Volume 69A
Number 6
Nov.–Dec. 1965

Physics and Chemistry

U.S. DEPARTMENT
OF COMMERCE

SECTION A

JOURNAL OF RESEARCH

NATIONAL BUREAU OF STANDARDS

Journal of Research

of the

National Bureau of Standards

A. Physics and Chemistry

Nov.–Dec. • 1965

Volume • 69A

NUMBER • 6

Editor: C. W. Beckett

Associate Editors: D. D. Wagman
J. M. Richardson

Publication dates:
Feb. 1, Apr. 1, June 1, Aug. 1, Oct. 1, Dec. 1, 1965

JOURNAL OF RESEARCH

The National Bureau of Standards Journal of Research reports research and development in the fields of activity shown at right. Also included from time to time are survey articles on topics closely related to the Bureau's scientific and technical program.

The Journal is published in three separate sections as follows:

A. Physics and Chemistry

Contains papers of interest primarily to scientists working in these fields. Issued six times a year. Annual subscription: domestic, $4.00; foreign, $4.75. Single copy, 70c.

B. Mathematics and Mathematical Physics

Presents studies and compilations designed mainly for the mathematician and the theoretical physicist. Issued quarterly. Annual subscription: domestic, $2.25; foreign, $2.75. Single copy, 75c.

C. Engineering and Instrumentation

Reports research and development results of interest chiefly to the engineer and the applied scientist. Issued quarterly. Annual subscription: domestic, $2.25; foreign, $2.75. Single copy, 75c.

The National Bureau of Standards is a principal focal point in the Federal Government for assuring maximum application of the physical and engineering sciences to the advancement of technology in industry and commerce. Its responsibilities include development and maintenance of the national standards of measurement, and the provision of means for making measurements consistent with those standards; determination of physical constants and properties of materials; development of methods for testing materials, mechanisms, and structures, and making such tests as may be necessary, particularly for government agencies; cooperation in the establishment of standard practices for incorporation in codes and specifications; advisory service to government agencies on scientific and technical problems; invention and development of devices to serve special needs of the Government; assistance to industry, business and consumers in the development and acceptance of commercial standards and simplified trade practice recommendations; administration of programs in cooperation with United States business groups and standards organizations for the development of international standards of practice; and maintenance of a clearinghouse for the collection and dissemination of scientific, technical and engineering information. The scope of the Bureau's activities is suggested in the following listing of its three Institutes and their organizational units.

Institute for Basic Standards. Applied Mathematics. Electricity. Metrology. Mechanics. Heat. Atomic Physics. Physical Chemistry. Laboratory Astrophysics.* Radiation Physics. Radio Standards Laboratory:* Radio Standards Physics & Radio Standards Engineering. Office of Standard Reference Data.

Institute for Materials Research. Analytical Chemistry. Polymers. Metallurgy. Inorganic Materials. Reactor Radiations. Cryogenics.* Materials Evaluation Laboratory. Office of Standard Reference Materials.

Institute for Applied Technology. Building Research. Information Technology. Performance Test Development. Electronic Instrumentation. Textile and Apparel Technology Center. Technical Analysis. Office of Weights and Measures. Office of Engineering Standards. Office of Invention and Innovation. Office of Technical Resources. Clearinghouse for Federal Scientific and Technical Information.**

*Located at Boulder, Colo. 80302.
**Located at 5285 Port Royal Road, Springfield, Va., 22171.

U.S. DEPARTMENT OF COMMERCE
John T. Connor, Secretary

NATIONAL BUREAU OF STANDARDS
A. V. Astin, Director

Order all publications from the Superintendent of Documents
U.S. Government Printing Office, Washington, D.C., 20402

Use of funds for printing this publication approved by the Director of the Bureau of the Budget (June 19, 1961).

JOURNAL OF RESEARCH of the National Bureau of Standards—A. Physics and Chemistry
Vol. 69A, No. 6, November–December 1965

Arc Measurement of Some Argon Transition Probabilities

C. H. Popenoe and J. B. Shumaker, Jr.

(July 29, 1965)

Transition probabilities and line shape parameters for three argon lines have been measured in a wall-stablilized argon arc containing a trace of hydrogen. The H_β line shape measurement and the assumption of local thermodynamic equilibrium provided the determination of the argon level populations. From these three lines ten other argon line transition probabilities have been obtained by relative measurements in a pure argon arc. The results are compared with those of other investigators and sources of error are discussed.

Key Words: Arc, argon, linewidth, plasma, spectroscopy, stark broadening, transition probability.

1. Introduction

The importance of argon transition probabilities for plasma diagnostics is reflected in the large amount of recent experimental work on the measurement of these quantities [1, 2, 3, 4].[1] The most fruitful source of these measurements has been the high current thermal arc, but unfortunately even here in similar sources the results of different investigators may differ by factors of two, well outside the error estimates attributed to the measurements by their authors. Consequently an additional attempt to measure argon transition probabilities in a thermal arc source was undertaken. The particular technique employed was one which has previously been used in these laboratories [5]. It consists of operating a wall-stabilized arc with a gas mixture containing a trace of hydrogen in the gas whose transition probability is to be measured, and then deducing the arc plasma temperature and composition from the spectral line shape of the 4861 Å hydrogen Balmer β line. From the plasma composition and absolute line intensity measurements the transition probabilities can be derived.

Absolute transition probabilities were determined in this manner for the two AI lines at 4300 and 6965 Å and for the AII line at 4806 Å. These lines were selected for their prominence, isolation from their neighbors, symmetry, relative freedom from self absorption, and location in wavelength regions favorable for photoelectric detection. Some additional transition probabilities were measured relative to one or another of these three reference lines in pure argon arcs. However, measurements on these lines are less satisfactory either because the lines are weak or because of ambiguity in the location of the background. Most of the prominent blue argon lines in this source are afflicted with this background problem due to the closeness of strong neighbors or asymmetric line shapes (see fig. 1) either of which can result in an uncertainty in the total intensity to be ascribed to the lines.

All of the data recording, handling, and calculations including the graphical presentation of the results were done by automatic machine methods to eliminate as many sources of error as possible. With the statistically large samples made possible by these methods along with elimination of subjective measurements and increased precision, it becomes possible to attempt a more thorough analysis of the errors and uncertainties involved in these measurements.

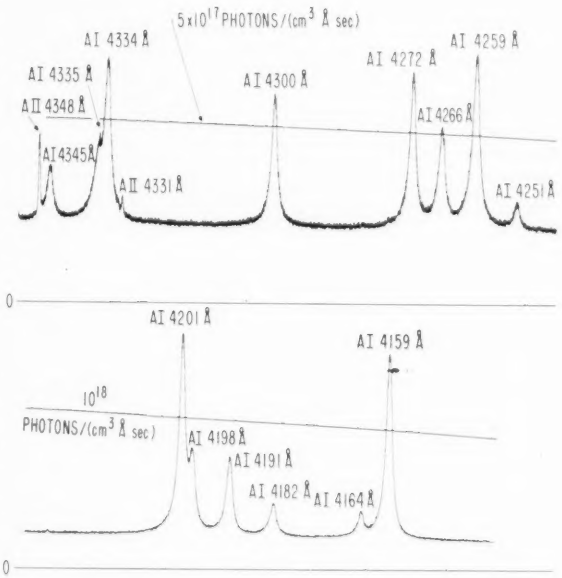

FIGURE 1. *Atmospheric pressure argon arc spectra after Abel inversion [ref. 19].*

The total intensity of AI 4300 Å yields an electron density of 6.9×10^{16} cm^{-3} and temperature of 12 060 °K assuming the transition probability value of table 3.

[1] Figures in brackets indicate the literature references at the end of this paper.

2. Experimental Details

2.1. Light Source

The radiation source is a wall-stabilized or cascade d-c arc of about 10 cm length and 5 mm diam. The arc chamber is similar to that described in reference [6] with the exception of improved water cooling for higher current operation. The graphite electrodes are surrounded by a separate flow of argon, preventing rapid electrode erosion and contamination of the test gas in the observation section. After passing through the arc the gases are exhausted to the atmosphere through large diameter ports. The arc characteristically operates stably for long periods of time for most test gases. For the experiments reported here arc currents of 40, 60, and 90 A were used.

The arc chamber is mounted on a carriage movable by means of a lead screw in a direction transverse to the optic axis of the monochromator. An electrically actuated single-revolution clutch couples an electric motor to the leadscrew drive providing for either continuous or incremental movement of the arc carriage. Variation in rate of scan or increment size is accomplished by a set of quick-change gears in the drive train.

Electrical power is supplied to the arc by either a bank of 100 6 V storage batteries, or a rotary converter of 500 kVA capacity and 650 V output as shown schematically in figure 2. Both power sources were used during this series of experiments with no observable difference in results. The voltage drop across the arc is typically 102 V in argon at 60 A, and 112 V with 1 percent hydrogen added to the test gas. The bulk of the power is dissipated in a large variable water resistor [7] in series with the arc supply.

The current is automatically regulated by a solid-state series current regulator (see fig. 2) consisting of 30 power transistors in parallel, with the current error signal being derived from a 0.2 Ω oil-cooled manganin shunt. The arc current is initially set and later monitored with a potentiometer and galvanometer by which variations in total arc current as small as 1 mA may be observed. A carbon pile rheostat is used to provide vernier adjustment of the ballast resistance.

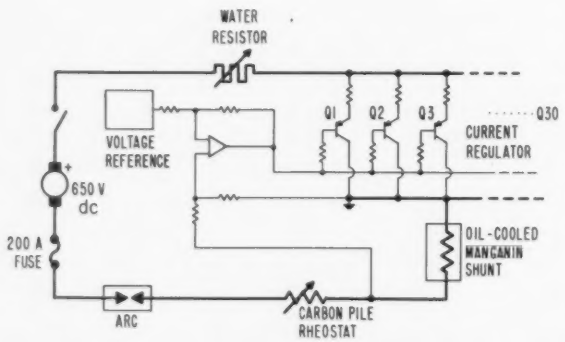

FIGURE 2. *Arc circuit schematic including some details of the transistorized automatic current regulator.*

2.2. Optical and Spectrographic Arrangement

The arc was viewed in a plane perpendicular to the arc axis with the image focused slightly enlarged on the monochromator entrance slit. A rectangular diaphragm opening at the lens formed the aperture stop of the system and limited the solid angle from the arc to 0.002 sr. The dispersing element was an 0.8 m Ebert-Fastie plane grating monochromator having a nominal dispersion of 10 Å/mm in the first order. Entrance and exit slits of 15 μ width were used in most of the experiments. The entrance slit height was masked to 1.2 mm to eliminate reflections from the copper plates adjacent to the observation section of the arc chamber and to minimize the effect of any slight variations of the arc column along its length. During the course of the experiments, RCA 931A (S–4 response), Hamamatsu R–136 and RCA 7265 (S–20 response), and ITT FW–118 (S–1 response) photomultiplier tubes were employed to detect the spectral intensity.

The monochromator grating drive is fitted with a single channel paper tape reader attached directly to the wavelength counter to allow direct digital control of the wavelength setting. An electrical signal causes the monochromator to scan in wavelength until a punched hole in the paper tape is sensed by the reader. A program paper tape may therefore be punched to direct the monochromator through a prescribed, not necessarily evenly spaced sequence of wavelengths in the spectrum. The resolution of the tape reader is 0.05 Å and the precision of the wavelength setting better than 0.01 Å.

2.3. Data Recording and Control System

The large quantity of data encountered in spectrometric studies involving spacial resolution of plasma characteristics invites the use of automatic digital techniques for data collection and reduction [8]. To facilitate data handling the response of the monochromator was recorded digitally on punched paper tape in a form compatible with electronic data processing equipment. In addition, the monochromator wavelength drive and arc carriage positioning mechanism were automatically actuated and coordinated so as to perform the proper variable changes during an experiment in the minimum time.

In essence, the data recorder consists of amplifying, digitizing and tape punching equipment. The small current output of the photomultiplier is amplified and converted to a voltage signal of the order of 1 V which in turn is converted to a pulse train whose frequency is proportional to this voltage. An electronic counter sums the pulses for a precise interval of time, resulting in a digitized integral of the applied voltage over the counting interval. Upon command, six digits of information from the counter are loaded simultaneously

into a shift register from which they may be shifted out serially into a code-conversion matrix and punched on paper tape in binary-coded-decimal form.

Movement of the arc carriage, changes in the monochromator wavelength and recording of photomultiplier current are all directed and coordinated automatically during a run by a central programmer. The heart of the programmer is a 25-step, 11 level stepping switch, wired in a closed-loop mode; i.e., a signal from the preceding operation verifying its successful completion is necessary to initiate a succeeding operation. With the above system the rate of data recording is limited by the tape punch to about two 8-character data points per second.

The possibility of erroneous recordings is greatly diminished by various self-checks incorporated into the system. The analog section of the system (current amplifier and voltage-to-frequency converter) is subject to the small errors inherent in analog devices and is therefore checked and calibrated several times during an experiment. The calibration is transferred directly to punched tape to preclude errors in recording. The nature of the digital section, and indeed of digital systems in general is such that the occurrence of small errors in transferring digits through the system is highly improbable. To ensure that such errors, if they occur, will be detected, an odd-bit parity check is made at the tape punch, and the recording process is automatically stopped if an added or dropped bit is detected on the tape. A second and independent parity check is made during the process of converting the tape to punched cards.

2.4. Experimental Method

A representative spectral line measurement consisted of the photoelectric recording of the arc intensity at each of perhaps 30 equally spaced positions across the width of the arc. This set of measurements was then repeated at each of usually 27 wavelengths spaced nonuniformly across the spectral line—spanning altogether about 10 times the maximum full halfwidth of the line. Finally, without turning off the electronics, recordings were made of the intensity of a calibrated tungsten strip pyrometer lamp at the same 27 wavelengths.

An intermittent arc traversing technique was used in which the motion of the arc carriage was momentarily stopped for an interval of time sufficient to overcome photomultiplier delay effects and to record the intensity at that point before resuming motion and proceeding to the next point. This eliminates the distortion of the arc profile which results from continuous movement of the arc carriage during the counting interval. Also, since the traverses always begin at precisely the same point (± 0.001 cm), each recorded point corresponds to a given point in space referenced to a laboratory coordinate system, not a function of time or scanning rate. The recording positions are therefore repeatable and the recorded intensities directly comparable from traverse to traverse.

The effect of integrating the intensity at a point for a finite interval of time is a temporal smoothing of noise at that point on the arc profile. Some further spacial smoothing occurs because of the necessity of observing a finite "slice" of the arc column. However, the additional loss of spacial resolution which would result from a continuous traversing or "scanning" of the arc image is effectively avoided by the intermittent traversing technique. In these experiments an integrating period of 0.1 sec was used. The width of the observed "slice" was determined by the slit width and in most experiments amounted to about 0.001 cm while the distance between samples was typically 0.03 cm.

The test gas—either pure argon or premixed mixture of argon and 1 percent hydrogen—was injected tangentially into the arc on both sides of the observation chamber at a rate of 1.2 liter/min and a differential pressure of a few millimeters of water. Gas flow rates were monitored by flowmeters and adjusted to minimize flow in the observation chamber. Separate flows of pure argon at about 0.2 liter/min were injected tangentially at the electrodes. The difference in flow rates insured a net gas flow away from the observation section, further precluding electrode vapor contamination by diffusion.

The intensity measurements are calibrated with a tungsten strip lamp at a brightness temperature at 6530 Å of 2340.3 °K (IPTS 1948). The lamp was periodically calibrated by the Temperature Physics Section of the National Bureau of Standards. At the conclusion of each arc experiment it was placed at the arc position with the quartz window from the arc placed in the optic path to eliminate the necessity for determination of window transmission. A well-regulated d-c power supply maintained the strip lamp current at a constant level within 0.01 percent. The same punched program tape used to direct the monochromator through the sequence of wavelengths for the experiment was then used to record the calibrated strip lamp intensity at the same wavelengths as those of the experiment.

3. Treatment of Data

3.1. Abel Inversion

In order to obtain the radial distribution of volume emission in the arc from side-on measurements it is necessary to solve the appropriate Abel integral equation [9] for each traverse across the arc. The technique employed is based upon one described by Freeman and Katz [10] in which the distribution of measured side-on intensities is fitted by a polynomial in the positional coordinate with origin at the center of symmetry. The solution of the integral equation is then obtained analytically for this polynomial and the volume emission at any desired point in the arc is calculated from this solution. By including odd powers in the fitting polynomial some minimal allowance is made for source asymmetry and for errors in locating the position of the arc "center of symmetry" [11].

The polynomial fitting was accomplished by the use of the orthogonal properties of the Jacobi [12] polynomials $P_n^{(a,\bar{a})}(x/R)$ whose inverse Abel transform is expressible in terms of $P_m^{(a-1/2,0)}(2[r/R]^2-1)$ with odd n terms treated in the approximation of Freeman and Katz [11]. R is the distance from the arc center beyond which the intensity is considered negligible. This technique results in the weighting of the data points by $(1-[x/R]^2)^a$. In the experiments reported here uniform weighting ($a=0$) was arbitrarily used after experiments revealed no appreciable difference in the results obtained using $a=0$ (corresponding essentially to the Freeman and Katz method) and $a=\frac{1}{2}$ (corresponding, except for the odd n terms, to a method described by Herlitz [13]). Individual arc traverses contained from 20 to 41 measurements at equally spaced x points and the resulting intensity profiles were fitted by the Jacobi polynomial expansions with 8 to 12 terms.

3.2. Line Shape Parameters

The volume emission intensities calculated from the Abel inversions were reassembled as a function of wavelength at each radial point and a suitable theoretical spectral line shape was fitted by an iterative least squares technique. In the case of the argon lines a dispersion (Lorentz) shape superimposed upon a linear background was used as the fitting function:

$$I=A+B(\lambda-\lambda_0)+\frac{C}{1+[(\lambda-\lambda_0)/\Delta]^2}$$

with A, B, C, λ_0, and Δ being adjusted to minimize the sum of the squares of the residuals. In the case of the hydrogen β lines the line shape fitting was preceded by subtracting from each experimental Abel inverted wavelength scan the corresponding pure argon arc spectrum at the same radial point. This pure argon background spectrum was obtained as a part of each experiment in the same manner and under the same arc conditions as was the argon-hydrogen mixture data. The red and blue wings of the resulting difference spectrum were then averaged and this line shape was fitted to an appropriate theoretical H_β line shape:

$$I=A+BS(\alpha)$$

where $\alpha=1.25\times10^{-9}|\lambda-\lambda_0|(N_e)^{-2/3}$, $S(\alpha)$ is a theoretical line shape [14], and A, B, and the electron density $N_e(\mathrm{cm}^{-3})$ are adjusted to minimize the residual function. The Griem, Kolb, and Shen tabulations of $S(\alpha)$ were fitted piecewise by cubics in all the tabulated intervals except the first where a parabola was used with the condition $\frac{dS}{d\alpha}=0$ at $\alpha=0$. The asymptotic wing formulas [15] were used beyond the range of the tables. In this manner piecewise analytic approximations to $S(\alpha)$ were constructed for H_β. In addition to the dependence of the H_β line shapes upon N_e implied by the definition of α, there is a further weak dependence upon N_e and T. This dependence was included in these calculations by the actual use of different piecewise line shapes calculated for $N_e=10^{17}$ and $T=13\,000$ °K, $N_e=10^{16}$ and $T=10\,000$ °K, and for $N_e=10^{15}$ and $T=7500$ °K—the first and last being obtained by interpolation in the Griem, Kolb, and Shen tables.

All of the above calculations as well as division by the strip lamp calibration data and conversion to absolute intensities are programmed to be performed in one pass through the IBM 7094 digital computer. At each radial point the computer plots the experimental radially-resolved wavelength scans and tabulates all of the line fitting parameters; in particular the argon line centers λ_0, $\frac{1}{2}$-halfwidths Δ, and total intensities $\pi C\Delta$, the hydrogen line total intensity $B\int S(\alpha)d\alpha$, and the electron density N_e.

No slit width corrections were necessary for the hydrogen lines because of their relatively great width. However, for the argon lines slit or apparatus function corrections were required. For this purpose the program for dispersion line shape fitting was systematically calibrated using various ratios of apparatus function width to dispersion line width and using various distributions of wavelength points of measurement across the line. The calibration was done for both Gaussian and triangular apparatus functions and resulted in the application of small slit width dependent corrections to the computed line widths and, for very wide slits, to the line intensities. This procedure should be quite reliable for lines which have nearly a dispersion shape.

The apparatus functions observed with the 15 μ entrance and exit slits used in most of these experiments were approximately Gaussian with $\frac{1}{2}$-halfwidths (one-half of the full width at the half maximum intensity level) of 0.1 Å. One experiment was performed with 150 μ slits in which the apparatus function was nearly triangular with a $\frac{1}{2}$-halfwidth of 0.75 Å.

Examples of the line shape fitting are given in figures 3 and 4. The AI 4300 Å line can be seen to exhibit some skewness. This skewness together with the unsymmetric disposition of the wavelength points [2] causes the dispersion shape fitting routine to produce a line shape which in this example is about 3 percent narrower than a good eye-fit would probably yield. The apparatus function for both lines in this example was the Gaussian shape with $\frac{1}{2}$-halfwidth of 0.1 Å. In figure 3 the computer-fitted $\frac{1}{2}$-halfwidth of 0.771 Å required a correction of 0.013 Å for apparatus function resulting in an estimate of 0.758 Å for the $\frac{1}{2}$-halfwidth of the spectral line itself. In figure 4 the intensity scale for H_β is displaced vertically by an amount which has no particular physical significance being determined by the subtracted hydrogen-free background spectrum.

Beyond a radial distance of 0.2–.25 cm, the line shape fitting procedure was considered unreliable due to the sharpness of the lines and the attendent small

[2] The asymmetric distribution of wavelength points apparent in figure 3 is, to some extent, unavoidable unless an excessive number of uniformly spaced wavelengths is used because of the dependence of the line shift upon the radial position of the observation.

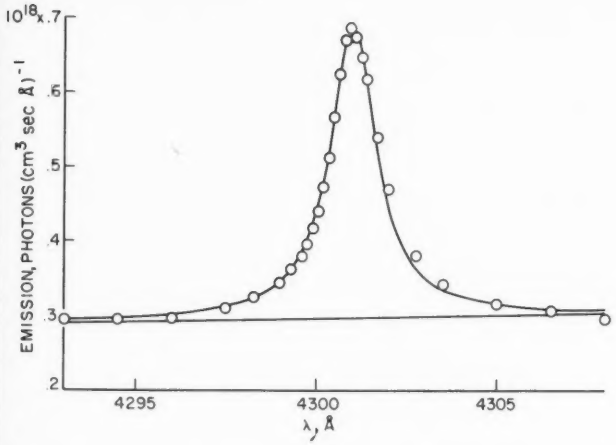

FIGURE 3. *Experimental intensity points in the neighborhood of AI 4300 Å after Abel inversion (0.13 cm from axis of 90 ampere arc in argon with ~ 1% H_2) showing computer fitted background and dispersion shape: ½-halfwidth = 0.771 Å, total line emission = 9.44×10^{17} photons cm^{-3} sec^{-1}*

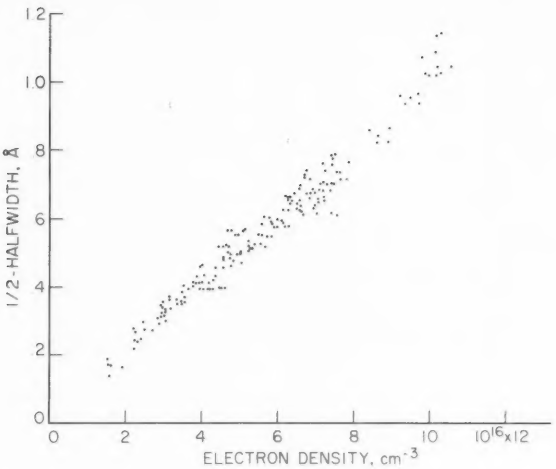

FIGURE 5. *Dependence of ½-halfwidth upon electron density for AI 4300 Å.*

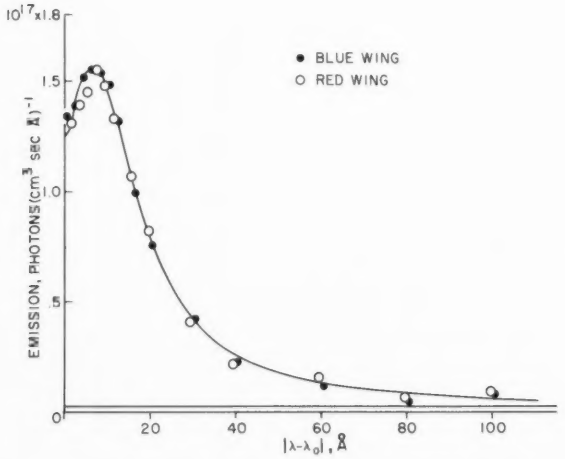

FIGURE 4. *Experimental intensity points in the neighborhood of H_β 4861 Å after Abel inversion (same conditions as fig. 3) showing computer fitted background level and theoretical line shape: electron density = 7.45×10^{16} cm^{-3}, total line emission = 8.10×10^{18} photons cm^{-3} sec^{-1}.*

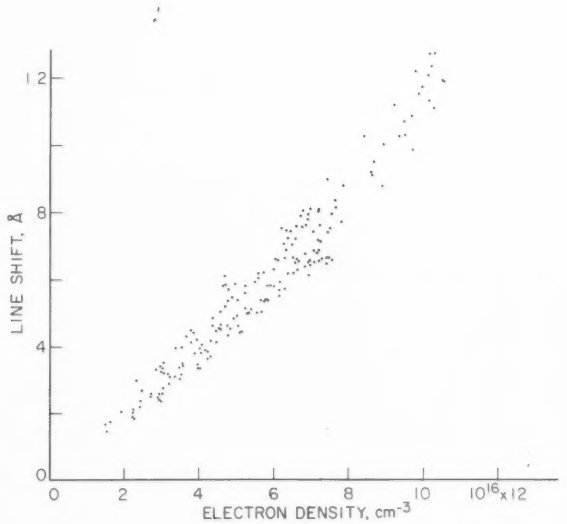

FIGURE 6. *Dependence of the red shift of the AI 4300 Å line upon electron density.*

number of points defining their shapes. At these distances, the low number density of the emitting species causes a reduction in the signal/noise ratio with the effect that the determination of the true line shape from a statistically small sample of noisy data is improbable. For these reasons, the data from regions lying beyond an arbitrarily chosen radial distance of 0.2 cm (0.16 cm for ionic lines) is not reported here.

Argon line shifts and ½-halfwidths corrected for the 0.1 Å Gaussian apparatus function are plotted in figures 5 to 10 against the electron density as determined from the H_β line shapes. The wavelengths for the unshifted lines were obtained by extrapolation to $N_e = 0$. Both the widths and shifts are seen to be approximately proportional to the electron density in rough agreement with theory [9]. The proportionality constants obtained by least squares fitting of this data are shown in table 1.

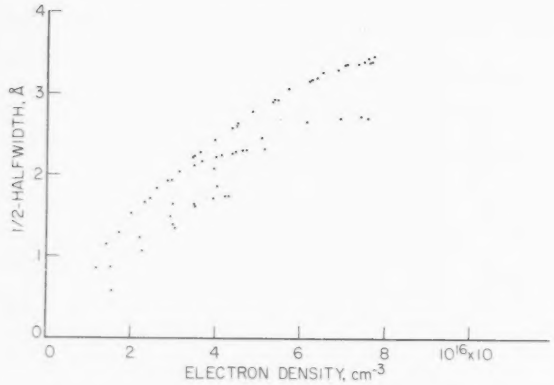

FIGURE 7. *Dependence of ½-halfwidth upon electron density for Al 6965 Å*

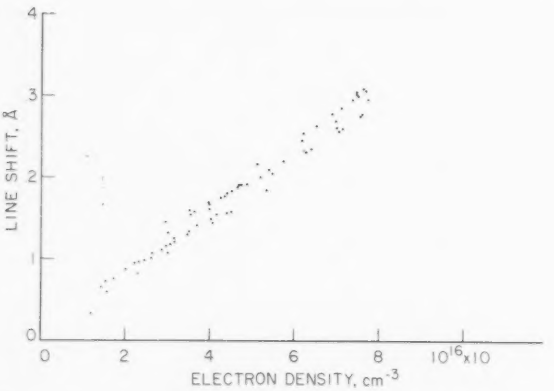

FIGURE 8. *Dependence of the red shift of the Al 6965 Å line upon electron density.*

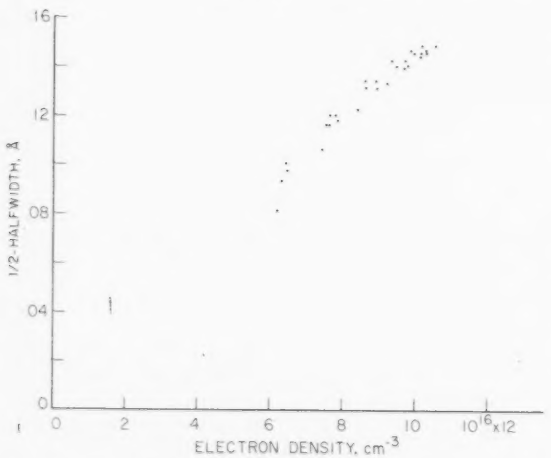

FIGURE 9. *Dependence of ½-halfwidth upon electron density for AII 4806 Å.*

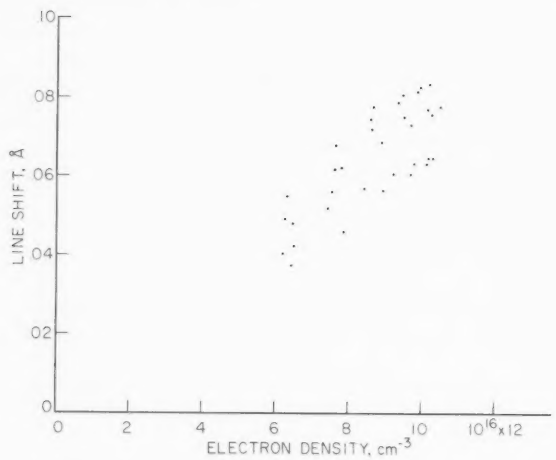

FIGURE 10. *Dependence of the blue shift of the AII 4806 Å line upon electron density.*

TABLE 1. *Stark 1/2-half widths,* w, *and shifts,* d, *for argon lines*

Line	$\frac{w}{N_e} \times 10^{16}$ [Å cm^3]		$\frac{d}{N_e} \times 10^{16}$ [Å cm^3]*	
	Expt.	Theor.	Expt.	Theor.
AI 4300 Å	0.100	0.124	0.103	0.132
AI 6965 Å	.048	.061	.039	.079
AII 4806 Å	.0148	.0058	−.0073	(−.0022)

*Shifts to the red are taken as positive.

3.3. Transition Probabilities

The calculation of the argon transition probabilities requires a knowledge of the plasma composition at each arc data point. For conditions of local thermodynamic equilibrium this can be computed in principle from the total pressure (1 atm), measured electron density, and total H_β line intensity assuming that only hydrogen and argon are present and using the theoretical H_β transition probability, Dalton's law, the condition for quasi-neutrality and the appropriate mass action laws (Saha equations) for the possible ionization and dissociation reactions. The fact that the hydrogen was present in trace amounts permitted some simplification of the calculations as has been discussed previously [5, 16]. This simplified calculation requires a table of the composition of a pure argon plasma at atmospheric pressure and employs small corrections computed iteratively from the observed H_β line intensity.

The pure argon plasma composition was machine computed by a method similar to that of Drellishak, Knopp, and Cambel [17] including first order Debye corrections. The partition functions as functions of the cutoff energy were analytically smoothed and made

to assume the asymptotic hydrogenlike form at the ionization energy limit (9). The number density of triply ionized argon atoms was assumed negligible thus limiting the calculations to temperatures below about 20 000 °K. The computed composition table including upper level populations pertinent to the present experiments is presented as table 2. Griem's treatment [18] of high density corrections to plasma composition calculations suggests that table 2 should be accurate to approximately 1 percent.

Finally the electron density and H_β line intensity obtained from the H_β line shape fitting are used iteratively in conjunction with this table to determine the total hydrogen content and the number density of excited argon atoms at the radial points considered. The argon transition probabilities are then found by division of the total line intensities (in photons per cubic centimeter per second) by these number densities at corresponding radii. The individual values of the transition probabilities obtained in this manner are presented in figures 11, 12, and 13. The averages of these experimental transition probabilities are given in table 3.

The transition probabilities of the lines other than 6965, 4300, and 4806 were determined relative to one or another of these three reference lines. The lines lying in the red and infrared were measured using the digital apparatus described above with full Abel inversion but with wider slits and with an abbreviated wavelength scan. The plasma composition was

TABLE 2. *Argon plasma composition at 1.00 atm pressure**

T	Z_0	Z_1	Z_2	U_0	U_1	U_2	N_e	N_0	N_1	N_2
5000	1.0000	5.3246	7.904	127106	222812	329954	1.322E 12	1.468E 18	1.322E 12	3.642E-07
5500	1.0000	5.3752	8.034	127101	222803	329940	7.174E 12	1.335E 18	7.174E 12	1.441E-04
6000	1.0000	5.4188	8.158	127093	222787	329916	2.944E 13	1.223E 18	2.944E 13	2.135E-02
6500	1.0000	5.4567	8.278	127081	222762	329879	9.746E 13	1.129E 18	9.746E 13	1.485E 00
7000	1.0000	5.4901	8.393	127063	222726	329825	2.724E 14	1.048E 18	2.724E 14	5.702E 01
7500	1.0000	5.5196	8.506	127039	222678	329753	6.648E 14	9.775E 17	6.648E 14	1.361E 03
8000	1.0000	5.5459	8.615	127009	222617	329662	1.453E 15	9.147E 17	1.453E 15	2.205E 04
8500	1.0000	5.5695	8.722	126971	222542	329549	2.898E 15	8.579E 17	2.898E 15	2.599E 05
9000	1.0001	5.5908	8.827	126926	222453	329415	5.352E 15	8.050E 17	5.352E 15	2.347E 06
9500	1.0001	5.6101	8.929	126875	222350	329261	9.254E 15	7.543E 17	9.254E 15	1.693E 07
10000	1.0003	5.6276	9.029	126818	222235	329089	1.511E 16	7.041E 17	1.511E 16	1.009E 08
10500	1.0005	5.6437	9.126	126755	222109	328900	2.342E 16	6.527E 17	2.342E 16	5.104E 08
11000	1.0009	5.6584	9.221	126688	221975	328699	3.466E 16	5.987E 17	3.466E 16	2.239E 09
11500	1.0015	5.6720	9.314	126618	221836	328491	4.910E 16	5.412E 17	4.910E 16	8.668E 09
12000	1.0025	5.6845	9.405	126549	221698	328283	6.672E 16	4.798E 17	6.672E 16	3.008E 10
12500	1.0039	5.6961	9.493	126482	221564	328082	8.705E 16	4.153E 17	8.705E 16	9.473E 10
13000	1.0061	5.7069	9.579	126421	221441	327898	1.091E 17	3.492E 17	1.091E 17	2.735E 11
13500	1.0093	5.7170	9.663	126367	221334	327738	1.315E 17	2.843E 17	1.315E 17	7.307E 11
14000	1.0140	5.7264	9.745	126325	221249	327610	1.525E 17	2.235E 17	1.525E 17	1.820E 12
14500	1.0208	5.7353	9.825	126294	221188	327517	1.705E 17	1.698E 17	1.705E 17	4.255E 12
15000	1.0304	5.7436	9.902	126275	221150	327462	1.846E 17	1.252E 17	1.845E 17	9.396E 12
15500	1.0441	5.7515	9.978	126268	221135	327439	1.942E 17	9.030E 16	1.942E 17	1.971E 13
16000	1.0630	5.7590	10.052	126269	221138	327443	1.998E 17	6.426E 16	1.997E 17	3.949E 13
16500	1.0890	5.7662	10.124	126277	221154	327467	2.022E 17	4.557E 16	2.020E 17	7.586E 13
17000	1.1241	5.7731	10.195	126289	221178	327504	2.021E 17	3.248E 16	2.018E 17	1.403E 14
17500	1.1706	5.7799	10.263	126304	221208	327559	2.004E 17	2.344E 16	1.999E 17	2.506E 14
18000	1.2315	5.7865	10.330	126321	221241	327608	76E 17	1.720E 16	1.967E 17	4.336E 14
18500	1.3099	5.7932	10.395	126337	221275	327648	1.9 3E 17	1.288E 16	1.928E 17	7.283E 14
19000	1.4093	5.7999	10.459	126354	221307	327697	1.907E 17	9.856E 15	1.883E 17	1.189E 15
19500	1.5334	5.8068	10.522	126369	221338	327744	1.870E 17	7.704E 15	1.833E 17	1.890E 15

T	N_e	4044 AI	4159 AI	4259 AI	4272 AI	4300 AI	4348 AII	4806 AII
5000	1.322E 12	1.153E 04	1.669E 04	2.054E 03	1.011E 04	1.760E 04	4.465E-08	6.290E-08
5500	7.174E 12	2.324E 05	3.252E 05	4.184E 04	1.968E 05	3.414E 05	1.467E-05	1.952E-05
6000	2.944E 13	2.818E 06	3.835E 06	5.118E 05	2.319E 06	4.009E 06	1.840E-03	2.333E-03
6500	9.746E 13	2.313E 07	3.073E 07	4.231E 06	1.858E 07	3.202E 07	1.099E-01	1.339E-01
7000	2.724E 14	1.397E 08	1.819E 08	2.572E 07	1.099E 08	1.890E 08	3.667E 00	4.314E 00
7500	6.648E 14	6.604E 08	8.450E 08	1.223E 08	5.102E 08	8.755E 08	7.675E 01	8.764E 01
8000	1.453E 15	2.557E 09	3.222E 09	4.758E 08	1.945E 09	3.331E 09	1.100E 03	1.223E 03
8500	2.898E 15	8.398E 09	1.044E 10	1.569E 09	6.298E 09	1.077E 10	1.153E 04	1.252E 04
9000	5.352E 15	2.401E 10	2.948E 10	4.503E 09	1.778E 10	3.037E 10	9.301E 04	9.901E 04
9500	9.254E 15	6.094E 10	7.404E 10	1.147E 10	4.464E 10	7.614E 10	6.016E 05	6.288E 05
10000	1.511E 16	1.395E 11	1.678E 11	2.633E 10	1.012E 11	1.723E 11	3.220E 06	3.310E 06
10500	2.342E 16	2.910E 11	3.471E 11	5.509E 10	2.092E 11	3.560E 11	1.462E 07	1.480E 07
11000	3.466E 16	5.581E 11	6.603E 11	1.059E 11	3.979E 11	6.764E 11	5.745E 07	5.738E 07
11500	4.910E 16	9.889E 11	1.161E 12	1.881E 11	6.997E 11	1.189E 12	1.985E 08	1.958E 08
12000	6.672E 16	1.624E 12	1.895E 12	3.096E 11	1.141E 12	1.937E 12	6.108E 08	5.957E 08
12500	8.705E 16	2.478E 12	2.873E 12	4.731E 11	1.730E 12	2.934E 12	1.690E 09	1.631E 09
13000	1.091E 17	3.513E 12	4.049E 12	6.719E 11	2.438E 12	4.133E 12	4.242E 09	4.055E 09
13500	1.315E 17	4.631E 12	5.311E 12	8.874E 11	3.198E 12	5.417E 12	9.722E 09	9.209E 09
14000	1.525E 17	5.689E 12	6.492E 12	1.092E 12	3.908E 12	6.616E 12	2.048E 10	1.924E 10
14500	1.705E 17	6.534E 12	7.423E 12	1.256E 12	4.468E 12	7.560E 12	3.991E 10	3.720E 10
15000	1.846E 17	7.063E 12	7.990E 12	1.359E 12	4.809E 12	8.133E 12	7.254E 10	6.713E 10
15500	1.942E 17	7.252E 12	8.171E 12	1.397E 12	4.918E 12	8.312E 12	1.240E 11	1.140E 11
16000	1.998E 17	7.147E 12	8.023E 12	1.379E 12	4.828E 12	8.157E 12	2.010E 11	1.836E 11
16500	2.022E 17	6.832E 12	7.642E 12	1.319E 12	4.599E 12	7.767E 12	3.116E 11	2.829E 11
17000	2.021E 17	6.394E 12	7.128E 12	1.236E 12	4.289E 12	7.241E 12	4.653E 11	4.201E 11
17500	2.004E 17	5.899E 12	6.557E 12	1.141E 12	3.945E 12	6.657E 12	6.732E 11	6.046E 11
18000	1.976E 17	5.394E 12	5.978E 12	1.045E 12	3.596E 12	6.067E 12	9.479E 11	8.470E 11
18500	1.943E 17	4.905E 12	5.421E 12	9.508E 11	3.261E 12	5.499E 12	1.303E 12	1.159E 12
19000	1.907E 17	4.445E 12	4.899E 12	8.624E 11	2.947E 12	4.968E 12	1.754E 12	1.553E 12
19500	1.870E 17	4.019E 12	4.419E 12	7.804E 11	2.658E 12	4.480E 12	2.313E 12	2.039E 12

T	N_e	6753 AI	6871 AI	6965 AI	7030 AI	9195 AI	9292 AI
5000	1.322E 12	1.016E 04	6.565E 03	1.626E 05	8.131E 03	1.891E 04	6.510E 03
5500	7.174E 12	2.072E 05	1.330E 05	2.460E 06	1.692E 05	3.478E 05	1.194E 05
6000	2.944E 13	2.537E 06	1.619E 06	2.348E 07	2.106E 06	3.908E 06	1.338E 06
6500	9.746E 13	2.099E 07	1.333E 07	1.574E 08	1.768E 07	3.007E 07	1.028E 07
7000	2.724E 14	1.277E 08	8.074E 07	7.994E 08	1.088E 08	1.719E 08	5.863E 07
7500	6.648E 14	6.072E 08	3.826E 08	3.251E 09	5.232E 08	7.745E 08	2.638E 08
8000	1.453E 15	2.364E 09	1.485E 09	1.104E 10	2.056E 09	2.876E 09	9.785E 08
8500	2.898E 15	7.798E 09	4.886E 09	3.228E 10	6.838E 09	9.103E 09	3.093E 09
9000	5.352E 15	2.238E 10	1.399E 10	8.323E 10	1.977E 10	2.518E 10	8.546E 09
9500	9.254E 15	5.703E 10	3.557E 10	1.926E 11	5.071E 10	6.207E 10	2.105E 10
10000	1.511E 16	1.310E 11	8.153E 10	4.058E 11	1.171E 11	1.384E 11	4.687E 10
10500	2.342E 16	2.741E 11	1.703E 11	7.853E 11	2.464E 11	2.819E 11	9.542E 10
11000	3.466E 16	5.270E 11	3.270E 11	1.407E 12	4.762E 11	5.289E 11	1.789E 11
11500	4.910E 16	9.362E 11	5.800E 11	2.341E 12	8.496E 11	9.186E 11	3.106E 11
12000	6.672E 16	1.541E 12	9.536E 11	3.632E 12	1.404E 12	1.482E 12	5.006E 11
12500	8.705E 16	2.356E 12	1.456E 12	5.256E 12	2.155E 12	2.223E 12	7.505E 11
13000	1.091E 17	3.346E 12	2.066E 12	7.098E 12	3.071E 12	3.102E 12	1.047E 12
13500	1.315E 17	4.420E 12	2.725E 12	8.948E 12	4.069E 12	4.032E 12	1.360E 12
14000	1.525E 17	5.438E 12	3.350E 12	1.054E 13	5.022E 12	4.888E 12	1.648E 12
14500	1.705E 17	6.256E 12	3.850E 12	1.165E 13	5.793E 12	5.545E 12	1.869E 12
15000	1.846E 17	6.773E 12	4.165E 12	1.214E 13	6.287E 12	5.925E 12	1.997E 12
15500	1.942E 17	6.963E 12	4.278E 12	1.205E 13	6.479E 12	6.018E 12	2.027E 12
16000	1.998E 17	6.871E 12	4.219E 12	1.150E 13	6.408E 12	5.871E 12	1.977E 12
16500	2.022E 17	6.576E 12	4.035E 12	1.067E 13	6.146E 12	5.559E 12	1.872E 12
17000	2.021E 17	6.161E 12	3.778E 12	9.710E 12	5.770E 12	5.156E 12	1.735E 12
17500	2.004E 17	5.691E 12	3.487E 12	8.724E 12	5.339E 12	4.717E 12	1.587E 12
18000	1.976E 17	5.209E 12	3.190E 12	7.780E 12	4.895E 12	4.279E 12	1.439E 12
18500	1.943E 17	4.741E 12	2.902E 12	6.909E 12	4.463E 12	3.862E 12	1.299E 12
19000	1.907E 17	4.300E 12	2.631E 12	6.122E 12	4.055E 12	3.475E 12	1.168E 12
19500	1.870E 17	3.891E 12	2.379E 12	5.419E 12	3.675E 12	3.121E 12	1.049E 12

*Z_0, Z_1, and Z_2 are internal partition functions for neutral, singly ionized, and doubly ionized argon atoms respectively.
U_0, U_1, and U_2 are effective ionization energies [cm^{-1}].
N_e, N_0, N_1, and N_2 are number densities of electrons, neutral, singly ionized, and doubly ionized argon atoms [cm^{-3}].
Columns headed by a wavelength contain number densities in the upper state of the line: e.g., under 4300 AI is tabulated $N_0 g_u \exp(-E_u/kT)/Z_0$ with $g_u = 5$, $E_u = 116999$ cm^{-1}.

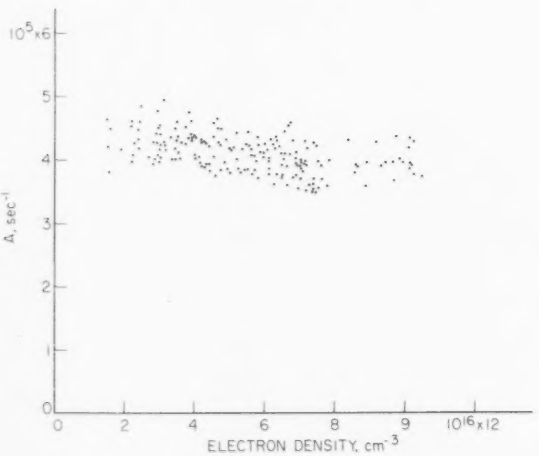

FIGURE 11. *AI 4300 Å transition probability values.*
Ave. = 4.11×10^5 sec^{-1}. Std. dev. = 0.29×10^5 sec^{-1}.

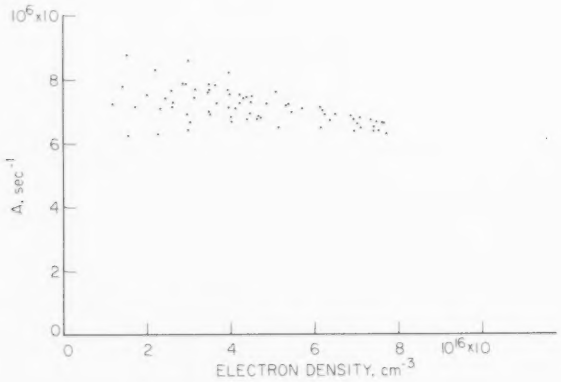

FIGURE 12. *AI 6965 Å transition probability values.*
Ave. = 7.10×10^6 sec^{-1}. Std. dev. = 0.55×10^6 sec^{-1}.

obtained from measurements of the AI 6965 Å intensity using a transition probability of 7.10×10^6 sec^{-1}. The lines in the blue were measured using an analog computer [19] for the direct recording of the Abel inverted spectra. In this way it was felt that the separation of overlapping lines (see fig. 1) could be better accomplished—although somewhat subjectively. The line intensities were determined by planimeter integration and the plasma composition was derived from the measured AI 4300 Å intensity (using $A = 4.11 \times 10^5$ sec^{-1}) for the neutral lines and from the AII 4806 Å intensity (using $A = 1.31 \times 10^8$ sec^{-1}) for the AII 4348 Å line. Because of the less satisfactory estimates of the line wing corrections, the limited number of experiments, and the uncertainty in the reference transition probabilities the A values for these lines are slightly less accurate than those for the 4300, 6965, and 4806 lines.

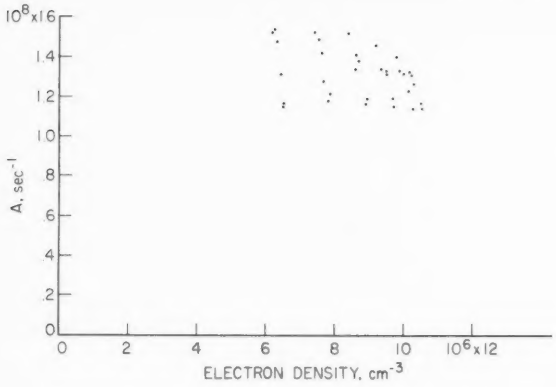

FIGURE 13. *All 4806 Å transition probability values.* Ave. = 1.31×10^8 sec^{-1}. Std. dev. = 0.21×10^8 sec.$^{-1}$.

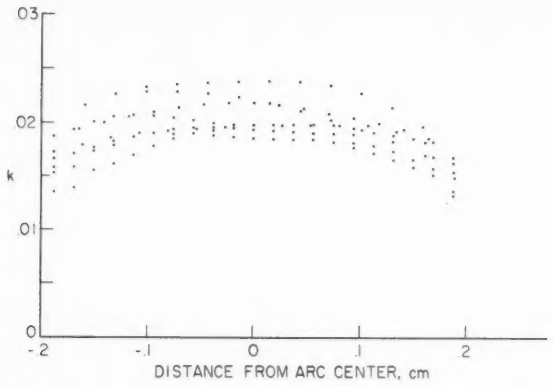

FIGURE 14. *The hydrogen/argon atomic ratio,* k, *as a function of radius for some 60 ampere experiments.*

TABLE 3. *Argon transition probabilities*

Wavelength	Transition	$A \times 10^{-8}$ [sec^{-1}]						
		This expt.	Drawin	Gericke	Olsen	Richter	Pery-Thorne	Garstang
Å								
4044 I	$1s_4 - 3p_5$	0.45 ± 13%	0.37			0.35		
4159 I	$1s_5 - 3p_8$	1.60 ± 13%	1.7	1.2	0.66			
4259 I	$1s_2 - 3p_1$	4.4 ± 14%	4.0	3.3	2.5			
4272 I	$1s_2 - 3p_7$	0.94 ± 14%	0.76	0.69	0.37			
4300 I	$1s_4 - 3p_8$	0.411 ± 11%	.36	.32				
4348 II	$4s^4P - 4p^4D^\circ$	240 ± 27%			115			128
4806 II	$4s^4P - 4p^4P^\circ$	131 ± 23%			79			79
6753 I	$2p_{10} - 4d_5$	2.9 ± 12%						
6871 I	$2p_{10} - 4d_5$	4.0 ± 13%						
6965 I	$1s_5 - 2p_2$	7.10 ± 11%			5.3		8.7	
7030 I	$2p_8 - 3s_5$	4.0 ± 12%						
9195 I	$2p_{10} - 2s_2$	2.2 ± 12%						
9292 I	$2p_{10} - 2s_3$	4.5 ± 12%						

3.4. Hydrogen-Argon Ratio

The ratio of the total hydrogen content to the total argon content as determined from the H_β shape and intensity measurements alone is shown in figure 14 as a function of radial position for some 60 A experiments. This ratio is defined as

$$k = (2N_{H_2} + N_H + N_{H+})/(N_A + N_{A+} + N_{A++} + \ldots)$$

where N_{H_2}, N_H, etc., are number densities of the species H_2, H, etc. All of the experiments in figure 14 utilized a premixed tank of the hydrogen-argon mixture with a value for this ratio of about 0.02 as determined by a mass spectrometric analysis. This figure illustrates the "demixing" effect [9] which precludes the use of cold gas composition data in determining the plasma composition in arcs containing gas mixtures.

4. Discussion of Errors

The recent appearance of a detailed and self-consistent theoretical treatment [9] of the problems of laboratory plasma sources and of spectroscopic plasma diagnostics together with the relatively large data sample sizes that can be accumulated with automatic recording and computing techniques makes possible a much more thorough error analysis than has heretofore been attempted. A discussion of several sources of error follows. In general it is found that the expected experimental and theoretical errors are of roughly comparable magnitudes.

4.1. Electronic

The maximum imprecision of the recorded intensities due to instrumental uncertainties was determined to be of the order of 0.15 percent. This figure results from the treatment as independent errors of the maxi-

mum effects of instrument nonlinearities and zero drift over a period of 1 hr with the combined effects of ambient temperature variations of plus or minus 5 °C and ± 10 percent line voltage fluctuations, and includes the contributions from the photomultiplier high-voltage power supply, the current amplifier, the voltage-to-frequency converter and the electronic counter.

An additional variation has been observed in the photomultiplier dark current on the higher gain range settings of the amplifier. This effect became noticeable after the dark current had been suppressed and appeared to consist of a long-term drift of the dark current of as much as 1 percent of full scale accompanied by short-term random noise of a similar magnitude.

The effects of photomultiplier fatigue on the photocurrent measurements were made negligible by restricting anode currents in the photomultiplier to less than 10^{-7} A, a value which previous investigations had shown to be below the threshold of fatigue effects for these tubes.

A certain amount of delay in the response of the photomultipliers to step inputs was observed. A rise time of about 0.2 sec was measured for the phototubes with S–20 response, while the delay was unmeasureable for the S–4 phototubes, implying some dependence on photocathode material. To ensure sufficient time for any effects of photomultiplier delay, mechanical relaxation or transient vibrations to decay, the recording of the photocurrent was postponed until 0.25 seconds after the arc chamber had completed its shift to a new position.

4.2. Calibration

The absolute calibration of the source intensities with a tungsten strip lamp is subject to a maximum uncertainty of about ± 5 percent. The brightness temperature calibration of the strip lamp at NBS is qualified by a certificated uncertainty of ± 7 °C relative to the IPTS which would produce uncertainties of about ± 3 percent in the transition probabilities of both neutral and ionic lines. For the calculation of the strip lamp emission at wavelengths other than the calibration wavelength (6530 A) the tungsten emissivities given by DeVos [20] were used. These are estimated to be accurate to within ± 2 percent. The maximum uncertainty due to this cause would therefore presumably be ± 2 percent in the blue and infrared spectrum and would decrease to zero at the calibration wavelength.

The errors in intensity due to uncertainties in determination of the correct strip lamp current are around ± 0.07 percent, almost two orders of magnitude below the errors discussed above and therefore negligible. The combined expected uncertainties are therefore ± 5 percent for blue and infrared lines decreasing to ± 3 percent for lines in the red.

4.3. Arc Source

The argon used in these experiments was technical grade argon with typically a purity of 99.996 percent containing mainly nitrogen and oxygen as contaminants. The gas flow system in the arc chamber is designed to prevent atmospheric and electrode contaminants from entering the observation chamber and indeed no impurities were observed spectroscopically during the experiments. From this observation the impurity upper limit and corresponding transition probability error of the order of 1 percent can be set based upon a minimum detectable signal and estimated transition probabilities for lines of the likely impurities, C, N, and 0.

The arc current regulator maintains the arc current constant to within 0.05 percent for periods of 1/4 or 1/2 hr. Effects of a long-term drift presumably due to ohmic heating of the oil-cooled regulator shunt were minimized by monitoring the arc current at intervals with a potentiometer and precision shunt and making small manual corrections. Oscilloscopic observation of the arc current reveals a 0.3 percent 360 cycle ripple when the rotary converter power supply is used. Assuming the totally unrealistic worst possible case—that the averaging over the 0.1 sec counting time results in a measurement of the electron density at one current extremum and of the line intensity at the other—then the ensuing error in the transition probabilities would be of the order of 0.5 percent and 1 percent for the AI and AII lines respectively.

The arc positioning mechanism is capable of locating the arc chamber to within 0.002 cm, with a repeatability an order of magnitude better. Since these positioning errors are attributed to the lead screw and are therefore noncumulative, they will appear on the recorded profile of the traverse as noise amounting at most to about 0.4 percent rms of the maximum signal.

The assumed total arc pressure of 1 atm is clearly an approximation. No record was kept of the prevailing atmospheric pressure during the experiments so that day-to-day pressure fluctuations of 2 or 3 percent must be expected. The over-pressure of the argon in the arc required to maintain the steady gas flow was 0.0003 atm. The arc column over-pressures due to magnetic self-compression and due to the momentum transport accompanying the heat transport can be estimated [9] for the 90 A arc as 0.0003 atm and 0.02 atm respectively. Thus the actual pressure at all points in the arc was at all times probably within 5 percent of the 1 atm assumed for the calculations. By repeating the plasma composition calculations (table 2) at other pressures the effect of this pressure uncertainty upon the transition probabilities can be evaluated. The result is that a ± 5 percent error in pressure produces a ∓ 1 percent error in the neutral line transition probabilities and a ± 8 percent error in the ionic line values.

4.4. Optical

Any nonuniformity of the arc in the axial direction within the observation chamber will result in transition probability errors due to the finite height of the spectrometer slit which collects light from a region 0.05 cm long in the axial direction and because of the resulting signal averaging which will be different for line widths, neutral line intensities, and ion line intensities. Estimates of the maximum errors from this source based upon measurements taken during a crude scan along the arc axis are 0.5 percent and 4 percent for neutral and ionic line transition probabilities respectively. Similar errors arise in the steep gradient regions of the arc because of imaging errors of the optical system and the finite width of the entrance slit. The combined lateral image smearing was determined to be less than 0.005 cm for the 15 μ slit by moving the edge of a tungsten strip filament lamp across the optic axis at the arc position and observing the "halfwidth" of the signal step. The corresponding maximum transition probability errors in this case are also 0.5 percent and 4 percent respectively at the edges of the arc. In all cases the experimental values should be too high. Turbulence, if present in the arc, would lead to similar errors. However, estimates of the Reynolds number for the conditions of these experiments lie well within the laminar flow region suggesting that this should not be a problem. Optical refractivity gradients in the arc are expected to cause a negligible distortion of the arc intensity profile even in the vicinity of strong lines [9]. This expectation was partially confirmed experimentally by the failure to detect a significant displacement of the apparent position of the edge of a tungsten strip lamp filament imaged into the arc plasma at any observing wavelength near the AI 6965 Å line.

Scattering of light by the optical elements and arc chamber windows would cause an increase in the apparent transition probabilities at the higher radii, i.e., at the edges of the luminous arc column. Since a slight variation of this type was indeed observed, several experiments were performed with no window in the arc chamber. These failed to show a significant difference at the arc edges from those in which the window was included in the optical path. Direct rough measurements of the light scattered by the optical elements showed this amount to be less than 0.3 percent of the maximum source intensity, which could not possibly account for the observed radial variation of the A-values.

The shot noise arising from statistical fluctuation in the arrival of photons at the photomultiplier can be estimated from the source intensity and the geometry of the optical train. It is estimated to be always less than 0.5 percent for the strip lamp calibration and less than 0.1 percent for the arc, except at the extreme edges.

For some experiments the limiting aperture of the optical system was reduced to one-half its original size. Any observed difference in the results of these experiments would have pointed out errors and misalinements of the optical system. No such differences were observed, indicating that the optical system was properly alined and that the original aperture was indeed limiting.

The degree of self-absorption can be estimated by calculating the optical depth $\tau = 2\int_0^R \kappa' dr$

where $$\kappa' = \epsilon / B(T)$$

and $$B(T) = 2hc^2\lambda^{-5}(e^{hc/\lambda kT} - 1)^{-1}$$

κ' is the effective absorption coefficient (cm^{-1}), and ϵ is the observed radially resolved emission coefficient per steradian (erg sec^{-1} cm^{-3} sr^{-1} cm^{-1}). The results of such calculations at the centers of the three lines at 4300, 6965, and 4806 Å are respectively 0.002, 0.11, and 0.002 for the optical depths, τ, in the worst cases encountered. Since the Abel inversion is most unstable near the center due to the infinite kernel at that point it is to be expected that the consequences of errors in the side-on intensity measurements due to self-absorption will normally be most severe in the radially inverted values near the center of the arc. This is borne out by exact analytic calculations of simple models and by the approximate Freeman and Katz [10] treatment of more realistic models. These calculations indicate that for small degrees of self-absorption and for bell-shaped profiles the relative error in the radially resolved emission coefficient is of the order of $\kappa_0' R$ at the arc center where κ_0' is the effective absorption coefficient at the center and R is, as before, the nominal arc radius. Thus only in the case of the AI 6965 Å line will self-absorption play a role leading to transition probabilities that are too low by about 5 percent ($\kappa_0' R$ averaged over the line shape) at the arc center and increasing to the correct value at the edge. To some extent this conclusion appears to be supported by the data of figures 11 and 12 which show for the 6965 Å line a more pronounced depression of the transition probabilities at high electron densities near the arc center.

4.5. Analytical and Theoretical

In general, the accuracy of an Abel inversion based on curve fitting techniques is dependent upon the form of the intensity profile of the arc traverse and the fitting function, the number of polynomials used in the fitting function, the number of increments examined during each arc traverse, and the noise present on the intensity profile. To assess the effects of these variables on the accuracy of the inversion, analytical test functions were constructed with varying amounts of superimposed noise drawn from a table of random normal deviates. These test functions, which are of the same general shape as the observed profile of the arc traverse, were then inverted by the machine program used in processing the experimental results. As expected, for data with a relatively high noise level a small number of polynomials in the fitting function produces the

best inversion in terms of accuracy of fit and minimum noise amplification. Conversely, no significant improvement in accuracy results from using large numbers of increments and terms unless the signal/noise ratio of the data is quite high. The accuracy of the inversion is, however, relatively insensitive to variations in number of increments for noise levels greater than 0.3 percent due to the smoothing inherent in the curve fitting process and in this range the relative noise level of the inverted profile is almost identical to that on the original recorded intensity profile.

The results of tests on analytical functions were borne out by further tests of the inversion on actual experimental profiles. The number of data points of representative many-point arc traverses was halved and quartered by systematically discarding alternate data points, and the resulting "thinned" traverses inverted and compared to the originals. These tests also showed that, at least for the data encountered here, no further accuracy could be attained by taking more than 20 or 30 measurements per arc traverse. Similarly, the use of more than 8 or 10 terms in the polynomial expansion was again not warranted and, in fact, increased the noise level in the results.

Numerical tests of the dispersion shape fitting program carried out by superimposing noise upon calculated dispersion shapes reveals that the relative rms noise on the computed line intensity and halfwidth is roughly equal to the relative noise in the input intensity data at the half maximum intensity level. Thus, little smoothing of the noise is accomplished in this step. This is due mainly to the influence of the noise upon the background or continuum level determination by the program. In these experiments this determination was dependent upon a comparatively small effective number of points due to the wavelength point distribution employed.

The use of the area of the fitted dispersion shape as the spectral line intensity obviates the necessity for correcting measured line intensities for that portion of the line lying below and beyond the end points of the wavelength scan. This is a significant correction amounting to 13 percent for scans of only ten halfwidths and may account for part of the difference between the transition probabilities observed here and the lower values of other workers. Since the experimental line shapes even after correction for apparatus functions are not expected to be quite dispersion shapes [9] it was necessary to ascertain the effect of departures from the dispersion shape upon the linewidth, shift, and intensity values as measured in these experiments. For this purpose the dispersion shape fitting program was applied to a theoretical complete asymmetric line shape [21] which appears to be reasonably representative of the experimental line shapes encountered here. The computed intensities and halfwidths were consistently low by 3 percent and 2 percent respectively. The line shifts were consistently overestimated by a magnitude approximately equal to the error in the $\frac{1}{2}$-halfwidth. No attempt was made to calibrate the dispersion shape fitting program for these theoretical line shapes because of the unavailability of sufficiently extensive tables of the necessary line shapes. Consequently, systematic errors can be expected in the results amounting to perhaps 5 percent and probably always in the direction indicated by this example.

At the heart of these measurements is the determination of the electron density by the H_β line shape measurement. Unfortunately a significant uncertainty in the results is associated with this step. For example, Griem [9] estimates that the electron densities obtained from H_β line shapes are probably reliable only to about 5 percent based upon an analysis of the theoretical approximations. In addition, as indicated in figure 4, some error is involved in the fitting of a theoretical line shape to the experimental data. Typically the rms deviation of the experimental points from the fitted curve is 2 or 3 percent of the maximum H_β intensity. (This is somewhat better than the dispersion shape fitting to the argon lines which typically has an rms deviation of 3 to 5 percent. However, in part this greater error is explained by the influence of the apparatus or slit function which is not taken into account in the fitting and by the approximation of the true theoretical shapes by the dispersion shape.) The subtraction of the pure argon spectrum from the argon + hydrogen spectrum removes the major part of any uncertainties in the H_β shape measurement due to irregularities in the argon continuum underlying the hydrogen line. Any errors in this step due to small changes in the radial temperature profile caused by the addition of the trace of hydrogen are expected to be negligible but presumably are included in this 2 or 3 percent deviation. As a partial check of these H_β measurements in two of the 60 A experiments H_α line shapes were also recorded. From the electron density, temperature, and hydrogen to argon ratio as determined from the H_β measurements the theoretical intensity and shape of the H_α lines were computed using the Griem, Kolb, and Shen tabulations. Figure 15 shows a comparison of an experimental H_α line shape (after the Abel inversion and subtraction of the pure argon spectrum) with the theoretical shape based upon the H_β measurements at the same radial point. The agreement is seen to be satisfactory in the wings and at the center but the halfwidth of the theoretical shape is 10 percent or so smaller than the experimental one. This difference appears to be in accord both in magnitude and direction with the correction to the theoretical H_α shapes which Griem et al., [14] estimate would accrue by taking into account the improved ion field strength distribution functions of Mozer and Baranger. Thus, in conclusion, it is reasonable to assume that the electron densities obtained in these experiments from the H_β line shapes should not be in error by much more than about 5 percent. This results in 8 and 20 percent uncertainties respectively in the AI and AII transition probabilities.

Griem [22] has discussed in detail the validity of the local thermodynamic equilibrium (L.T.E.) assumption in laboratory plasmas. Using his criteria one finds

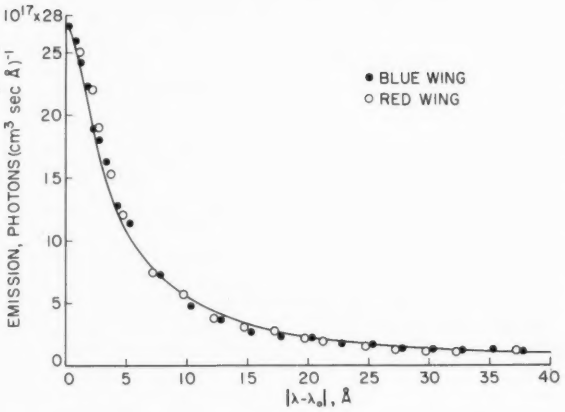

FIGURE 15. *Experimental intensity points in the neighborhood of* H_α *6563 Å after Abel inversion (on axis of 60 ampere arc in argon with* ~ *1%* H_2*) with theoretical* H_α *line shape computed from parameters obtained by* H_β *measurements:* $N_e = 7.35 \times 10^{16}$ *cm*$^{-3}$, $k = 0.0197$.

that for homogeneous plasmas of the dimensions of the arcs of these experiments complete L.T.E. would be probable down to the lowest electron densities actually utilized in the measurements—2×10^{16} for neutral species and 5×10^{16} for ionic species. Again following Griem's treatment one finds that the greatest average distance traveled by any species in the arc between equilibrating collisions is that of the ground state neutrals of the order of 10^{-2} cm at the axis. Thus, the measured electron density and line intensities at a particular point in the arc are not to be interpreted as corresponding exactly to L.T.E. conditions at the local electron temperature at that point but rather as appropriate to some kind of averaging of near-equilibrium distributions which exist over a distance of the order of 10^{-2} cm. The use of this distance, then, permits some estimate of the effects of the temperature and composition gradients present in the arc upon the accuracy of the transition probability determinations. Clearly an over-estimate of the errors is obtained by coupling line intensity measurements at one point with equilibrium calculations based upon electron density measurements 10^{-2} cm away. Such a procedure results in error estimates of 1 percent for the neutral lines and 2 percent for the ionic lines at the center of the 90 A arc. Away from the center this equilibrating collision distance is not a proper measure of the L.T.E. smearing because of the additional equilibrating influences of the diffusion of ions and excited atoms from the hot core and the absorption of resonance radiation from the core. The fact that the measured transition probabilities show no strong dependence upon the electron density, however, suggests that if departures from L.T.E. are not serious at the arc center they are probably also not serious at least out to 0.2 cm where the lowest electron density measurements were taken.

5. Discussion of Results

The estimated transition probability uncertainties resulting from this error analysis assuming the errors are independent are included in table 3 together with transition probability values obtained by other investigators. Most of the errors which have been discussed are systematic. However, a few—the electronic noise, the numerical curve fitting errors, the day-to-day pressure variation, and the dark current drift errors—are not and will tend to be reduced in magnitude by the averaging over the many experiments or radii. In arriving at the uncertainty estimates in table 3 due allowance for this kind of error was taken, where appropriate, by division by the square root of the sample number. A similar calculation applied to the neutral line width and shift measurements gives an estimated 6 percent uncertainty.

The three dominating errors in the average transition probability values determined here are the absolute intensity calibration errors, the systematic errors in the argon line shape fitting due to apparatus functions and asymmetry, and the estimated uncertainty in the hydrogen line broadening theory. It is now possible to reduce the effect of calibration uncertainties from the 3 to 5 percent estimated in these experiments to about 1 to 2 percent, by means of new NBS radiometric calibration services which have become available on a limited basis [24] since these experiments were undertaken. Also, with some effort, the argon line shape fitting can be improved by the calculation and use of more extensive theoretical line shape tables including asymmetry and possibly with apparatus and Doppler broadening properly folded in. Thus the experimental errors can probably be reduced by a factor of two without excessive effort. However, without a concomitant improvement in the accuracy of the electron density determination these experimental improvements would only marginally reduce the estimated overall errors. The uncertainty in this step is the major contribution to the error estimates in table 3. Griem's estimate of the accuracy of the hydrogen line shape calculation is not significantly changed by consideration of the small amount of relatively contradictory experimental evidence [9]. Further experimental or theoretical studies should permit a better assessment of the accuracy of this extremely useful plasma diagnostic technique.

The origin of the apparent decrease of the transition probabilities with increasing electron density (see e.g., fig. 11) is unknown. Of the error sources described above, the only pertinent ones estimated to be of sufficient magnitude to encompass this effect are hydrogen line broadening theory errors, line shape fitting errors, and possibly departures from L.T.E. This deviation from a constant transition probability agrees qualitatively with the discrepancies observed by Wiese et al. [25] in pure hydrogen arcs.

The scatter of the transition probability values (figs. 4 to 13) is in agreement with the noise level estimates described above. These were mainly electronic and

amounted to 1 or 2 percent of the maximum signals. When expressed in terms of the half-intensity of a line this relative noise level is higher by a factor of two or more, and, consequently, since neither the Abel inversion nor the dispersion line fitting seems to modify the noise level, the line intensities should exhibit a scatter of several percent. When combined with a similar noise in the electron density values,a resultant scatter of the transition probability values of the order of 5 to 10 percent is to be expected.

The theoretical transition probabilities of Garstang [23], the "hook" method values of Pery-Thorne and Chamberlain [1], and the arc measurements of Drawin [4] appear to agree generally with the present values in the sense that the error ranges assigned by the investigators overlap the present ones. (The theoretical values are good to perhaps a factor of two, Pery-Thorne and Chamberlain estimate an accuracy of 20 to 30 percent for their values, and Drawin assigns error limits ranging from 10 percent for AI 4044 Å to 20 percent for AI 4300 Å.) Drawin's measurements were carried out in an arc containing a hydrogen-argon mixture. However, since his diagnostics were based upon hydrogen line intensity measurements and the use of the cold gas composition there is a possibility of a systematic error due to demixing.

Gericke's argon transition probabilities [3] are based upon an argon arc temperature profile derived from measurements of the AII 4348 Å line intensity using a transition probability value of 68×10^6 sec^{-1}. The value obtained in the present work for this transition probability is 240×10^6 sec^{-1}. If this is correct then Gericke's transition probability values should be increased by about 35 percent[3] and would agree well with the present values. These same comments apply to Richter's value for the AI 4044 A line (27) which was evidently obtained similarly. The corresponding adjustments to Gericke's electron density values result, in the case of the AI 4300 Å line, in values (in Å) for the $\frac{1}{2}$-halfwidth and shift both approximated by $0.12 \times 10^{-16}[N_e]$ where N_e is the number of electrons per cm^3. This compares reasonably well with the present values (table 1) of $0.10 \times 10^{-16}[N_e]$. Thus the measurements reported here are evidently well in accord with Gericke's on a relative basis but the absolute results differ through the use of the H_β line shape for the arc diagnostics rather than the AII 4348 Å transition probability used by Gericke.

In the case of Olsen's results an estimate of the degree of self-absorption at the center of the AII 4806 Å line[4] under his arc conditions leads to values for the optical depth, τ, of 0.7 or 0.3 depending upon whether the line halfwidth is estimated from Griem's theoretical calculations [9] or is extrapolated from the experimental data of figure 9. In either case the magnitude is sufficient to cause a serious error in the radially resolved emission coefficient and to raise doubts about whether Olsen's observed apparent off-axis maximum was not in fact a consequence of this absorption rather than a manifestation of the Larenz and Bartels [28] "normal" temperature effect. In this event Olsen's temperature determinations and transition probabilities are open to radical reinterpretation.

Table 1 compares the measured values of the line widths and shifts (averaged assuming they are proportional to the electron density) with theoretical values computed from Griem's tables [9] for a temperature of 12 000 °K. Fortunately the theoretical values of the reduced widths and shifts are not strongly temperature dependent so that the difference between 12 000° and whatever effective temperature is introduced by the averaging of the experimental values will cause a difference of only a few percent in the tabular entries. For the neutral argon lines the agreement of theory and experiment is roughly within the expected accuracy of 8 percent for the experiments and 20 percent for the theory. The ion line results, however, are in very poor agreement with theory. For the line shift this is understandable since the theoretical Stark shift for the line does not include the plasma polarization blue shift [9] which rough calculations indicate will be larger than the Stark shift. For the width of the AII 4806 Å line errors due to both Doppler broadening and the slit width correction procedure are important but do not appear to be sufficient to resolve the discrepancy between theory and experiment. The consequences of neglecting the Doppler broadening were estimated by folding the Doppler line shape (Gaussian with $\frac{1}{2}$-halfwidth of approximately 0.03 Å) into the apparatus function to give a broadened effective apparatus function. The use of this modified apparatus function (which significantly affects only the narrow ionic line) reduces the widths of figure 9 by approximately 0.005 Å and decreases the proportionality constant in table 1 by about 5 percent. The error in this proportionality constant stemming from the application of the slit width correction procedure to the AII 4806 Å line where the line and apparatus function widths are comparable (line width: 0.08 Å to 0.15 Å: apparatus width: 0.1 Å) is estimated at 10 or 20 percent. This figure is based upon the results of the 150 μ slit width experiment in which the apparatus function was wider than the AI 4300 Å line at all radii. In this case application of the slit width correction procedure to the computer fitted line widths resulted in an average value for $\frac{w}{N_e} \times 10^{16}$ of 0.089 compared to the average 0.100 for all the narrow slit experiments.

[3] This includes a correction discussed by Griem (26) to the ionization potential lowering.

[4] There appears to be an error in the equation for self-absorption in reference 2 (eq (6)). g_0 should probably be replaced by $\frac{1}{2}\pi$.

6. References

[1] A. Pery-Thorne and J. E. Chamberlain. Proc. Phys. Soc. (London) **82,** 133 (1963).
[2] H. N. Olsen. J. Quant. Spectr. Radiative Transfer **3,** 59 (1963).
[3] W. E. Gericke. Z. Astrophysik **53,** 68 (1961).
[4] H. W. Drawin. Z. Physik **146,** 295 (1956).
[5] W. L. Wiese and J. B. Shumaker, Jr., J. Opt. Soc. Am. **51,** 937 (1961).

[6] J. B. Shumaker, Jr., Rev. Sci. Instr. **32,** 65 (1961).
[7] C. R. Yokley and J. B. Shumaker, Jr., Rev. Sci. Instr. **32,** 6 (1961).
[8] D. R. Paquette and W. L. Wiese, Applied Optics **3,** 291 (1964).
[9] H. R. Griem, Plasma Spectroscopy (McGraw-Hill Book Co., New York, N.Y., 1964).
[10] M. P. Freeman and S. Katz, J. Opt. Soc. Am. **50,** 826 (1960).
[11] M. P. Freeman and S. Katz, J. Opt. Soc. Am. **53,** 1172 (1963).
[12] A. Erdélyi, Higher Transcendental Functions, Vol. **2** (McGraw-Hill Book Co., New York, N.Y., 1953).
[13] S. I. Herlitz, Arkiv för Fysik. **23,** 571 (1963).
[14] H. R. Griem, A. C. Kolb, and K. Y. Shen, Astrophys. J. **135,** 272 (1962).
[15] H. R. Griem, Astrophys. J. **136,** 422 (1962).
[16] J. B. Shumaker, Jr., and W. L. Wiese, Temperature—Its Measurement and Control in Science and Industry, Vol. **3,** Pt. 1, pp. 575–579, (Reinhold Pub. Corp., New York, N.Y., 1962).
[17] K. S. Drellishak, C. F. Knopp, and A. B. Cambel, Arnold Engineering Development Center Tech. Documentary Report AEDC-TDR-63-146 (1962).
[18] H. R. Griem, Phys. Rev. **128,** 997 (1962).
[19] C. R. Yokley and J. B. Shumaker, Rev. Sci., Instr. **34,** 551 (1963).
[20] J. C. DeVos, Physica **20,** 690 (1954).
[21] O. Roder and A. Stampa, Z. Physik **178,** 348 (1964).
[22] H. R. Griem, Phys. Rev. **131,** 1170 (1963).
[23] R. H. Garstang, Mon. Not. R. Astr. Soc **114,** 118 (1954).
[23] N.B.S. Tech. News Bull. **49,** 14 (1965).
[25] W. L. Wiese, D. R. Paquette, and J. E. Solarski, Phys. Rev. **129,** 1225 (1963).
[26] H. R. Griem, Phys. Rev. **128,** 515 (1962).
[27] J. Richter, Z. Astrophysik **53,** 262 (1961).
[28] R. W. Larenz and H. Bartels, Naturwiss. **37,** 164 (1950).

(Paper 69A6–370)

JOURNAL OF RESEARCH of the National Bureau of Standards—A. Physics and Chemistry
Vol. 69A, No. 6, November–December 1965

Theoretical Interpretation of the Third Spectrum of Gold (Au III)*

Y. Shadmi[1]

(July 23, 1965)

The levels belonging to the configurations $5d^9+5d^86s$ and $5d^86p$ of Au III were calculated and compared with experiment with an rms error of about 260 cm^{-1}. By using semiempirical methods and theoretical calculations it is shown that these configurations are best described by use of the j–j coupling scheme.

Key Words: Analysis, atomic energy levels, atomic spectra, doubly ionized gold, j–j coupling, theoretical

1. Introduction

In a paper by L. Iglesias [1][2] an analysis of the spectrum of Au III is reported. Seventeen even levels are reported, belonging to the configurations $5d^9$ and $5d^86s$. The baricenter of the configuration d^8s is about 40000 cm^{-1} higher than the baricenter of d^9. Only the highest level of d^8s was not observed. Forty-three odd levels reported in reference [1] belong to the configuration $5d^86p$. Two of these levels are doubtful. For the d^8p configuration, the theory predicts 45 levels. In reference [1] the even levels are grouped into terms. The assignments given to the odd levels are tentative. Only their total J is really known.

The use of L–S coupling assignments for the even levels of Au III seemed to us rather problematical for the following reasons: (1) The spread of some terms is of the order of magnitude of 10000 cm^{-1}, (2) many terms overlap, (3) from the distance between the two levels of d^9, which are practically unperturbed, one sees that the spin-orbit interaction parameter ζ_d is larger than 5000 cm^{-1}. This is much larger than the approximate values of the electrostatic parameters as estimated from previous calculations [2] on Pt II, while the necessary presumption for L–S coupling is that the electrostatic interaction is considerably stronger than the spin-orbit interaction.

Because of this situation we thought it worthwhile to try to interpret the levels of Au III by use of the j–j coupling scheme. In this scheme it is assumed that the spin-orbit interaction is much stronger than the electrostatic interaction. Thus for every electron its orbital angular momentum is first coupled with its spin. We designate by small j the total angular momentum of an individual electron, which is a good quantum number in this scheme.

In d^9 only two states occur, which differ by their total J. Hence all the coupling schemes are equivalent. In d^8s and d^8p we first have to specify the "parent state" generated by the d electrons. Then we add the angular momentum of the outer electron to the total angular momentum J_d of all the d electrons and obtain the total angular momentum J of the state. For d electrons, j may be either 3/2 or 5/2. Thus the configuration d^8 splits into three fundamental groups:

$$(1)\quad d^4_{3/2}d^4_{5/2}, \qquad (2)\quad d^3_{3/2}d^5_{5/2}, \qquad (3)\quad d^2_{3/2}d^6_{5/2}.$$

The superscript gives the number of d electrons having the given j. Since we are dealing with an almost closed shell of d electrons, it is more convenient to characterize the parent states by counting the number of d-electron "holes" in the two subshells with $j=3/2$ and $j=5/2$. From now on "$d_{3/2}$" and "$d_{5/2}$" will not symbolize electrons but electron holes. The three fundamental groups will be designated:

$$(1)\quad d^2_{5/2}, \qquad (2)\quad d_{3/2}d_{5/2}, \qquad (3)\quad d^2_{3/2}.$$

Since we are dealing with holes, the spin-orbit interaction is negative. Hence the first group is the lowest one, the second group is the intermediate one and the third group is the highest group.

In groups (1) and (3) we have two equivalent holes. Thus, in order to get antisymmetric states J_d can assume only even values. For group (2), J_d can assume any value which is consistent with the triangular condition. Now we have the full list of the parent states. The different states belonging to the same group are distinguished by their values of J_d. The degeneracy of these states is removed by introducing a weak electrostatic interaction. We shall write J_d as a subscript. We get the list of 9 parent states, as follows:

$$(1)\quad (d^2_{5/2})_0, \qquad (d^2_{5/2})_2, \qquad (d^2_{5/2})_4$$

*This paper was partially supported by the National Bureau of Standards, Washington, D.C. and by the A.F.C.S. through the European Office, Aerospace Research, U.S. Air Force.

[1] The Hebrew University of Jerusalem, Jerusalem, Israel.

[2] Figures in brackets indicate the literature references at the end of this paper.

(II) $(d_{3/2}d_{5/2})_1$, $(d_{3/2}d_{5/2})_2$, $(d_{3/2}d_{5/2})_3$, $(d_{3/2}d_{5/2})_4$

(III) $(d^2_{3/2})_0$, $(d^2_{3/2})_2$.

In order to get the states of d^8s, we have to add to J_d the j of the s electron which has the magnitude 1/2. For d^8p, one has to add to J_d the j of the p electron, 1/2 or 3/2.

We shall describe separately the treatment of these two configurations.

The Qualitative Treatment of the Configuration $5d^86s$. First we shall write down the list of j–j states for d^8s. It is sufficient to check which parent-states of d^8 appear for each total J. They are:

$J=1/2$	$J=3/2$	$J=5/2$	$J=7/2$	$J=9/2$
$(d^2_{5/2})_0$ $(d_{3/2}\ d_{5/2})_1$ $(d^2_{3/2})_0$	$(d^2_{5/2})_2$ $(d_{3/2}\ d_{5/2})_1$ $(d_{3/2}\ d_{5/2})_2$ $(d^2_{3/2})_2$	$(d^2_{5/2})_2$ $(d_{3/2}\ d_{5/2})_2$ $(d_{3/2}\ d_{5/2})_3$ $(d^2_{3/2})_2$	$(d^2_{5/2})_4$ $(d_{3/2}\ d_{5/2})_3$ $(d_{3/2}\ d_{5/2})_4$	$(d^2_{5/2})_4$ $(d_{3/2}\ d_{5/2})_4$

In this list we have 7 parents with $J_d \neq 0$ occurring twice and 2 terms belonging to the parents $(d^2_{5/2})_0$ and $(d^2_{3/2})_0$ occurring once.

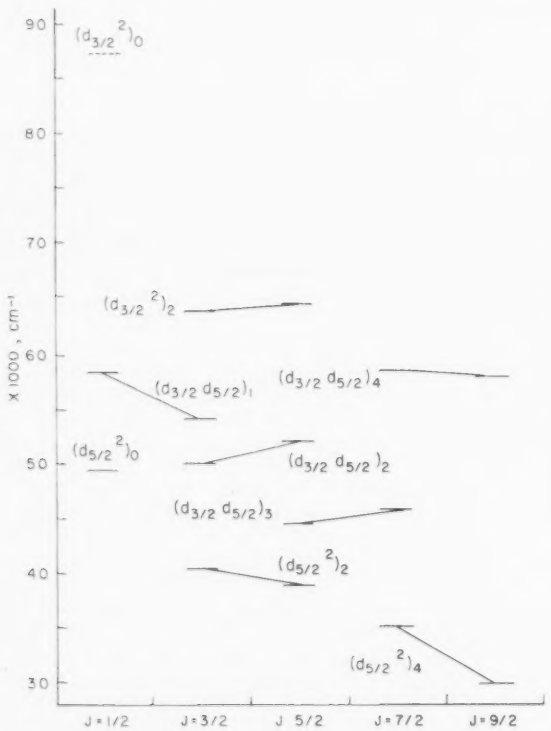

FIGURE 1. *The levels of the configuration* $5d^86s$.

Now we can compare this list with figure 1, where the observed levels of d^8s are represented. For $J=1/2$, 9/2 the situation is very simple, since only one representative (at most) of each of the three fundamental groups of parents (defined earlier) appears in them. Hence, for $J=9/2$ it is obvious that the low-lying level belongs to $(d^2_{5/2})_4$ and the high one to $(d_{3/2}\ d_{5/2})_4$. For $J=1/2$ it is clear that the low lying level is the singlet belonging to $(d^2_{5/2})_0$. The second level having $J=1/2$ belongs to $(d_{3/2}\ d_{5/2})_1$. The level belonging to $(d^2_{3/2})_0$ is the highest level of the configuration and was not observed.

For $J=3/2$, 5/2, 7/2 we always have 2 levels belonging to 2 parent terms which are both members of group II. For example, for $J=5/2$ we know that the lowest level belongs to $(d^2_{5/2})_2$ and the highest one belongs to $(d^2_{3/2})_2$, but we do not know which of the remaining levels belongs to $(d_{3/2}\ d_{5/2})_2$ and which one belongs to $(d_{3/2}\ d_{5/2})_3$. But this difficulty can be easily overcome if we start from the two levels with $J=9/2$ and connect each of them with the nearest level having $J=7/2$. The only remaining level with $J=7/2$ obviously belongs to the parent $(d_{3/2}\ d_{5/2})_3$, which is not represented in $J=9/2$. Now we can proceed from $J=7/2$ to $J=5/2$, and so on. By this way the j–j coupling classification can be very easily and uniquely completed. Only on the passage from $J=5/2$ to $J=3/2$ are there two levels with $J=3/2$ which apparently could be connected with the level belonging to $(d_{3/2}\ d_{5/2})_2$. However, only the highest of these two levels can be connected to the level with $J=1/2$ belonging to $(d_{3/2}\ d_{5/2})_1$. Thus, the uniqueness of the classification is preserved.

The classification could also be done by calculating the diagonal elements of a weak electrostatic interaction as a function of J_d, but in this section we wanted to show that such a classification can be performed without any theoretical calculation.

Several problems remain open. First of all, we did not *prove* the assumption that the actual states of Au III are j–j states, but we showed that this assumption leads to a reasonable interpretation. Next, even if the j–j coupling scheme is the best one, one can hardly expect pure states, so that it is interesting to have information on mixtures of states. It is also very interesting to check whether the empirical grouping of levels (in reference [1] and in the present section as well) is consistent with the theoretical assignments which one can get by diagonalization of the complete Hamiltonian including the spin orbit interaction and the electrostatic interaction as well.

To answer all these questions a quantitative treatment of the spectrum of Au III is necessary.

2. Notations and Definitions

Before we start to describe the quantitative treatment we shall give short definitions of the parameters used in the calculations.

The parameter A is an additive constant common to all the levels of a configuration.

The parameters B and C are linear combinations of Slater integrals: $B = F_2(d^2) - 5F_4(d^2)$, and $C = 35F_4(d^2)$. The parameter $G = G_2(ds)$ measures the exchange interaction between d and s electrons. The quantity $H = (1/35)R^2(dd, ds)$ is the parameter of the interaction of the configuration d^8s with the configuration d^9. The term α is the parameter of the $L(L+1)$ correction. The term ζ_d is the parameter of the spin-orbit interaction of a d electron-hole. The configurations $d^9 + d^8s$ were calculated together and their parameters are given in table 1. In order to distinguish between parameters which appear in both configurations we use the symbols A and ζ_d for d^9 and the symbols A′ and ζ_d' for d^8s.

For the configuration d^8p we use also the electrostatic parameters A, B, C. In addition we need three parameters to describe the interaction between d and p electrons: $F_2 = F_2(dp)$ describes the direct interaction between them, while $G_1 = G_1(dp)$ and $G_3 = G_3(dp)$ describe their exchange interaction. In addition to ζ_d we use also ζ_p, which is the parameter of spin-orbit interaction of the p electron.

"Diag." is an abbreviation for "diagonalization" and "L.S." is an abbreviation for "least-squares calculation."

The quantitative treatment of the configurations ($d^9 + d^8s$). We estimated starting values for the parameters in the first diagonalization in the following way. From a preliminary calculation on the isoelectronic spectrum of Pt II [2] we took the values of B, C and G. Vaules for H and α were taken from a general treatment of the first spectra of the Pt group [3], which was then in progress. ζ_d, A and A′ were estimated from the experimental levels of Au III, and ζ_d' was set equal to ζ_d. All these parameters are given in table 1 under the column "Diag. 1." In the following least-squares calculation (L.S. 1) we got an rms error of ± 276 cm^{-1}. The parameters C and G changed rather strongly. For α we got the value -1 ± 33; also the uncertainty of H is bigger than its value.

In the following diagonalization (Diag. 2) we used for the parameters the values obtained in L.S. 1. The parameter α was given the value zero. Diag. 2 was followed by two least-squares calculations. In L.S. 2a all the parameters are free and we got an rms error of ± 298. For H and α we got the values -120 ± 907 and -10 ± 47, respectively. Both are meaningless and equal to zero within their statistical errors. In L.S. 2b, α was forced to be equal to zero. The rms error reduced to ± 281 cm^{-1}, but H remained meaningless and equal to zero within its uncertainty. This means that the interaction between the configurations d^9 and d^8s is very weak.

In the third diagonalization (Diag. 3) the parameters of L.S. 2b were used; both H and α were given the value zero. In the following least-squares (L.S. 3) α and H were forced to remain equal to zero and we got an rms error of ± 266 cm^{-1}. The values of all the parameters of L.S. 3 are equal to their values in Diag. 3. This indicates that convergence of the mathematical process was reached. Thus, the calculated levels of L.S. 3 are the best theoretical predictions, within the approximation we use. The parameters of the various stages of the calculation are given in table 1.

The elements of the energy matrices are usually calculated in the L–S coupling scheme. Thus the process of diagonalization gives us directly the eigenvectors in this scheme. They are simply the rows of the diagonalizing orthogonal matrix. The j–j coupling eigenvectors are calculated in the following way. Let us denote by H_1 the energy matrix in the L–S coupling scheme and by H_2 the energy matrix in the j–j coupling scheme. E is the diagonalized energy matrix. We define three orthogonal matrixes Ω_1, Ω_2 and T by the following equations:

$$\Omega_1 H_1 \tilde{\Omega}_1 = E, \tag{1a}$$

$$\Omega_2 H_2 \tilde{\Omega}_2 = E, \tag{1b}$$

$$T H_1 \tilde{T} = H_2. \tag{1c}$$

Of course, the rows of Ω_1 are the L–S coupling eigenvectors, the rows of Ω_2 are the j–j coupling eigenvectors, and T is the transformation matrix from the L–S scheme to the j–j scheme. It is not necessary to calculate H_2 and diagonalize it in order to obtain Ω_2.

TABLE 1. *Parameters of the configurations* $d^9 + d^8s$ *in the various stages of the calculation*

	Diag. 1	L.S. 1	Diag. 2	L.S. 2a	L.S. 2b	Diag. 3	L.S. 3
A	6000	5063 ± 460	5063	4917 ± 594	5002 ± 411	5000	5002 ± 380
A′ − A	44000	44762 ± 602	44762	45039 ± 824	44900 ± 458	44900	44899 ± 407
B	540	596 ± 35	596	597 ± 42	605 ± 16	605	605 ± 13
C	2700	3782 ± 309	3782	3794 ± 423	3711 ± 138	3710	3711 ± 106
G	3200	2802 ± 112	2800	2815 ± 119	2812 ± 111	2810	2812 ± 105
H	500	253 ± 322	270	−120 ± 907	46 ± 415	0	.....
α	30	−1 ± 33	0	−10 ± 47	.....	0	.....
ζ_d	5300	5068 ± 176	5068	5050 ± 196	5068 ± 166	5070	5068 ± 157
ζ_d'	5300	5426 ± 62	5426	5395 ± 72	5402 ± 62	5400	5401 ± 59
Δ	.....	± 276	.....	± 298	± 281	.....	± 266

Δ designates the rms error in the calculated levels.

Instead, we use the relation

$$\underline{\Omega_2 = \Omega_1 \cdot \tilde{T}.} \qquad (2)$$

The matrix T is calculated by performing diagonalization with fictitious parameters in which ζ_d is given a very large value. B is given a very small value and all other parameters are equal to zero. In this case the diagonalized energy matrix is in the j–j scheme, so that the diagonalizing matrix is equal to T. It is necessary to give B a nonzero value in order to remove the degeneracy between states which differ only by their values of J_d.

The computer program which we use for the abovementioned calculations is described in a paper by G. Racah [4].

The results of our calculations on the configurations $5d^9 + 5d^8 6s$ are given in table 2. The levels are grouped according to their j–j classification. This arrangement practically avoids overlapping. In addition to the j–j percentage composition the square of the largest component of the L–S eigenvector is also given. For d^9 both couplings are equivalent.

TABLE 2. *Observed and calculated levels of the configurations* $5d^9 + 5d^8 6s$

Conf.	j–j Coupling Assignment	J	L–S coupling largest component	Observed	Calculated	O–C
d^9	100% $d_{5/2}$	5/2	100% ^{2}D	0.0	0	0
d^9	100% $d_{3/2}$	3/2	100% ^{2}D	12694.0	12694	0
d^8s	93% $(d^2_{5/2})_0 s_{1/2}$	9/2	96% (^{3}F)^{4}F	29753.6	30240	−486
	83% $(d^2_{5/2})_0 s_{1/2}$	7/2	58% (^{3}F)^{4}F	35076.7	34906	171
d^8s	93% $(d^2_{5/2})_2 s_{1/2}$	5/2	45% (^{3}P)^{4}P	38822.2	38781	41
	85% $(d^2_{5/2})_2 s_{1/2}$	3/2	45% (^{1}D)^{2}D	40345.6	40307	39
d^8s	76% $(d_{3/2}d_{5/2})_2 s_{1/2}$	5/2	72% (^{3}F)^{4}F	44425.9	44461	−35
	87% $(d_{3/2}d_{5/2})_2 s_{1/2}$	7/2	56% (^{3}F)^{2}F	45740.5	45524	217
d^8s	63% $(d^2_{3/2})_0 s_{1/2}$	1/2	87% (^{3}P)^{4}P	49438.9	49233	205
d^8s	[47% $(d_{3/2}d_{5/2})_2$ + 39% $(d_{3/2}d_{5/2})_2]s_{1/2}$	3/2	64% (^{3}P)^{4}P	49969.4	49779	190
	81% $(d_{3/2}d_{5/2})_2 s_{1/2}$	5/2	50% (^{3}F)^{2}F	52059.6	51723	336
d^8s	[57% $(d_{3/2}d_{5/2})_2$ + 18% $(d_{3/2}d_{5/2})_2]s_{1/2}$	3/2	49% (^{3}P)^{2}P	54133.2	54388	−254
	81% $(d_{3/2}d_{5/2})_2 s_{1/2}$	1/2	81% (^{3}P)^{2}P	58327.1	58523	−196
d^8s	93% $(d_{3/2}d_{5/2})_4 s_{1/2}$	9/2	96% (^{1}G)^{2}G	57818.6	58026	−207
	96% $(d_{3/2}d_{5/2})_4 s_{1/2}$	7/2	93% (^{1}G)^{2}G	58584.6	58407	178
d^8s	72% $(d^2_{3/2})_2 s_{1/2}$	3/2	50% (^{1}D)^{2}D	63670.9	63837	−166
	93% $(d^2_{5/2})_2 s_{1/2}$	5/2	45% (^{1}D)^{2}D	64244.0	64286	−42
d^8s	79% $(d^2_{3/2})_0 s_{1/2}$	1/2	84% (^{1}S)^{2}S		87357	

For the 16 levels of d^8s the situation is as follows: In the j–j scheme 15 levels have a definite assignment, while only 10 have an assignment in L–S scheme. Also, the j–j purities generally are much better.

In table 3 we arrange the observed levels of d^8s in L–S terms. First we give the arrangement deduced in reference [1]. Then in the two columns under theory, we arrange the observed levels according to the largest of the calculated L–S components. Comparison with table 2 clearly shows the superiority of the j–j coupling arrangement. We can conclude that the theoretical calculations on the configuration $5d^8 6s$ justify the qualitative treatment, by showing that the j–j coupling scheme has more physical significance.

The Quantitative treatment of the configuration 5d^{8}6p. This configuration is more complicated than the even configurations. Hence we preferred the

TABLE 3. L–S *coupling arrangement of the levels of* 5d^{8}6s

Term	J	Published analysis ref. [1]	Theory	
			Purity	Level (observed)
			%	
(^{3}F)^{4}F	9/2	29753.6	96	29753.6
	7/2	35076.7	58	35076.7
	5/2	38822.2	72	44425.9
	3/2	40345.6	33	*40345.6
(^{3}P)^{4}P	5/2	44425.9	45	38822.2
	3/2	49969.4	64	49969.4
	1/2	49438.9	87	49438.9
(^{3}F)^{2}F	7/2	45740.5	56	45740.5
	5/2	52059.6	50	52059.6
(^{3}P)^{2}P	3/2	63670.9	49	54133.2
	1/2	58327.1	81	58327.1
(^{1}G)^{2}G	9/2	57818.6	96	57818.6
	7/2	58584.6	93	58584.6
(^{1}D)^{2}D	3/2	54133.2	50	63670.9
	5/2	64244.0	45	64244.0
(^{1}S)^{2}S	1/2	.....	84	.....

*45 percent of the state belonging to this level is $^2D_{3/2}$

theoretical treatment from the beginning. Starting values for B, C, α, and ζ_d were taken from the treatment of d^8s. Values for $F_2 = F_2(dp)$, $G_1 = G_1(dp)$, $G_3 = G_3(dp)$ and ζ_p were estimated from the configuration $5d^8 6p$ of Hg III. The first diagonalization was followed by three least-squares calculations which we call "L.S. 1a," "L.S. 1b," and "L.S. 1c." In these three calculations the parameters B, C, α, ζ_d, which we believed to be known rather well, were "fixed" i.e., forced not to change their values. In L.S. 1a, 40 observed levels were fitted with the calculated levels. This was done by grouping together all the levels with the same total J, and then by arranging them according to increasing value and finally by fitting them with the calculated levels according to this arrangement. No attention was given to the assignments of the observed levels. In L.S. 1a we did not include 3 levels. For $J = 1/2$ there are two levels with values 113749.9 cm^{-1} and 113764.9 cm^{-1}. They are designated in reference [1] as $18^\circ_{1/2}$ and $19^\circ_{1/2}$, respectively. We could fit only one of them, and arbitrarily chose the first one. Also we did not include the two levels designated as $33^\circ_{1/2}$ and $36^\circ_{1/2}$ which are reported in reference [1] as doubtful. The rms error of L.S. 1a is ± 2592 cm^{-1}. This is a very bad result, and we tried to improve it in L.S. 1b. For this purpose three more levels were excluded from the calculation and some assignments were changed. However, the rms error was only reduced to ± 1723 cm^{-1}, which is still very bad. The additional levels discarded in L.S. 1b are $23^\circ_{7/2}$, $42^\circ_{5/2}$, and $43^\circ_{5/2}$. In L.S. 1c we also discarded the levels $5^\circ_{1/2}$ and $34^\circ_{3/2}$. On the other hand it was possible to add the level $43^\circ_{5/2}$. Thirty-six observed levels were included in L.S. 1c which gave an rms error of ± 568 cm^{-1}.

For further improvement of the calculation better derivatives are necessary. Thus, we performed a second diagonalization (Diag. 2) with the parameters of L.S. 1c. The derivatives of Diag. 2 were used for 2 least-squares calculations: L.S. 2a. and L.S. 2b. In both calculations all the 36 levels of L.S. 1c were

TABLE 4. *Parameters of the various stages of calculation of the configuration* $5d^86p$

	Diag. 1	L.S. 1a	L.S. 1b	L.S. 1c	Diag. 2	L.S. 2a	L.S. 2b	Diag. 3	L.S. 3a	L.S. 3b
A	114000	111236 ± 825	111338 ± 552	112155 ± 195	112000	112113 ± 197	111786 ± 211	111786	111819 ± 200	111703 ± 149
B	620	Fixed	Fixed	Fixed	620	539 ± 21	597 ± 28	600	596 ± 28	587 ± 20
C	3850	Fixed	Fixed	Fixed	3850	3673 ± 162	3225 ± 215	3225	3247 ± 203	3373 ± 146
α	0	Fixed	Fixed	Fixed	0	Fixed	68 ± 24	68	62 ± 2ₑ	60 ± 17
F_2	550	503 ± 105	624 ± 70	518 ± 24	520	521 ± 20	514 ± 18	514	509 ± 18	509 ± 14
G_1	600	637 ± 110	631 ± 74	549 ± 25	550	563 ± 21	565 ± 18	565	561 ± 17	551 ± 12
G_3	50	81 ± 100	114 ± 68	83 ± 22	100	84 ± 19	88 ± 17	88	91 ± 16	99 ± 12
ζ_d	5500	Fixed	Fixed	Fixed	5500	5457 ± 71	5440 ± 64	5440	5430 ± 63	5497 ± 48
ζ_p	7000	8736 ± 923	8519 ± 626	8605 ± 205	8600	8849 ± 170	8789 ± 154	8790	8815 ± 155	8744 ± 126
Δ	–	± 2592	± 1723	± 568	–	± 426	± 381	–	± 373	± 257

Δ designates the rms error in the calculated levels.

included. In L.S. 2a α was forced to remain zero (as it was in d^8s) and the rms error reduced to ± 426 cm^{-1}. In L.S. 2b all the parameters were allowed to change freely and we got an rms error of ± 381 cm^{-1}. A third diagonalization (Diag. 3) was performed with the parameters of L.S. 2b. It was also followed by 2 least-squares calculations: L.S. 3a, and L.S. 3b. In L.S. 3a all the 36 observed levels used in the previous iteration were included. We obtained an rms error of ± 373 cm^{-1}. In L.S. 3b we excluded also the levels $24^{\circ}_{3/2}$ and $8^{\circ}_{11/2}$. The level $20^{\circ}_{7/2}$ was replaced by the level $23^{\circ}_{7/2}$. Theoretically there is room for only one of these levels, and the second one gives a much better fit.

The parameters of the various stages of the calculation are given in table 4. The observed levels and the calculated levels of L.S. 3b are given in table 5. Observed levels enclosed in parentheses were not included in the calculation. In table 6 we summarize the situation of the problem levels. Eleven levels were discarded in various stages of the calculation, but two of them were reintroduced later. Under the column "present situation" we designate by "+" two levels which turned out to be good ones. We designate by "–" six levels which are discarded by theory without any doubt. One of them is also doubtful in reference [1]. Three levels are assigned as doubtful. Two of them (8° and 24°) have large deviations from the corresponding theoretical levels, while the third one (36°) was excluded mainly because the experimental evidence was doubtful.

The components of the eigenvectors in the j–j coupling scheme were calculated by the method described in the previous section. In the diagonalization with fictitious parameters which calculates the transformation matrix T from L–S coupling to j–j coupling scheme we chose $\zeta_d = 100000$, $\zeta_p = 100$, $B = 0.1$ and all other parameters were equal to zero. In table 5, for each level both the j–j coupling assignment and the largest L–S component are given. The levels are grouped according to j–j assignments.

Now we can compare the validity of the two coupling schemes for the configuration $5d^86p$. Out of 45 levels, 39 levels have a j–j component which is at least 50 percent. Only 14 levels have an L–S component which is at least 50 percent. For 41 levels the main j–j component is larger than the main L–S component, for two levels the L–S component is larger, and for two levels both components are equal. Thus, for this configuration the superiority of the j–j coupling scheme is clearly demonstrated. Actually, for most levels the L–S assignments are meaningless.

In table 5 we see that several states are mixed, showing a tendency towards intermediate coupling. Most mixtures are one of the two following types:

(a) $(d^2_{5/2})\ J_d p_{3/2} + (d_{5/2}d_{3/2})\ J'_d p_{1/2}$,
(b) $(d_{3/2}d_{5/2})\ J_d p_{3/2} + (d^2_{3/2})\ J'_d p_{1/2}$.

TABLE 5. *Observed and calculated levels of the configuration* $5d^86p$

j–j coupling assignment	J	L–S coupling largest component	Observed	Calculated	O–C
91% $(d^2_{5/2}) J_d p_{1/2}$	7/2	63% $(^3F)^4D$	88788.5	89052	– 263
94% $(d^2_{5/2}) J_d p_{1/2}$	9/2	36% $(^3F)^2G$	91409.4	91115	295
97% $(d^2_{5/2}) J_d p_{1/2}$	3/2	26% $(^1D)^2D$	95740.0	96012	– 272
87% $(d^2_{5/2}) J_d p_{1/2}$	5/2	26% $(^1D)^2F$	96094.5	96152	– 58
69% $(d_{5/2}d_{3/2}) J_d p_{1/2}$	5/2	45% $(^3F)^4D$	101728.2	101645	84
78% $(d_{5/2}d_{3/2}) J_d p_{1/2}$	7/2	59% $(^3F)^4G$	102320.2	102033	287
95% $(d^2_{5/2}) J_d p_{3/2}$	11/2	95% $(^3F)^4G$	(102993.7)	102069	
94% $(d^2_{5/2}) J_d p_{3/2}$	9/2	66% $(^3F)^4F$	104564.6	104491	74
57% $(d^2_{5/2}) J_d p_{3/2}$ + 20% $(d_{5/2}d_{3/2}) J_d p_{1/2}$	7/2	61% $(^3F)^2F$	105809.1	106088	– 279
52% $(d^2_{5/2}) J_d p_{3/2}$ + 27% $(d_{5/2}d_{3/2}) J_d p_{1/2}$	5/2	44% $(^3F)^4D$	108221.2	108481	– 260
57% $(d^2_{5/2}) J_d p_{1/2}$ + 26% $(d^2_{5/2}) J_d p_{3/2}$	1/2	26% $(^3P)^4D$	104348.3	104637	– 289
61% $(d_{5/2}d_{3/2}) J_d p_{1/2}$	3/2	31% $(^3P)^4D$	106263.1	106508	– 244
50% $(d^2_{5/2}) J_d p_{3/2}$ + 32% $(d_{5/2}d_{3/2}) J_d p_{1/2}$	5/2	29% $(^3P)^4P$	107554.2	107116	437
45% $(d^2_{5/2}) J_d p_{1/2}$ + 20% $(d_{5/2}d_{3/2}) J_d p_{3/2}$	5/2	35% $(^3F)^2F$	122530.3	122423	107
57% $(d^2_{5/2}) J_d p_{1/2}$ + 21% $(d_{5/2}d_{3/2}) J_d p_{3/2}$	3/2	47% $(^3F)^4D$	128250.9	128154	97
58% $(d^2_{5/2}) J_d p_{3/2}$ + 12% $(d^2_{5/2}) J_d p_{1/2}$	3/2	30% $(^3P)^4D$	123179.0	122639	540
67% $(d_{5/2}d_{3/2}) J_d p_{3/2}$	5/2	42% $(^3P)^4D$		125580	
82% $(d_{5/2}d_{3/2}) J_d p_{3/2}$	3/2	40% $(^3P)^4S$	127467.6	127490	– 23
75% $(d_{5/2}d_{3/2}) J_d p_{3/2}$	1/2	48% $(^3P)^4S$	125846.2	125930	– 84
95% $(d_{5/2}d_{3/2}) J_d p_{3/2}$	11/2	95% $(^4G)^2H$	(127467.0?)	127104	
92% $(d_{5/2}d_{3/2}) J_d p_{3/2}$	9/2	82% $(^4G)^2G$	132353.0	132346	7
85% $(d_{5/2}d_{3/2}) J_d p_{3/2}$	7/2	74% $(^4G)^2G$	130978.2	131145	– 167
74% $(d_{5/2}d_{3/2}) J_d p_{3/2}$	5/2	70% $(^4G)^2F$	128512.7	128390	122
88% $(d^2_{3/2}) J_d p_{3/2}$	7/2	48% $(^1D)^2F$		135014	
77% $(d^2_{3/2}) J_d p_{3/2}$	5/2	28% $(^1D)^2D$	134953.0	135392	– 439
86% $(d^2_{3/2}) J_d p_{3/2}$	3/2	26% $(^1D)^2P$		133181	
63% $(d^2_{3/2}) J_d p_{3/2}$	1/2	45% $(^1D)^2P$		137443	
76% $(d^2_{3/2}) J_d p_{1/2}$	1/2	74% $(^1S)^2P$		144606	
79% $(d^2_{3/2}) J_d p_{3/2}$	3/2	80% $(^1S)^2P$		156369	
89% $(d_{3/2}d_{3/2}) J_d p_{3/2}$	1/2	61% $(^3P)^4P$		108293	
53% $(d_{3/2}d_{3/2}) J_d p_{3/2}$ + 23% $(d^2_{3/2}) J_d p_{3/2}$	3/2	35% $(^3P)^2P$	(116892.1)	115987	
88% $(d^2_{5/2}) J_d p_{3/2}$	7/2	44% $(^1D)^2F$	110984.1	111042	– 58
42% $(d^2_{5/2}) J_d p_{3/2}$ + 20% $(d_{5/2}d_{3/2}) J_d p_{3/2}$	5/2	30% $(^3F)^4D$	112879.6	113102	– 223
38% $(d^2_{5/2}) J_d p_{3/2}$ + 22% $(d_{3/2}d_{5/2}) J_d p_{3/2}$	3/2	20% $(^3P)^4P$	109387.6	109071	316
67% $(d^2_{5/2}) J_d p_{3/2}$	1/2	34% $(^1D)^2P$	113749.9	113664	86
74% $(d_{3/2}d_{3/2}) J_d p_{3/2}$	9/2	68% $(^4G)^2H$		115091	
50% $(d_{3/2}d_{3/2}) J_d p_{3/2}$ + 32% $(d_{3/2}d_{5/2}) J_d p_{3/2}$	7/2	42% $(^4G)^2F$	118324.6	118125	200
81% $(d_{3/2}d_{5/2}) J_d p_{3/2}$	9/2	43% $(^3F)^2G$	115724.2	115595	129
60% $(d_{3/2}d_{5/2}) J_d p_{3/2}$	7/2	47% $(^3F)^4F$	116293.8	116220	73
77% $(d_{3/2}d_{5/2}) J_d p_{3/2}$	5/2	29% $(^3F)^4D$	115374.2	115414	– 40
42% $(d_{3/2}d_{5/2}) J_d p_{3/2}$ + 22% $(d^2_{3/2}) J_d p_{3/2}$	3/2	29% $(^1D)^2P$	118561.7	118601	– 39
83% $(d_{3/2}d_{5/2}) J_d p_{3/2}$	7/2	44% $(^3P)^4D$	121826.4	121838	– 11
44% $(d_{3/2}d_{5/2}) J_d p_{3/2}$ + 31% $(d^2_{3/2}) J_d p_{1/2}$	5/2	26% $(^3P)^4P$	120027.3	119922	105
38% $(d_{3/2}d_{5/2}) J_d p_{3/2}$ + 15% $(d^2_{3/2}) J_d p_{1/2}$	3/2	27% $(^3P)^2P$	121943.5	122156	– 213
50% $(d_{3/2}d_{5/2}) J_d p_{3/2}$ + 28% $(d^2_{3/2}) J_d p_{3/2}$	1/2	55% $(^3F)^4D$	122407.0	122333	74

TABLE 6. *The dubious levels in the configuration* $5d^8 6p$

Assignment	J	Level	Excluded	Retained	Present situation
5°	1/2	98559.1	L.S. 1c	.....	−
8°	11/2	102993.7	L.S. 3b	.....	?
19°	1/2	113764.9	L.S. 1a	.....	−
20°	7/2	115339.9	L.S. 3b	.....	−
23°	7/2	116293.8	L.S. 1b	L.S. 3b	+
24°	3/2	116892.1	L.S. 3b	.....	?
33°	9/2	123508.8?	L.S. 1a	.....	−
34°	3/2	125767.9	L.S. 1c	.....	−
36°	11/2	127467.0?	L.S. 1a	.....	?
42°	5/2	133058.9	L.S. 1b	.....	−
43°	5/2	134953.0	L.S. 1b	L.S. 1c	+

In both types the difference between the first component and the second one is that a $d_{3/2}$ is replaced by a $d_{3/2}$ and the $p_{3/2}$ is replaced by a $p_{1/2}$. Now let us compare the energies:

$$\mathrm{E}\,(p_{3/2}) - \mathrm{E}\,(p_{1/2}) = 1.5\,\zeta_p = 13100\ \mathrm{cm}^{-1},$$
$$\mathrm{E}\,(d_{5/2}) - \mathrm{E}\,(d_{3/2}) = 2.5\,\zeta_d = -13750\ \mathrm{cm}^{-1}.$$

We see that energetically both changes cancel each other. In the j–j scheme the diagonal elements corresponding to the two states represented in the mixture are rather close, and the nondiagonal elements which are of the order of magnitude of the electrostatic parameters can strongly mix them. This is an interesting example that for configurations containing nonequivalent electrons (in nonclosed shells) the requirement that all spin-orbit interactions be much larger than the electrostatic interactions is not a sufficient condition for pure j–j coupling. A similar situation was found by Mrs. Z. Goldschmidt [5] for the configuration $4f^2 6p$ in the isoelectronic spectra of Ce II and Pr III.

The author is grateful to Professor G. Racah for his kind interest and most valuable advice.

3. References

[1] L. Iglesias, J. Res. N.B.S **64A** (Phys. and Chem.) No. 5, 481 (1960).
[2] G. Racah, private communication.
[3] Y. Shadmi, to be published.
[4] G. Racah, Bull. Res. Council of Israel **8F**, 1 (1959).
[5] Z. Goldschmidt, private communication.

(Paper 69A6–371)

JOURNAL OF RESEARCH of the National Bureau of Standards—A. Physics and Chemistry
Vol. 69A, No. 6, November–December 1965

Photopolarographic Behavior of Inorganic Depolarizers

R. A. Durst* and J. K. Taylor

(July 21, 1965)

Nickel(II), cobalt(II), and uranium(VI) were studied polarographically to determine the effect of uv-visible irradiation on their reduction characteristics. Photoeffects were observed in all cases. Two mechanisms are proposed for the nickel photokinetic prewave, and the complex photoeffects observed with cobalt and uranium are described. Proposals are made for further studies to clarify and elucidate the photochemical reactions and to apply this technique in the study of the activated states of ions prior to reduction.

Key words: Cobalt(II), depolarizers, nickel(II), photoactivation, photochemical effects, photopolarographic effects, polarographic measurements, radiation effects, uranium (VI).

1. Introduction

Although the effects of uv-visible irradiation on organic compounds have been studied for some time [1],[1] the application of photopolarography to inorganic systems has received little attention. This paper describes some previously unreported phenomena observed during the photopolarographic reduction of nickel(II), cobalt(II), and uranyl ions. The data obtained to date are still mostly qualitative and descriptive with only tentative explanations and interpretations given. The present preliminary work has been concerned primarily with surveying possible systems for future detailed study.

This investigation was stimulated by a research proposal for the study of the activation overpotential of irreversible redox systems presented at the Massachusetts Institute of Technology in February 1962 [2] in which it was proposed to activate certain irreversible couples by irradiation with uv-visible light and determine the magnitude of the activation by the shift in the half-wave potential of the irreversible electrode reaction. It was presumed that a study of this type in which the activation energies are evaluated could lead to an understanding of the structural changes taking place in the course of the electrochemical reaction.

Vlček [3] has suggested that since the activation energy is a direct measure of the energy necessary for the formation of the transition state, by comparing the values of the activation energy with known constants of the particular substance, such as the energies of the spectral transitions, structural changes may be estimated and an insight into the mechanism of the whole reaction can be obtained.

Before the electron transfer process can occur, the electronic states of the depolarizer and of the electrode must be nearly equal and, in addition, the electron is always accepted by the lowest unoccupied (or singly occupied) orbital in the depolarizing particle. However, when there is no low-lying orbital available, electronic rearrangement must take place to create a vacant orbital into which subsequently an electron can be accepted and retained [4]. Since the electron transfer itself is always very rapid, the cause of irreversibility in these cases is that these particles cannot accept or retain the electrons without first undergoing some change in their electronic structure.

In this investigation, an attempt was made to produce these necessary electronic changes by irradiation with high-intensity, uv-visible light. The promotion of the electrons to higher orbitals by the absorption of radiation should make lower lying orbitals available for the electron transfer. This means that the energy requirement for the formation of the transition state and consequently the electron transfer should be reduced by an amount equivalent to the energy of the spectral transition. Similarly, the electrode potential necessary for the electron transfer should be reduced but in a more complex manner since both the transfer coefficient and the heterogeneous rate constant must be considered.

In attempting to apply polarography to this type of study, two serious problems immediately arise. One is obtaining the required resolution in the half-wave potentials of the waves for the reduction of the activated and ground-state ions, and the other is measuring the small photokinetic current produced by the activation. Since photoactivation is basically a very inefficient process, the concentration of activated ions in the vicinity of the electrode will be very low, necessitating an extremely sensitive polarograph. Fortunately, the activated species will be reduced at potentials more anodic than the ground-state ions so that the interference from the much larger concentration of unactivated ions will not be as serious. Furthermore, the steady-state concentration of the activated species will be proportional to the intensity of the radiation although limits in this respect are set by available equipment and the necessity of avoiding heating effects in the solution. In addition, the steady-state con-

* Chemistry Department, Boston College, Chestnut Hill, Mass.

[1] Figures in brackets indicate the literature references at the end of this paper.

centration of the activated ions, and consequently the photokinetic current observed, will depend on the rate of decay or half-life of the activated ions.

From the above discussion, it is expected that the shift of the half-wave potential for an irreversible reduction to more anodic values during irradiation should result in a photokinetic prewave: the degree of anodic shift being dependent on the wavelength (energy) of absorbed radiation and the transfer coefficient, the wave height (photokinetic current) dependent on the concentration of the ground-state ions, radiation intensity, and decay rate of the activated ions. Conversely, no prewave should occur upon irradiation of an inorganic depolarizer which is reversibly reduced under normal conditions.

2. Apparatus

The polarograph used in this study was an electronic-scan, controlled-potential type incorporating several features [5, 6] advantageous in achieving the resolution and sensitivity required to detect and measure the small photokinetic prewave. These features include a derivative mode of operation which permits the separation of the prewave from the main reduction wave, and parallel-T RC filters which remove the charging current oscillations to further increase the resolution of the derivative polarograms. In addition, the use of a three-electrode system consisting of the dropping mercury electrode (DME), an asbestos-fiber saturated calomel electrode (SCE), and a platinum working electrode eliminates the need for iR drop corrections. The peak follower was also used to eliminate oscillations for the recording of maximum current polarograms with an insignificant amount of damping.

The polarographic cell consists of a single-compartment rectangular Corex cell ($5 \times 5 \times 2$ cm) with optically flat surfaces covered by an aluminum foil light shield with circular openings 1 cm in diameter in the center of the front and rear surfaces. An opaque plastic top has openings for the three electrodes and the nitrogen deaeration inlet and outlet tubes. These components are arranged in such a way that only the mercury drop is in the excitation light beam.

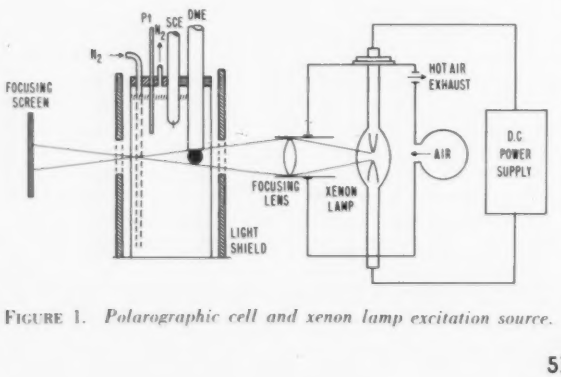

FIGURE 1. *Polarographic cell and xenon lamp excitation source.*

The excitation source is a quartz high-pressure xenon lamp which produces an intense uv-visible continuum in the range from 0.25 to 0.75 microns and is powered by a d-c power supply. The lamp is mounted in a special chamber fitted with a focusing lens and forced-air cooling device (fig. 1). The light from the xenon lamp is focused by positioning the lens so that the light beam is almost completely blocked by the mercury drop at maximum size. This is accomplished by observing the drop image on the focusing screen and adjusting accordingly.

3. Results

3.1. Nickel(II)

The first inorganic depolarizer to be studied by photopolarography was the aquo nickel(II) ion. The reduction of nickel from noncomplexing media is irreversible, as indicated by the half-wave potential being more than 0.5 V more negative than would be predicted from the reversible potential of the Ni^{++}–Ni couple [7]. In order to produce a measurable steady-state concentration of the activated nickel(II), it was necessary to use a relatively high concentration of the nickel salt. Therefore, 0.50 *M* reagent-grade nickel sulfate solutions were used. Since this work was primarily concerned with observing photoeffects and not with quantitative results, no supporting electrolyte was used. Also, inasmuch as the prewave of interest is a kinetic wave rather than a diffusion wave, it is unnecessary to eliminate the migration current. Actually, the migration of nickel ions to the electrode is desirable insofar as enhancement of the photokinetic wave is concerned. In order to avoid any side photoreactions, the use of a maximum suppressor was also omitted. In order to obtain the optimum resolution and sensitivity, derivative polarograms were taken using the 1–2–4–10 filters. The polarograms are shown in figure 2.

Due to the high concentration and sensitivity, the nickel(II) derivative wave begins at about -0.65 V versus SCE, and the half-wave potential occurs at approximately -1.1 V. With irradiation, a photokinetic wave precedes this main nickel reduction wave. The separation is not great enough to allow the prewave to develop fully, but using derivative polarography the half-wave potential is easily obtained. During the continued irradiation, the half-wave potential of the photokinetic prewave shifts between -0.70 and -0.75 V versus SCE in an irregular manner, and the peak current fluctuates between 2 and 6 μA. The heating effect in the solution and especially around the dropping mercury electrode (DME) is small as evidenced by the very small anodic shift of the rising portion of the ground-state nickel wave.

Since the principal absorption band for nickel (II) occurs at 3950 A, the amount of energy absorbed by the $Ni(H_2O)_6^{++}$ ions is equal to 72.2 kcal/mol (energy $= Nhc/\lambda$) or 3.13 electron volts. According to the ligand field theory [8], this corresponds to a *d-d* transition in Ni(II) which has eight 3*d* electrons. In octahedral coordination, as in the case of $Ni(H_2O)_6^{++}$, the ground state electronic configuration of Ni(II) is $^3A_{2g}(t_{2g})^6(e_g)^2$. The absorption of energy at 3950 Å

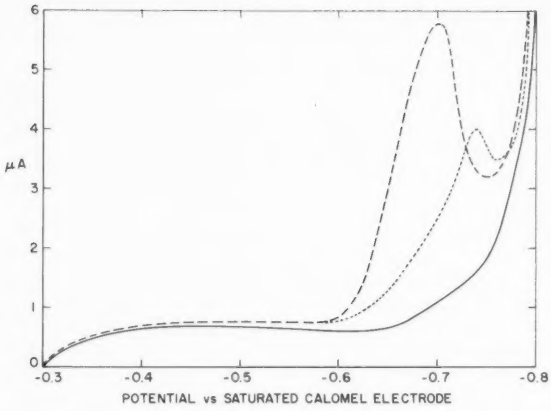

FIGURE 2. *Polarographic reduction waves of nickel(II).*
Solution, 0.50 *M* nickel sulfate; scan rate, 0.1 V/min; derivative mode of operation; 1–2–4–10 filters.
———— No irradiation.
- - - - - - - - With irradiation (anodic extreme).
. . . . . With irradiation (intermediate).

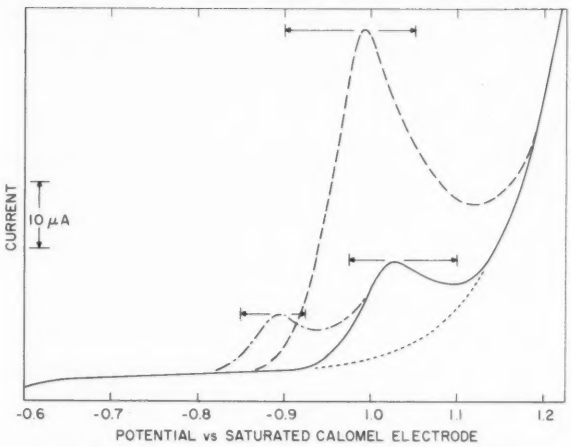

FIGURE 3. *Polarographic reduction waves of cobalt(II).*
Solution, 0.10 *M* cobaltous chloride; scan rate, 0.1 V/min; 1–2–4–10 filters.
. . . . . With or without irradiation, deaerated, pH < 6.5.
———— No irradiation, pH ≥ 7.0, not deaerated (Brdička hydrolysis wave).
- - - - - - - - With irradiation, not deaerated, pH ≥ 6.5.
. . . . . No irradiation, trace of H_2O_2 added.

(25,300 cm^{-1}) corresponds to the transition: $^3A_{2g} \rightarrow {}^3T_{1g}(P)$, or more simply, a transition from the $(t_{2g})^6(e_g)^2$ configuration to the $(t_{2g})^4(e_g)^4$ configuration. Since e_g electrons are antibonding, i.e., their presence tends to weaken and thus lengthen the metal-ligand bonds ($Ni^{++} - H_2O$) while t_{2g} electrons are nonbonding and have little effect on the metal-ligand bond lengths [9], this transition whould result in a weakening of the aquonickel complex. As it is necessary to remove the complexing water molecules during the reduction of nickel to the metal form (zero oxidation state), this weakening of the nickel-water bonds could result in the smaller energy requirement for the reduction as is observed in figure 2.

Another possible explanation of the activation of the Ni(II) as evidenced by its more reversible reduction during irradiation is by the method originally proposed. That is, when electrons are raised to higher energy orbitals (e_g), lower energy orbitals (t_{2g}) are made available for the acceptance of the reducing electrons. Either one or both of these mechanisms could explain the increased reversibility and, for the present, this problem cannot be unequivocally answered.

3.2. Cobalt(II)

Hexaquo cobaltous ions are irreversibly reduced in noncomplexing media at a half-wave potential of about −1.4 V versus SCE. In cobaltous chloride solutions containing no supporting electrolyte, the cobalt is present as the pink $Co(H_2O)_6^{++}$ ion which is reduced at a potential several tenths of a volt more negative than would be predicted from the reversible potential of the $Co^{++} - Co$ couple [10]. To be able to detect any activation effects, the relatively high concentration of 0.10 *M* reagent-grade cobaltous chloride was used in the polarographic solutions. Again, it was unnecessary and undesirable to use a supporting electrolyte and maximum suppressor for the reasons previously stated in the discussion of the Ni(II) reduction.

In figure 3, the preliminary results of the Co(II) study are summarized. Due to the large separation of the prewave from the main reduction wave, it was unnecessary to use the derivative mode of operation of the polarograph to obtain resolution of the waves. The peaks on these waves are, therefore, maxima and not to be confused with derivative peaks which would indicate the half-wave potential. The polarograms were taken using the 1–2–4–10 filters to eliminate drop oscillations and give smooth average current traces. From the figure, it is seen that the Co(II) wave in solutions of pH less than 6.5 begins at about −1.0 V versus SCE at the cobalt concentration and instrument sensitivity used. This is the typical, irreversible reduction wave of $Co(H_2O)_6^{++}$ as would be expected. Upon irradiation, no observable changes are produced in this wave which would indicate either the activation effect does not occur with cobalt or the rate of decay of the activated species is too rapid to allow the buildup of a detectable concentration.

In neutral or slightly basic solutions, however, a prewave does occur at potentials between −1.0 and −1.1 V versus SCE (as indicated by the arrows extending from the peak of the wave). This wave occurs in the absence of irradiation and is most certainly the hydrolysis wave reported by Brdička [11]. The prewave described by Brdička is attributed to reduction of the hydrolysis product of the hexaquo cobaltous ions:

$$[Co(H_2O)_6]^{++} \rightleftharpoons [Co(H_2O)_5OH]^{+} + H^{+}.$$

The hydrolysis equilibrium is established at a rate slow enough for each ion to be reduced at its own potential. The absence of the prewave in acid solution is caused by the suppression of hydrolysis according to the above equilibrium.

With irradiation, a very large prewave occurs in solutions of *p*H equal to or greater than 6.5 at potentials between −0.9 and −1.05 V versus SCE. Although the prewave produced on irradiation generally occurs at potentials about 0.05 V more anodic than the hydrolysis wave, the overlap of potentials is considerable, and one is tempted to interpret the waves as being identical except in their magnitude. Although Brdicka noted that heating increased the size of the hydrolysis wave, the position of the rising portion of the main Co(II) wave is not shifted anodically and thus precludes heating as a significant effect.

For reasons still not understood, prewaves could not be produced, either with or without irradiation, when the solutions were deaerated. Indeed, it appeared that the size of the wave produced with irradiation increased with increasing oxygen concentration. This observation led to the conjecture that the irradiation prewave might be due wholly or in part to the production of hydrogen peroxide by the action of uv radiation on the oxygen and water. This hypothesis was tested by the addition of trace amounts of H_2O_2 to the polarographic solutions. At the lowest concentrations, a wave of the type shown in figure 3 was obtained at potentials of about −0.9 V versus SCE. In general, the hydrogen peroxide wave occurred at potentials more anodic than the irradiation prewave although there was considerable overlap. In addition to the H_2O_2 wave, the hydrolysis wave appeared at potentials between the peroxide and hexaquo Co(II) waves. Since the prewave caused by irradiation arises at potentials between the H_2O_2 and hydrolysis waves, another possible interpretation of the wave produced during irradiation is a merging of these two waves. This seems unlikely, however, since one would expect to see a double-peaked prewave at some point of development during irradiation if this were the case. At higher hydrogen peroxide concentrations, it appears that the Co(II) catalyzes the reduction of H_2O_2 as reported by Strnad [12] and the oxidation of mercury. Moreover, at these concentrations of H_2O_2, there is considerable distortion of the polarogram in the region of the prewaves and of the main Co(II) reduction wave. Since such high hydrogen peroxide concentrations do not arise by irradation, these effects may be disregarded and further discussion of this type of interfering reaction omitted.

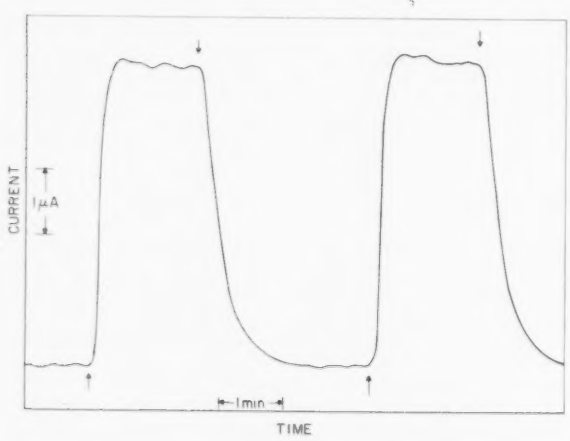

FIGURE 4. *Photoenhancement and decay of the Co(II)* prewave.
Solution, 0.10 *M* cobaltous chloride, *p*H = 6.7, potential at peak of photoinduced wave, half-life of photoactivated species = 12 seconds.
↑ Xenon lamp—ON.
↓ Xenon lamp—OFF.

Although these complicating side reactions prevent the use of Co(II) in the manner originally intended, i.e., in an investigation of changes in the electronic configuration during electrochemical reduction, the very large enchancement of the prewave during irradiation stimulated one additional study. When the potential is set at the peak of the photoinduced prewave and the irradiation applied periodically, the current variations clearly show the production and decay of the photoactivated species. Figure 4 shows a typical current versus time curve for the prewave during alternate periods of irradiation and darkness. The activation process is very rapid, reaching equilibrium in approximately ½ min. The decay of the activated species is considerably slower, being on the order of 1½ min for equilibrium and exhibiting a half-life of about 12 sec. The peak current trace shown in this figure was obtained by connecting the maximum current oscillations of the polarograms recorded without damping or filtering. The current fluctuations during the period of irradiation are probably due to variations in the intensity of the xenon lamp.

Except for the rather interesting occurrences noted above in the reduction of Co(II), the results obtained do not warrant further study of cobalt under the original project. Although solutions of cobaltous chloride show definite photoeffects, these seem not to be of the electronic configuration type desired in this investigation, but rather due to photochemically induced side reactions which complicate the interpretation of the results and thereby prevent the use of cobalt in this type of study.

3.3. Uranium(VI)

The use of the UO_2^{++} ion in a study of photopolarographic behavior is also complicated by side reactions. However, the well-known behavior of uranyl ion as a photosensitizer makes this ion an interesting prospect even though it is reversibly reduced and should not exhibit an activation prewave. The polarographic reduction of uranyl ions may take place in as many as four steps corresponding to reduction to the (V), (IV), (III), and metal amalgam states [13]. However, at all acidities, the reduction corresponding to the first wave is

$$UO_2^{++} + e^- \rightarrow UO_2^{+},$$

although in nearly neutral solutions, the hydrolysis of

the uranyl ion

$$UO_2^{++} + H_2O \rightarrow UO_2OH^+ + H^+$$

causes a decrease in the magnitude of the first wave [14]. The hydrolysis product, UO_2OH^+, is irreversibly reduced at about −0.6 V versus SCE and overlaps the U(V)→U(IV) wave.

A summary of typical results is given in figure 5. The uranyl reduction derivative peak occurs at approximately −0.24 V versus SCE and exhibits a slight maximum (as indicated by the dip in the curve between −0.3 and −0.4 V). During irradiation, there is not the slightest trace of a prewave which is in agreement with what would be expected for a reversible reduction, but a series of "postwaves" do occur. On a normal polarogram, these postwaves would appear as a series of maxima or undulations on the upper part of the wave and on the plateau. Even more curiously, these undulations (except for the first) seem to continuously shift in an anodic direction during continued irradiation. The first peak at −0.28 V is the most prominent and stable of these current fluctuations. Over an irradiation time of more than an hour, this peak shifts less than 10 mV either anodically or cathodically, although its height varies by about 15 μA (fig. 5 shows the maximum height of all the peaks). The second peak (at −0.32 V in fig. 5) has been followed by successive polarograms over a period of an hour and was found to shift 60 mV anodically. It has been difficult to follow the remainder of the peaks from one polarogram to the next since the peak heights vary considerably, and an individual peak usually cannot be unequivocally distinguished on successive polarograms. However, in some cases this was achieved, and these smaller peaks seem to follow the anodic-shift trend.

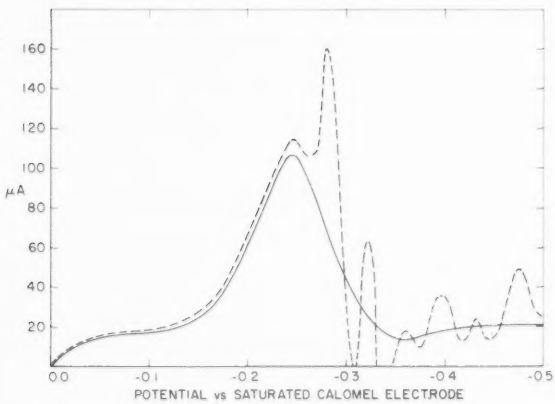

FIGURE 5. *Polarographic reduction waves of* UO_2^{++}.

Solution, 0.020 *M* UO_2SO_4 + 0.1 *M* Na_2SO_4; scan rate, 0.1 V/min; derivative mode of operation: 1–2–4–10 filters.
———— No irradiation.
- - - - - - - - With irradiation.

Although a rigorous interpretation cannot be made at the present time for these fluctuations in the uranyl reduction current, two observations would seem to eliminate hydrolysis as the cause of the observed photoeffect. The first is the fact that the main uranyl peak height does not decrease during irradiation as would be expected if hydrolysis occurred. And second, polarograms recorded to −0.8 V versus SCE do not show any indication of the hydrolysis wave which should occur at −0.6 V. All that is certain at the present time is that a definite photoeffect does occur with the uranyl ion, and an explanation of its cause must await further polarographic studies.

4. Discussion and Future Considerations

Since this study was intended as a preliminary survey of possible systems for further detailed research, many points remain to be clarified and evaluated. For example, the effect of different wavelengths of light on the activation process could provide information on the actual energies required for maximum activation. This would further elucidate the electronic transitions taking place during the electrochemical reduction. Eventually it may be possible to apply mathematical treatments such as those of Koutecky [15] and Koutecky and Brdička [16] for the kinetics of irreversible reductions and reductions involving the generation of the depolarizer in the vicinity of the electrode, and also correlate these with the observed photokinetic currents. In addition, it is presently unknown what effect the irradiation has on the mercury drop itself. Since mercury is a known photosensitizer, the results observed may be due to a transfer of energy from the mercury rather than direct absorption of energy by the ions in solution. Perhaps the spectral studies or studies with other types of electrodes will provide the answers.

Although the use of cobalt(II) and uranium (VI) can be eliminated from consideration in the present investigation due to their complex photoeffects, their study has indicated additional areas in which photopolarography may be applied to induce and analyze different types of photoreactions which have heretofore gone unreported. Certainly phenomena of this type deserve more attention as they may lead to greater understanding of the reactions of simple and complex ions in excited states.

From the reported observations, it appears that the aquo nickel(II) ion is the most likely prospect for further research into the photoactivation of an irreversibly reduced species. The two mechanisms proposed for the apparent increased reversibility of nickel during irradiation gives some indication of the profound changes that may be induced by this technique. Since nickel is but one of the many species which are irreversibly reduced, inorganic photopolarography could have wide application in studying and elucidating these reductions, and it is to be hoped that these initial results will stimulate further research into these phenomena.

5. References

[1] H. Berg and H. Schweiss, Nature **191,** 1270 (1961).
[2] R. A. Durst, Photo-voltammetric studies of the activation overpotential of irreversible systems, Analytical Chemistry Proposition I, M.I.T., Feb. 5, 1962 (unpublished report).
[3] A. A. Vlček, Collection Czechoslov. Chem. Communs. **24,** 3538 (1959).
[4] A. A. Vlček, Disc. Faraday Soc. **26,** 164 (1958).
[5] M. T. Kelley, H. C. Jones, and D. J. Fisher, Anal. Chem. **31,** 1475 (1959).
[6] M. T. Kelley, D. J. Fisher, and H. C. Jones, Anal. Chem. **32,** 1262 (1960).
[7] I. M. Kolthoff and J. J. Lingane, Polarography, **II,** p. 486 (Interscience Publishers, New York, 1952).
[8] C. J. Ballhausen, Introduction to Ligand Field Theory, p. 261 (McGraw-Hill Book Co., New York, N.Y., 1962).
[9] F. A. Cotton, J. Chem. Ed. **41,** 466 (1964).
[10] R. Brdička, Collection Czechoslov. Chem. Communs. **2,** 489 (1930).
[11] Ibid. **3,** 396 (1931).
[12] F. Strnad, Collection Czechoslov. Chem. Communs. **11,** 391 (1939).
[13] I. M. Kolthoff and P. J. Elving, Treatise on Analytical Chemistry, p. 115, P. II, **9,** (Interscience Pub., New York, 1962).
[14] W. E. Harris and I. M. Kolthoff, J. Amer. Chem. Soc. **69,** 446 (1947).
[15] J. Koutecky, Collection Czechoslov. Chem. Communs. **18,** 597 (1953).
[16] J. Koutecky and R. Brdička, Collection Czechoslov. Chem. Communs. **12,** 337 (1947).

(Paper 69A6–372)

JOURNAL OF RESEARCH of the National Bureau of Standards—A. Physics and Chemistry
Vol. 69A, No. 6, November–December 1965

Spectral Structure of Critical Opalescence: Binary Mixture

Raymond D. Mountain*

(June 29, 1965)

The linearized hydrodynamic equations of irreversible thermodynamics are used to obtain the time dependence of the kth Fourier component of a concentration fluctuation in the one-phase region of a binary mixture. The frequency of the light scattered by concentration fluctuations near the critical mixing point is found to be broadened into a Lorentzian distribution with a half-width proportional to the mass diffusion coefficient, D. The possibility of detecting space dispersion in D is discussed.

Key Words: Binary diffusion coefficient, concentration fluctuations, critical opalescence, gas laser, optical hetrodyne system, spectral distribution of scattered light.

1. Introduction

According to the Einstein [1][1]-Smoluchowski [2] theory of light scattering in a fluid, scattering results from fluctuations in the dielectric constant in small volumes of the fluid. Since static inhomogeneities do not exist in fluids, these fluctuations vary in time and this results in a spectrum of frequencies of the scattered light [3].

Critical opalescence refers to the anomalously large amount of scattering which occurs in the vicinity of a critical point [4]. In this paper we are concerned with the spectrum of critical opalescence in the one phase region of a binary mixture. Here the fluctuating quantity is the concentration of one of the components of the mixture [5]. Large fluctuations in the concentration are possible near the critical mixing point because the chemical potentials of the components vary quite slowly with concentration in that region [6].

Although the spectrum of the scattered light is confined to a narrow range of frequencies, it is now possible to investigate the spectrum using a gas laser and an optical heterodyne system [7]. This type of system has been used to examine critical opalescence in a cyclohexane and aniline mixture [8].

2. Formulation of the Problem

We shall determine the time dependence of concentration fluctuations by calculating the decay of a fluctuation in time using the linearized equations of irreversible thermodynamics [9]. For a binary mixture, these are the continuity equation

$$\partial\rho/\partial t+\rho_0 \text{ div } \mathbf{v}=0, \tag{1}$$

the Navier-Stokes equation (only the longitudinal part of $\mathbf{v}$ is included)

$$\rho_0\partial\mathbf{v}/\partial t=-\text{grad } p+\left(\frac{4}{3}\eta_s+\eta_B\right)\text{grad div } \mathbf{v}, \tag{2}$$

the energy transport equation

$$\rho_0 c_p\partial T/\partial t-\rho_0 k_T(\partial\mu/\partial c)_{p,T}\partial c/\partial t + \rho_0 T_0(\partial S/\partial p)_{T,c}\partial p/\partial t=\kappa\nabla^2 T, \tag{3}$$

and the equation of continuity for the concentration

$$\rho_0\partial c/\partial t=\rho_0 D[\nabla^2 c+(k_T/T_0)\nabla^2 T+(k_p/p_0)\nabla^2 p]. \tag{4}$$

In these equations, ρ is the density, T is the temperature, p is the pressure and c is the concentration; equilibrium values are denoted by a subscript zero (ρ_0). Other quantities are the thermal conductivity κ, the shear and bulk viscosities η_s and η_B, the diffusion coefficient D, the thermal diffusion ratio k_T and the barodiffusion ratio k_p. The thermodynamic derivatives involve the entropy S and the chemical potential μ of the mixture. The notation is that of reference 9.

A light scattering experiment provides a Fourier analysis of the fluctuations in the scattering medium. If both the scattering angle and the frequency of the scattered light are measured precisely, both the space and the time variation are Fourier analyzed [3]. Using the hydrodynamic equations, eqs (1 to 4), we can determine the time dependence of the kth Fourier component, $c(k, t)$, of a concentration fluctuation in terms of an initial fluctuation $c(k)$. The intensity of the scattered light is proportional to $\langle c(k, \omega)c(-k)\rangle$ where the $\langle \ldots \rangle$ indicate an equilibrium average over initial ($t=0$) values and

$$c(k, \omega)=2 \text{ Re}\int_0^\infty c(k, t)e^{i\omega t}\,dt. \tag{5}$$

*NAS–NRC postdoctoral Fellow at the National Bureau of Standards.

[1] Figures in brackets indicate the literature references at the end of this paper.

In eq (5) $k = 2k_i \sin \theta/2$ is the *change* in the wave vector which occurs when light with wave vector k_i in the medium is scattered through an angle θ. The *change* in the angular frequency is denoted by ω.

It is a straightforward, if involved, procedure using eqs (1 to 4) to obtain $c(k, t)$ in terms of the initial fluctuation $c(k)$ [10]. As expected, two propagating (phonon) modes and two diffusive modes are obtained. The diffusive modes are a combination of thermal diffusion and mass diffusion. Near the critical mixing point, where c_p is anomalously large and D is small [11], the situation is appreciably simpler. There eqs (3) and (4) may be used to describe the diffusive modes. The pressure terms may be neglected because the pressure is insensitive to the local concentration in the vicinity of the critical point [6].

In the next section, we shall obtain an expression for the spectral structure of critical opalescence using the constant pressure versions of eqs (3) and (4). The results are identical to those obtained using the full set of equations.

3. Calculation

The equations governing the temperature and the concentration are

$$\partial T/\partial t - k_T/c_p(\partial \mu/\partial c)_{P,T}\partial c/\partial t = (\kappa/\rho_0 c_p) \nabla^2 T \tag{6}$$

and

$$\partial c/\partial t = D[\nabla^2 c + (k_T/T_0) \nabla^2 T]. \tag{7}$$

The first step is to obtain the Fourier (space) and Laplace (time) transforms of eqs (6) and (7). The transform of the concentration is

$$c(k, s) = \int_v \int_0^\infty e^{-i\mathbf{k}\cdot\mathbf{r}} e^{-st} c(r, t) d\mathbf{r} dt. \tag{8}$$

Equations (6) and (7) become

$$sT(k, s) - sk_T/c_p(\partial \mu/\partial c)_{P,T} c(k, s) + (\kappa k^2/\rho_0 c_p) T(k, s) = T(k) - k_T/c_p(\partial \mu/\partial c)_{P,T} c(k) \tag{9}$$

and

$$sc(k, s) + Dk^2 c(k, s) + (Dk_T k^2/T_0) T(k, s) = c(k). \tag{10}$$

Neglecting $T(k)$ because $\langle \Delta T \Delta c \rangle = 0$ [12], we obtain

$$\frac{c(k, s)}{c(k)} = \frac{s + \chi k^2 + \xi k^2}{s^2 + sk^2(\chi + D + \xi) + \chi D k^4} \tag{11}$$

where

$$\chi = \kappa/\rho_0 c_p$$

and

$$\xi = (Dk^2/c_p T_0)(\partial \mu/\partial c)_{P,T}.$$

From this it follows that

$$\frac{c(k, t)}{c(k)} = \frac{\frac{1}{2}\mathscr{D} + \frac{1}{2}(\chi - D) + \frac{1}{2}\xi}{\mathscr{D}} \exp\left[-\tfrac{1}{2}(\mathscr{C} - \mathscr{D})k^2 t\right] + \frac{-\frac{1}{2}\mathscr{D} + \frac{1}{2}(\chi - D) + \frac{1}{2}\xi}{\mathscr{D}} \exp\left[-\tfrac{1}{2}(\mathscr{C} + \mathscr{D})k^2 t\right] \tag{12}$$

where

$$\mathscr{D} = [(\chi - D)^2 + 2(\chi + D)\xi + \xi^2]^{1/2}$$

and

$$\mathscr{C} = \chi + D + \xi.$$

Near the critical point both χ and $D (\chi > D)$ are small [11] so that

$$\mathscr{D} \approx \chi - D \tag{13}$$

and eq (12) simplifies to

$$\frac{c(k, t)}{c(k)} = e^{-Dk^2 t} + \varphi(D^2). \tag{14}$$

Equation (14) is based on the reasonable assumption that $(\chi - D)^2$ vanishes more slowly than D^2/c_p. Combining eqs (5) and (14) we find that

$$\langle c(k, \omega) c(-k) \rangle = \langle c(k) c(-k) \rangle \frac{2Dk^2}{(Dk^2)^2 + \omega^2}. \tag{15}$$

An equation equivalent to eq (14) has been derived by Debye [14]. His derivation is based on the assumption that there is no dynamical coupling between the concentration and the temperature. We have shown this to be the case when $D < \chi$ and both quantities are small. Then it is possible to separate the two diffusive modes into one dominated by the thermal diffusity χ and one dominated by the diffusion coefficient D. The mode dominated by the thermal diffusity has effectively zero weight in the sum rule, eq (16), for the intensity of the scattered light.

$$\frac{1}{2}\frac{1}{\pi}\int_{-\infty}^{\infty} \langle c(k, \omega) c(-k) \rangle d\omega = \langle c(k) c(-k) \rangle. \tag{16}$$

(The phonon modes, which we have not explicitly considered, also have zero weight.)

If only the intensity of the scattered light is observed, $\langle c(k) c(-k) \rangle$ is obtained. Near the critical point $\langle c(k) c(-k) \rangle$ is commonly assumed to be of the form $(k^2 + \kappa^2)^{-1}$ where κ^{-1} is the range of the two particle correlation function [13]. Away from the critical point, $\langle c(k) c(-k) \rangle$ is independent of the wave vector and equals the mean square fluctuation in the concentration.

4. Discussion

The spectrum of critical opalescence is that of a Lorentzian distribution with a half width of Dk^2/π cycles/sec. Recent measurements of the spectrum of critical opalescence in a mixture of cyclohexane and aniline are of this type [8]. Measurements of the spectral structure of critical opalescence provide a gradient-free method of determining the diffusion coefficient.

The type of calculation presented above is certainly appropriate when the range of the two particle correlations is small compared to the wavelength of the light which is scattered. Near the critical point, the range of the correlations is on the order of the wavelength of visible light. It is not unreasonable to expect that near the critical point, transport coefficients may reflect the long range of these correlations by becoming k-dependent [15]. This interesting possibility could be checked by seeing whether or not the half width of the Lorentzian distribution varies linearly with k^2. Any deviation from linearity would suggest that the diffusion coefficient D should be replaced by $D(k)$, a k-dependent diffusion coefficient.

(Paper 69A6–373)

5. References and Notes

[1] A. Einstein, Ann. Physik **33,** 1275 (1910).

[2] M. V. Smoluchowski, Ann. Physik **25,** 205 (1908).

[3] L. D. Landau and E. M. Lifshitz, Electrodynamics of Continuous Media ch. 14 (Reading, Mass.: Addison-Wesley Publishing Co., 1960).

[4] P. Debye, J. Chem. Phys. **31,** 680 (1959); B. Chu, J. Chem. Phys. **41,** 226 (1964) and the references contained in this paper.

[5] H. C. Brinkman and J. J. Hermans, J. Chem. Phys. **17,** 574 (1949); John G. Kirkwood and Richard J. Goldberg, J. Chem. Phys. **18,** 54 (1950); W. H. Stockmayer, J. Chem. Phys. **18,** 58, (1950).

[6] J. R. Partington, An Advanced Treatise on Physical Chemistry, Vol. **IV,** pp. 588–591 (New York: Longmans, Green and Co., Inc., 1953).

[7] H. Z. Cummins, N. Knable, and Y. Yeh, Phys. Rev. Letters **12,** 150 (1964).

[8] Y. Yeh, S. S. Alpert, E. Lipworth, L. Seigel, and D. Balzarini, Bull. Am. Phys. Soc. **10,** 310 (1965); S. Alpert, Y. Yeh, and E. Lipworth, Phys. Rev. Letters **14,** 486 (1965).

[9] L. D. Landau and E. M. Lifshitz, Fluid Mechanics, pp. 219–226 (Reading, Mass., Addison-Wesley Publishing Co., 1959).

[10] This program has been carried out by the author.

[11] I. R. Krichevskii, N. E. Khazanova, and Yu. V. Tshkhanskaza, Russ. J. P. Chem. **34,** 598 (1960); G. Jura, D. Fraga, G. Maki, and J. H. Hildebrand, Proc. Natl. Acad. Sci. U.S. **39,** 19 (1953).

[12] L. D. Landau and E. M. Lifshitz, Statistical Physics, p. 362 (Reading, Mass.: Addison-Wesley Publishing Co., 1958).

[13] There is some experimental evidence that this Ornstein-Zernike-Debye result for the correlation function is not applicable very near the critical point. D. McIntyre, A. Wims, and M. S. Green, J. Chem. Phys. **37,** 3019 (1962); B. Chu and W. P. Kao, J. Chem. Phys. **42,** 2608 (1965).

[14] P. Debye, Phys. Rev. Letters **14,** 783 (1965).

[15] Some of the effects of k-dependence have been discussed by Marshall Fixman, J. Chem. Phys. **36,** 310 (1962).

JOURNAL OF RESEARCH of the National Bureau of Standards—A. Physics and Chemistry
Vol. 69A, No. 6, November–December 1965

Irregularities in the NBS (1955) Provisional Temperature Scale

Hans M. Roder

Institute for Materials Research

(August 5, 1965)

This paper presents evidence for small irregularities in the temperature scales employed between 50 and 100 °K. The results are derived from the raw data defining the PVT surface of parahydrogen and are given in terms of temperature adjustments to the NBS (1955) scale. The results suggest that an improvement of the temperature scales presently in use would be desirable.

Key Words: Gas thermometer, international practical temperature scale, NBS (1955) provisional temperature scale, platinum resistance thermometer.

The purpose of this report is to illustrate several irregularities in the NBS (1955) scale for low temperatures and to estimate their values. In addition, the junction of the NBS (1955) scale with the lower end of the International Practical Temperature Scale (IPTS), near 90 °K, is examined for irregular behavior. The NBS (1955) provisional scale for low temperatures is based on a comparison of platinum resistance thermometers with a helium gas thermometer between 14 and 83 °K [1].[1] The scale is used in the U.S. to calibrate precision resistance thermometers between 10 and 90 °K. Irregularities in the scale are known to exist [2]; however, the irregularities are less than ±0.02 °K, the accuracy claimed for the original experiment. The International Practical Temperature Scale (IPTS) [3] is the working scale adopted by international agreement for use at temperatures above 90 °K. Earlier experiments [see, for instance, ref. 4] show how this scale differs between 90 and 300 °K from the Kelvin scale. A good summary of all experiments of this type is given by Stimson [5]. It is interesting to note that recent accurate computations of thermodynamic functions take the difference between the IPTS and the Kelvin scale into account [6].

Low level irregularities in temperature scales become troublesome as the accuracy in experiments improves, especially so if the variable measured is expected to vary continuously (smoothly) with absolute temperature. Recent experimental evidence [2, 6, 7, 8] suggests that this level of experimental accuracy has been reached. Irregularities in heat capacities are attributed to imperfections in the temperature scales employed [9]. These imperfections can also be derived from the PVT surface of a gas, provided that the experimental data are sufficiently accurate, and, further, that the data were taken along lines of constant volume. Given these conditions, each line of constant volume may be treated as an independent gas thermometric experiment where the pressures are obtained as a function of temperature in a closed system, and the assumption is made that for each line of constant volume the values of pressure should vary continuously (smoothly) with absolute temperature.

The results of the present analysis are based on 920 of the 1200 points recently obtained by Goodwin et al., [10] defining the PVT surface of parahydrogen. Table 1 of reference [10] presents the experimental values in terms of lines of nearly constant volume called pseudo-isochores. Each experimental point is considered as an independent determination. Pseudo-isochores at high densities which do not include pressure entries at 50 °K or higher have been omitted from the analysis for reasons to be discussed later. On all other pseudo-isochores the pressure entries below 50 °K were included in the least squares fitting of the analytical representation, but as explained later these pressures could not be utilized in the analysis. The pseudo-isochores are used rather than the partially smoothed data (lines of constant volume, table 2 of reference [10]) because the smoothing may have introduced an additional error, and because it was desired to retain the weighting in density as given by the experiment.

Ideally, the analysis should be performed by treating the temperature as a function of pressure and obtaining the desired temperature adjustments directly. Lack of a suitable analytical representation for $T=f(P)$

[1] The present NBS provisional temperature scale is designated NBS (1955) and is defined to be 0.01 deg lower than the scale given in reference [1], found in the referenced literature at the end of this paper.

787-221 O-65—3

forced us to approach the problem indirectly in the four steps given below:

1. Fit each pseudo-isochore with an appropriate analytical representation:

2. obtain deviations in pressure ($P_{calc} - P_{experimental}$) for each pseudo-isochore at each temperature;

3. convert each deviation in pressure to an equivalent deviation in temperature:

4. seek a consistent pattern of temperature deviations by considering all pseudo-isochores together: i.e., temperature scale shifts which would improve the smoothness of the raw data and cause the deviations in pressure to appear random. (For a given temperature the temperature adjustment was established by averaging the equivalent temperature deviations obtained in step 3 for all pseudo-isochores.)

The analytical representation used in step 1 above is of critical importance to the analysis performed. Many of the pseudo-isochores exhibit inflection points, and a few of these occur at temperatures as high as 50 °K. As many as five different analytical representations might be required to define the PVT surface accurately at lower temperatures [11]. The analysis, therefore, was restricted to temperatures above 50 °K, using the same analytical representation employed recently in a compilation of thermodynamic functions [12]:

$$P_{calc} = AT^2 + BT + C + D/T + E/T^2. \qquad (1)$$

The analysis was also performed by smoothing fourth differences [13], and by a technique which places certain restraints on the derivatives; i.e., a "spline-fit" [14], yielding results essentially identical to the ones presented here.

The total deviation in pressure obtained in step 2 above arises from the following contributions:

E_1 the error made in the actual measurement of pressure;

E_2 the error made in the experimental determination of temperature on the NBS (1955) scale or on the IPTS;

E_3 the irregularities in the temperature scale used—NBS (1955) and the lower end of the IPTS scale;

E_4 the deviation between the Kelvin scale and the scale fashioned by the particular analytical representation used.

In the analysis we attempt to separate the error E_3 from the others. Maximum values for the error E_1 have been estimated by Goodwin [15, table 2]. It is pertinent to use the rms combination of his various uncertainties resulting in the following values: 0.00408 atm at a total pressure of 2 atm, 0.00435 at 20 atm, and 0.00830 at 200 atm. The error E_2 arises from the experimental uncertainty and a certain reproducible error. The uncertainty expresses the ability of the experimenter to maintain a certain desired temperature during data recording and has been estimated to be 0.00025 °K [11]. This uncertainty and the error E_1 are random; combined, they cause the spread in deviations illustrated in figure 1. The reproducible

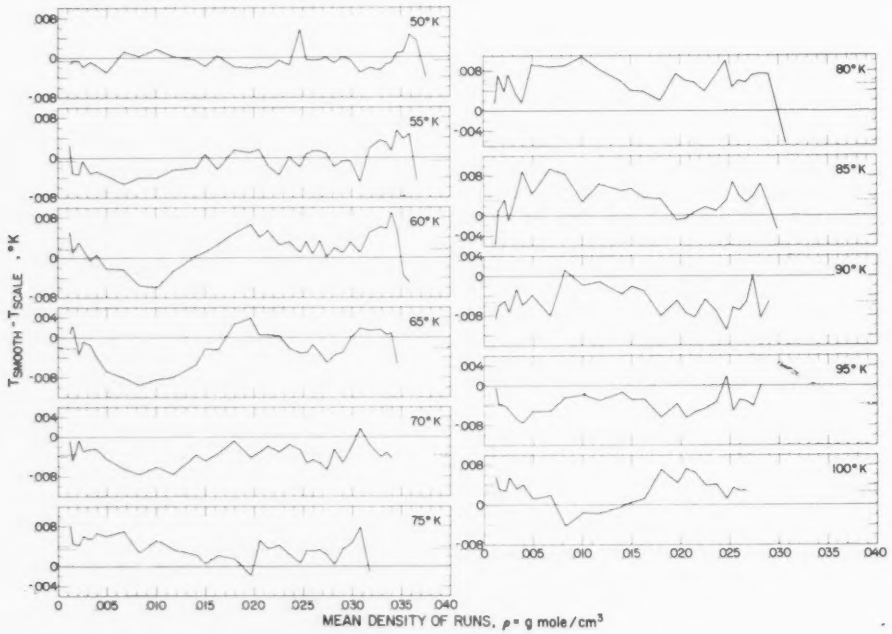

FIGURE 1. *The individual temperature deviations.*

Equivalent temperature deviations of observed pressures from values calculated using equations fitted to the data (pseudo-isochores). Every junction of the broken straight lines represents the deviation of the observed pseudo-isochore at the temperatures indicated. The results from the same pseudo-isochores are found along vertical lines and those from different pseudo-isochores along horizontal lines.

part of the error E_2 assumes a given value for each temperature attained in the experiment. It is based on consideration of the various components of the experiment; certain maximum values have been estimated by Goodwin [15, table 3]. By the nature of this analysis the reproducible part of the error E_2 will be lumped with the error E_3 which we wish to determine. The error E_4 has been included to indicate that a constant or slightly varying "offset" in temperature may exist between the smooth analytical representation used and the assumed ideal, but unknown, function of pressure versus thermodynamic temperature. This error also includes the continuously (smoothly) changing "offset" which may be introduced by using pseudo-isochores rather than the true line of constant volume. Results obtained from the other smoothing techniques indicated previously and from fitting the isochores of table 2 in reference [10] permit an estimate of ± 0.001 °K as the maximum "offset" caused by the error E_4. Any small error made in the assignment of density to a particular pseudo-isochore has been shown to be constant for that pseudo-isochore [10] and will not affect this analysis.

TABLE 1. *Results of the Analysis*

Temperature	Mean temperature adjustment, $T_{scale} - T_{smooth}$	Standard error of the mean temperature adjustment	Number of runs on which columns 2 and 3 are based
°K	°K	°K	
50	0.0006	0.0003	38
55	.0006	.0005	37
60	−.0017	.0006	36
65	.0022	.0006	34
70	.0036	.0004	33
75	−.0035	.0004	30
80	−.0054	.0006	29
85	−.0031	.0007	28
90	.0053	.0006	27
95	.0037	.0004	26
100	−.0026	.0006	24

The results of the analysis are shown in figure 1, where the individual equivalent temperature deviations, $T_{smooth} - T_{scale}$, have been plotted, for each temperature considered, as a function of the mean density of the pseudo-isochores (runs). The results are summarized in table 1, where the temperature adjustments shown are the averages of the equivalent temperature deviations for all pseudo-isochores at a given temperature. These averages or mean values are indicated by dashed lines in the ordinates of figure 1. The standard errors of the mean temperature adjustments are given in column 3 of table 1 and are indicated in figure 2. The mean temperature adjustments are 2 to 9 times larger than the corresponding standard errors except for 55 °K, so that, based on the number of runs in column 4, table 1, these mean adjustments are significantly different from zero. The temperature adjustments are presumed to be a good indication of the irregularities in the temperature scales because

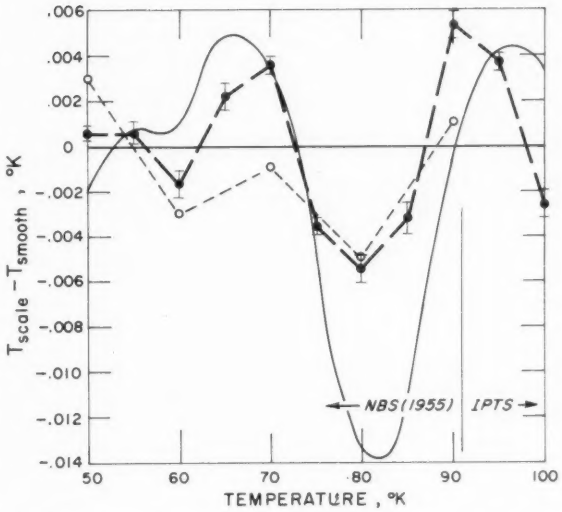

FIGURE 2. *The irregularities of the NBS (1955) scale and the IPTS.*
—•—•— this paper relative to the "smoothed" scale, where I is the standard error of the temperature adjustment—see text.
– – – Barber [2] relative to the average of the four scales considered—see text.
——— Furukawa and Reilly [9] relative to their smoothed scale.

if they are applied to the raw data the absolute sum of the pressure deviations is reduced from 3.27 atm to 2.16 atm. For comparison we have computed the sum of the errors E_1 linearly interpolating between the estimates of error established previously. The sum so obtained is 2.30 atm, in excellent agreement with the value 2.16 atm above.

The temperature adjustments between the NBS (1955) scale or the IPTS and the "smoothed" scale are plotted in figure 2. For ease of comparison the ordinate has been reversed and is now $T_{scale} - T_{smooth}$. The resemblance between the present work and the results of Barber [2] and of Furukawa and Reilly [9] is striking. Barber considered the temperature scales established at the National Physical Laboratory [2], at the National Bureau of Standards [1], at the Pennsylvania State University [16], and at the Physicotechnical, Radio-technical Measurements Institute [17]. He compared these scales on common terms by using a "best" value of the oxygen point on the thermodynamic scale, and by adjusting them to the same virial coefficients and to the same expansion data for copper. The deviation of the NBS scale from the mean of the four scales considered by Barber is also plotted in figure 2. The resemblance to the work of Furukawa and Reilly is perhaps superficial. However, their process permits the establishment of a uniform degree from 20 to 380 °K while keeping the average size of the degree in this interval the same as for NBS (1955)-IPTS.

The results given in this paper illustrate certain irregularities in the temperature scales employed between 50 and 100 °K. They indicate that the NBS (1955) scale is slightly irregular and does not join smoothly to the lower end of the IPTS scale. The adjustments obtained for the lower end of the IPTS scale are qualitatively in agreement with earlier experiments [4] and with the evaluation based on the heat capacity data [9]. Thus, the deviation pattern established from the PVT surface of parahydrogen reinforces earlier work and suggests that an improvement in the temperature scales would be desirable.

The author is indebted to R. J. Corruccini, R. D. Goodwin, L. A. Weber, and B. A. Younglove for many valuable comments and discussions.

References

[1] H. J. Hoge and F. G. Brickwedde, Establishment of a temperature scale for the calibration of thermometers between 14 and 83 °K, J. Res. NBS **22,** 351 (March 1939).

[2] C. R. Barber, The establishment of a practical scale of temperature for the range 10–90 °K, Brit. J. Appl. Phys. **13,** 235 (May 1962).

[3] H. F. Stimson, International practical temperature scale of 1948. Text revision of 1960, J. Res. NBS **65A** (Phys. and Chem.) No. 3, 139 (May 1961).

[4] W. H. Keesom and B. G. Dammers, Comparison of some platinum thermometers with the helium thermometer between 0 and −183 °C, Physica **2,** 1080 (1935).

[5] H. F. Stimson, Heat units and temperature scales for calorimetry, American Journal of Physics **23,** 614 (Dec. 1955).

[6] W. de Graaff, Compressibility isotherms and thermodynamic functions of hydrogen and deuterium. Conclusions regarding the intermolecular field, Thesis, University of Amsterdam, 29 June 1960, page 13.

[7] G. T. Armstrong, Calorimetry, Physics Today **17,** 50 (Feb. 1964).

[8] G. T. Furukawa, M. L. Reilly, and J. H. Piccirelli, Calorimetric properties of some alkali pentaborate hydrates from 15 to 370 °K, J. Res. NBS **68A** (Phys. and Chem.) No. 4, 381 (July 1964).

[9] G. T. Furukawa and M. L. Reilly, Application of precise heat-capacity data to the analysis of the temperature intervals of the NBS (1955) and the International Practical Temperature Scales in the region of 90 °K, J. Res. NBS **69A** (Phys. and Chem.) No. 1, 5 (Jan. 1965).

[10] R. D. Goodwin, D. E. Diller, H. M. Roder, and L. A. Weber, Pressure-density-temperature relations of fluid para-hydrogen from 15 °K to 100 °K at pressures to 350 atmospheres, J. Res. NBS **67A** (Phys. and Chem.) No. 2, 173 (March 1963).

[11] R. D. Goodwin, private communication.

[12] H. M. Roder, L. A. Weber, and R. D. Goodwin, Thermodynamic and related properties of parahydrogen from the triple point to 100 °K at pressures to 340 atm., NBS Monograph 94 (1965).

[13] C. Lanczos, Applied Analysis, pp. 316–320 (Prentice Hall, Englewood Cliffs, N.J., 1956).

[14] F. Landis and E. N. Nielson, The determination of thermodynamic properties by direct differentiation techniques, Progress in International Research on Thermodynamic and Transport Properties, Second Symposium on Thermophysical Properties, pp. 218–227 (Academic Press, New York, N.Y., 1962).

[15] R. D. Goodwin, Apparatus for determination of pressure-density-temperature relations and specific heats of hydrogen to 350 atmospheres at temperatures above 14 °K, J. Res. NBS **65C** (Eng. and Instr.) No. 4, 231 (Oct. 1961).

[16] G. W. Moessen, J. G. Aston, and R. G. Ascah, The Pennsylvania State University thermodynamic temperature scale below 90 °K and the normal boiling points of oxygen and normal hydrogen on the thermodynamic scale, Temperature, Its Measurement and Control in Science and Industry, Vol. **3,** pt 1, p. 91 (Reinhold Publishing Corp., New York, N.Y., 1962).

[17] A. C. Borovick-Romanov, P. G. Strelkov, M. P. Orlova, and D. N. Astrov, The I.M.P.R. temperature scale for the 10 to 90 °K region, Temperature, Its Measurement and Control in Science and Industry, Vol. **3,** pt 1, p. 113 (Reinhold Publishing Corp., New York, N.Y., 1962).

(Paper 69A6–374)

JOURNAL OF RESEARCH of the National Bureau of Standards—A. Physics and Chemistry
Vol. 69A, No. 6, November–December 1965

Isotherms Determined by the National Bureau of Standards Acoustical Thermometer in the Liquid Helium Temperature Range

G. Cataland and H. Plumb

(July 7, 1965)

Isotherms of the speed of sound in helium 4 gas as a function of pressure have been measured. Five of the isotherms in the liquid helium 4 temperature range have been analyzed, and the results are discussed. The acoustically determined values of temperature are consistently higher than the values of temperature associated with the liquid helium 4 vapor pressure scale (T_{58}). The deviations are 0.006 °K at 2.323 °K, 0.007 °K at 2.807 °K, 0.008 °K at 3.211 °K, 0.010 °K at 4.212 °K and 0.012 °K at 5.024 °K.

Key Words: Acoustical thermometer, isotherm at low temperature, Speed of sound in helium gas, thermometry at low temperature.

1. Introduction

A program of absolute and secondary low temperature thermometry has been conducted for some years at the National Bureau of Standards. Certain of the results are in the process of being reported and this paper presents absolute temperature determinations in the lower range of investigation.

Thus far, absolute thermometry at these temperatures has been conducted by employing either a gas thermometer or apparatus designed for P-V isotherm determinations. Each of these methods is subject to inaccuracies which require corrections in order to obtain "the thermodynamic temperature." The corrections are caused by or related to "dead space volumes", deviations of the thermometric fluid from "ideal gas" behavior, conservation of the thermometric fluid during measurements, and volume changes accompanying necessary temperature changes. In some cases the pressure measurements, the requirements of which are far from being trivial, must be modified to allow for thermomolecular effects. To some extent, these corrections have been considered as existing nuisances but not always necessarily crucial in determining the end result, a temperature. While it is not the intention of this paper to treat the preceding corrections, the investigation being reported was initiated with an intention of avoiding them. Additionally we felt that a fundamentally different approach to low temperature thermometry was completely justified and would prove to be beneficial in contributing knowledge about existing temperature determinations and scales.

A salient feature of gas thermometry should be mentioned. The thermometer must be filled with the thermometric gas and the pressure measured at some assumed value of temperature. This assumption is critical and receives careful consideration, naturally, but a cascading of errors from one temperature range to another is possible. This type of error is also avoided in our approach to thermometry.

The method of temperature determinations which we have pursued is based on the speed of sound in helium gas as a function of the gas pressure. Since translational dispersion of speeds in our experiments is negligible, one can proceed from the basic equation $W=\sqrt{E/\rho}$ where W is the speed of sound:

E, the adiabatic bulk (1)

modulus of the medium: and ρ the density. This can be written as

$$W=\sqrt{-\frac{v^2}{M}\left(\frac{\delta p}{\delta v}\right)_S}=\sqrt{-\frac{C_p}{C_v}\frac{v^2}{M}\left(\frac{\delta p}{\delta v}\right)_T}. \tag{2}$$

If the equation of state for helium gas is assumed to be of the form

$$pv=RT\left(1+\frac{B}{v}+\frac{C}{v^2}+\ldots\right) \tag{3}$$

the partial derivative, $\left(\frac{\delta p}{\delta v}\right)_T$, can be substituted into eq (2) and C_p/C_v can be related to an ideal gas with the result

$$W^2=\left(\frac{C_p}{C_v}\right)_{p=0}\frac{R_M T}{M_{\mathrm{He}}}(1+\alpha p+\beta p^2+\ldots). \tag{4}$$

In eq (4), T is the desired temperature:

$\left(\frac{C_p}{C_v}\right)_{p=0} = 5/3$: $R_M = 8.314 \times 10^7$ (erg/°K mol);[1]

$M_{He} = 4.0026$ g/mol [2];[2]

and $\alpha = \frac{1}{RT}\left(2B + \frac{4}{3}T\frac{dB}{dT} + \frac{4}{15}T^2\frac{d^2B}{dT^2}\right)$. B and C are the second and third virial coefficients, respectively, for helium 4 gas. Equation (4) suggests the form

$$W^2 = W_0^2(1 + \alpha p + \beta p^2 + \ldots),$$

$$\text{where } W_0^2 = \left(\frac{C_p}{C_v}\right)_{p=0}\frac{R_M T}{M_{He}} \qquad (5)$$

in which W_0 is the speed of sound in an ideal gas. W and p are measured experimentally and treated so that W_0^2 may be determined. In practice this may be done in two ways. W^2 and p as in eq (5) may be fitted by a least squares method with the intercept W_0^2, at $p = 0$ resulting. Another approach is to obtain W_0 or W_0^2 from a linear extrapolation (either graphically or analytically). The implication is, naturally, that in eq (5) αp is small compared with 1, and terms involving higher orders of pressure negligible. Values of W_0^2 obtained by the methods described afford a simple calculation of the temperature. Obviously, this treatment can produce information on helium 4 virial coefficients, but this will be presented in a following paper.

The experimentally determined quantity, speed, has been obtained with an apparatus which is generally called an acoustical interferometer [3]. This instrument employs a quartz crystal, operating at its resonant frequency (1 megahertz), and it is assumed that the crystal acts as a plane wave radiator. Pressure measurements are made with a mercury manometer which is accurate to 70 μ of mercury in the range of measurements. While there are a few references to our instrument in the literature [4, 5, 6], a detailed description has not been published (see footnote 3).

2. Results

There are listed in table 1 values of pressure, speed and speed squared for each isotherm. The temperature of an "isotherm" was maintained nearly constant by an automatic regulator which operated from a germanium resistor connected to a Wheatstone bridge. This and other germanium resistors were located in thermal contact with the acoustical thermometer apparatus so that allowance could be made for small relative temperature changes which occurred during measurements of an isotherm. Since four or five pressure-speed determinations on a given isotherm require a day it was not possible for all points on an isotherm to be taken at exactly the same temperature. Consequently, small deviations in temperature occurred (not exceeding 3 mdeg) and the speeds were corrected using the germanium thermometer indications. The speeds in table 1 have been treated in this manner.

TABLE 1. *Isotherm data (speed—meters/sec; pressure—atmospheres)*

1. 2.323 °K				4. 4.212 °K			
p	W	W^2	Δ^a	p	W	W^2	Δ
0.0135	88.991	7,919.4	−12.4	*0.0322*	120.241	14,461	−9.5
.01541	88.968	7,915.3	−1.1	*.0328*	120.182	14,444	−21.6
.02005	88.806	7,886.5	−7.6	.0501	120.030	14,407	4.0
.0251	88.528	7,837.2	−1.0	.0507	119.996	14,391	−1.9
.0251	88.527	7,837.4	−1.2	.06638	119.76	14,342	−2.2
.02076	88.740	7,874.8	1.6	.0668	119.766	14,344	−0.7
.02966	88.292	7,795.5	−5.9	.0801	119.566	14,287	.6
.02991	88.312	7,799.0	−0.4	.0997	119.262	14,223	−1.6
.03837	87.942	7,733.7	2.7	.10211	119.232	14,216	−.1
				.10271	119.268	14,225	10.7
2. 2.807 °K				.1204	118.968	14,145	2.8
				.1505	118.498	14,042	−0.7
				.1674	118.25	13,975	1.2
0.01601	98.043	9,612.5	−8.4	.1986	117.786	13,874	3.8
.0233	97.879	9,612.3	3.5	.1976	117.76	13,867	−5.9
.03011	97.648	9,535.1	−0.6	.2017	117.707	13,855	−3.7
.03666	97.445	9,495.4	−.7	(.2357)	117.281	13,746	
.04333	97.241	9,455.8	−.1	(.3024)	116.139	13,481	
				(.2555)	116.859	13,646	
3. 3.211 °K				(.3805)	114.743	13,160	
				5. 5.024 °K			
0.03048	104.647	10,951.	−5.3				
.04007	104.448	10,909.4	3.7	*0.0644*	131.178	17,208	−12.5
.0501	104.162	10,849.7	−3.0	.0988	130.90	17,135	6.2
.0568	103.996	10,815.2	−3.3	.1340	130.51	17,033	−2.0
.0668	103.769	10,768.0	3.4	.1676	130.166	16,943	2.2
.08366	103.324	10,675.8	.2	.1978	129.87	16,866	1.2
.0989	102.942	10,597.	1.9				
.1003	102.884	10,585.1	−2.6				
(.1340)	101.995	10,403.0					
(.1672)	101.049	10,210.9					
(.2036)	99.975	9,995.0					

[a] The columns under Δ contain the difference between the experimental W^2 at the indicated pressures and the W^2 of linear function determined by the computer least squares fitting.

For each isotherm, values of p and W^2 have been treated analytically by computer and graphically to obtain W_0^2. Equation (5) demonstrates that a linear treatment of the data will be inadequate at sufficiently high pressures. It is not surprising, therefore, that in figure 1, which depicts the 3.2 °K isotherm, the data points markedly depart from a straight line above 0.17 atm of pressure. In order to represent the isotherms linearly, we noted the departure of the highest point and, assuming that such departures are proportional to p^2, discarded all points for which the deviation from linearity would exceed the experimental reproducibilities. Accordingly, the data above 0.1003 and 0.2017 atm for isotherms 3.2 and 4.2 °K, respectively, were omitted in the linear computer analysis. For the remaining isotherms, comparable data selection was unnecessary since correspondingly high pressure data had not been acquired.

In general, the lowest pressure points on an isotherm warrant lesser weightings. The inaccuracy of these

[1] The value of the gas constant is taken from reference [1].
[2] Figures in brackets indicate the literature references at the end of this paper.
[3] Note added in proof: The instrument is described in Science **150**, No. 3693, p. 155 (8 Oct. 1965).

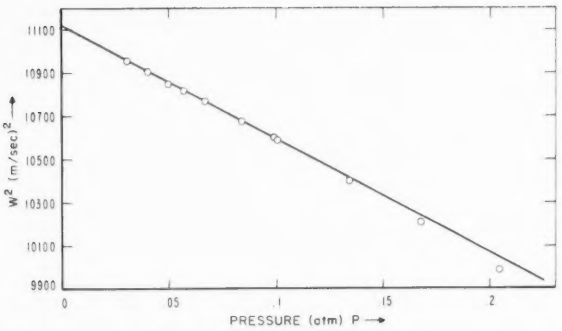

FIGURE 1. W^2 *as a function of pressure at 3.211 °K.*

points is caused by a lack of resolution resulting from the high attenuation of sound energy in the thermometric gas. Consequently, the italicized data received one quarter weights in all computer fits.

Column 1 of table 2 contains the W_0^2 intercepts obtained from graphical treatment of the data where W^2 was plotted as a function of p. The procedure was straightforward in that straight lines were obvious representations in the graphs if the highest pressure points for the 3.2 and 4.2 °K isotherms were not considered. Column 8 of table 2 contains the temperatures derived from the W_0^2's of column 1.

In the computer analysis of the apparently linear data, each isotherm was fitted by the method of least squares to a polynomial in which the square of the speed is equated to a power series of the pressure, i.e., $W^2 = W_0^2 + W_0^2\alpha p + W_0^2\beta p^2 + W_0^2\gamma p^3 + \ldots$. The first analysis involved the constant and linear terms, the second included the quadratic, and for the third the cubic was also added. Each of these cases yields a value for W_0^2. Columns 2 and 9 of table 2 list the intercepts and temperatures obtained from the linear computer fitting. The higher order fits, with one exception, proved to be of little significance since the additional coefficients were statistically uncertain. The exception was the quadratic fit for the 4.2 °K isotherm. In this case a W_0^2 value of 14.570 with an uncertainty of 6 was obtained from which a temperature of 4.209 (±0.002) °K resulted.[4] In the above analyses the bracketed high pressure data points for the 3.2 and 4.2 °K were not included.

Equation (5) can be accurately represented by a linear expression (for a constant α) if the pressure is sufficiently low. (Our input data for the majority of isotherms have been selected to meet this criterion or, more specifically, data have been used that graphically exhibit a linear relationship within the limits of the experimental error.) For this reason we believe that the most accurate determinations of isotherm temperatures are those which have resulted from a linear treatment. Nevertheless for completeness, it is necessary to extend the computer analysis to higher orders of pressure and include the higher pressure data for isotherms 3.2 and 4.2 °K. In this case the linear representation is inaccurate, but there exists no a priori approach to predict the significance of particular higher order pressure terms since the analytical representation of higher order virial coefficients is unknown. Consequently we have approached the analyses empirically, by including quadratic, and quadratic and cubic terms for the pressure.

When only the quadratic term is added, a statistically meaningful coefficient for p^2 of eq (5) results. Columns 5 and 11 list the W_0^2 and T values which result from extrapolations of the quadratic analyses. The addition of a cubic term was not helpful since the

[4] The values reported here are not to be confused with the value resulting from the more complete quadratic fitting as reported in columns 5, 6, and 7 of table 2.

TABLE 2. *Summary of data derived from isotherms*

W^2 Extrapolations from							Temperatures derived from					$T_{isotherm} - T_{68}$
Linear analysis of data				Quadratic analysis of data			Linear analysis			Quadratic Analysis		
Graphical	Computer			Computer			Graphical	Computer	Computer	Computer		ΔT
W_0^2	W_0^2	δ^a	σ^c	W_0^2	δ^a	σ^c	T	T	δT^b	T	δT^b	
Column No. 1	2	3	4	5	6	7	8	9	10	11	12	13
17.393	17.392	9.6	5.4				5.024	5.024	0.002			0.012
14.580	14.583	3.1	5.0	14.568	6.	7.2	4.211	4.212	.001	4.208	0.002	.010
11.123	11.117	3.7	3.1	11.104	4.4	2.9	3.213	3.211	.001	3.207	.001	.008
9.722.5	9.717.5	6.2	3.1				2.808	2.807	.002			.007
8.037.5	8.040.5	6.9	4.5				2.322	2.323	.002			.006

[a] The δ's in columns 3 and 6 of table 2 contain the uncertainties of the coefficients, W_0^2, in columns 2 and 5.
[b] The δ's of columns 10 and 12 are the corresponding uncertainties of the temperatures in columns 9 and 11.
[c] σ is the standard deviation in the least squares fitting of an isotherm.

statistical significance of coefficients was lost. The analysis was not extended for we felt that to be meaningful it should include data over the largest possible range of pressures. Column 13 contains the temperature differences, $T_{\text{isotherm}} - T_{58}$, where T_{58} is derived from the helium 4 vapor pressure scale [7]. These were obtained by calibrating germanium resistors directly against measured vapor pressures and comparing them, in the acoustical thermometer, with germanium resistors which had been calibrated by the acoustical thermometer. In one or two cases, a resistor associated with the acoustical thermometer during an isotherm measurement had been previously calibrated at one or more vapor pressure temperatures. The temperature values of T_{isotherm} are from column 9.

Thus our values of isotherm temperatures, column 9, and the indicated departures from T_{58} (column 13) afford a comparison with the T_{58} scale as portayed in figure 2. Except for out data points, figure 2 is taken from Van Dijk [8]. In essence he has plotted values of absolute temperature determination, in the liquid helium range, relative to the T_{58} scale. While we are not prepared to present a value for the absolute accuracy of our values of temperature, if one believes that the T_{58} scale is smooth with respect to the true thermodynamic temperature scale, the plot suggests that perhaps the present data are the most self consistent of any temperature measurements that have been made below 5 °K. (The dispersion in temperature values resulting from our different methods of isotherm analyses indicates that our deduced values of temperature are not critically dependent upon a particular method of analysis.)

The reproducibility of points on an isotherm appears to be within ± 0.002 °K although it is obvious that most of the isotherms need a better definition, that is, a greater number of points. Nevertheless, we do feel that the indicated conclusions of our measurements are important enough to be presented now rather than be delayed until the complete program in this temperature range has been finished.

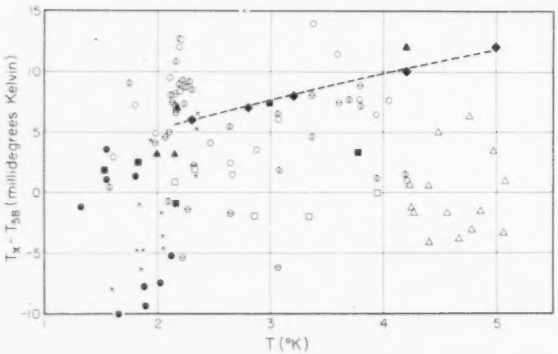

FIGURE 2. *A comparison with* T_{58} *of temperatures derived from isotherm measurements, gas thermometry and the acoustical interferometer.*

◑⊖○–Schmidt and Keesom [9] (gas thermometer, 1937).
●–Kistemaker [10] (gas thermometer, 1946).
×–Kistemaker [10] (isotherms, 1946).
△–Berman and Swenson [11] (gas thermometer, 1954).
□–Keller [12] (helium 4 isotherms, 1955).
■–Keller [12] (helium 3 isotherms, 1955).
▲–Preliminary results [4,5] (velocity of sound in helium 4 gas, acoustical interferometer, 1962).
◆–Present work (isotherms determined by the NBS acoustical thermometer).

3. References

[1] NBS Tech. News Bull. 47, 175 (1965); NBS Misc. Publ. 253 (Nov. 1963).

[2] F. Everling, L. A. König, H. E. Mattuch, and A. H. Wapstra, Relative nuclidic masses, Nuclear Phys. **18**, 529 (1960).

[3] J. L. and E. S. Stewart, J. Acoust. Soc. Am. **24**, 22 (1952); M. Greenspan, Physical Acoustics **2A**, 30 (Academic Press, Inc., New York, 1965).

[4] G. Cataland, M. Edlow, and H. H. Plumb, Temperature, Its Measurement and Control in Science and Industry, C. M. Herzfeld, ed., **3**, F. G. Brickwedde, ed., Pt 1 (Reinhold Publishing Corp., New York, 1962).

[5] G. Cataland and H. H. Plumb, J. Acoust. Soc. Am. **34**, 1145 (1962).

[6] G. Cataland and H. H. Plumb, Proceedings of the Eighth International Conference on Low Temperature Physics (Butterworths, Washington, 1963).

[7] F. G. Brickwedde, H. van Dijk, M. Durieux, J. R. Clement, and J. K. Logan, J. Research NBS **64A** (Phys. and Chem.) No. 1, 1 (1960).

[8] H. van Dijk, Progress in Cryogenics, p. 123 (Heywood and Company, Ltd., London, 1960).

[9] G. Schmidt and W. H. Keesom, Leiden Commun. No. 250b; Physica **4**, 963 (1937).

[10] J. Kistemaker and W. H. Keesom, Leiden Commun. No. 269b; Physica **12**, 227 (1946).

[11] R. Berman and C. A. Swenson, Phys. Rev. **95**, 311 (1954).

[12] W. E. Keller, Phys. Rev. **97**, 1 (1955); Phys. Rev. 100, 1790 (1955).

(Paper 69A6–375)

JOURNAL OF RESEARCH of the National Bureau of Standards—A. Physics and Chemistry
Vol. 69A, No. 6, November–December 1965

Synthesis of D-Glucose-*3*-^{14}C and Related Compounds[1, 2]

Harriet L. Frush, Lorna T. Sniegoski, Nancy B. Holt, and Horace S. Isbell

(July 29, 1965)

D-Glucose-3-^{14}C has been prepared by means of three, successive Kiliani syntheses. The process consists of (a) the addition of ^{14}C-labeled cyanide to D-glyceraldehyde; (b) hydrolysis of the cyanohydrins and conversion of the resulting epimeric D-tetronic-*1*-^{14}C acids into D-tetroses-*1*-^{14}C by way of an improved Rosenmund reduction of the acetylated tetronyl chlorides; (c) addition of nonlabeled cyanide to the mixture of the *aldehydo* acetates of D-threose-*1*-^{14}C and D-erythrose-*1*-^{14}C; (d) hydrolysis of the cyanohydrins, and lactonization of the resulting mixture of four D-pentonic-*1*-^{14}C acids; (e) chromatographic separation of these into three fractions; (f) reduction of the fraction containing D-arabinono-2-^{14}C- and D-xylono-2-^{14}C-lactone to the corresponding sugars, and chromatographic separation of these; and (g) conversion of D-arabinose-*2*-^{14}C into D-glucose-*3*-^{14}C and D-mannose-*3*-^{14}C by a third Kiliani synthesis. Approximately 3 percent of the radioactivity was obtained in the form of D-glucose-*3*-^{14}C. The process results in the production of a large number of intermediate labeled compounds.

Key Words: Aldonic acids; carbon-14-labeled carbohydrates; chromatography, paper; glucose-3-carbon-14; hexoses-3-carbon-14; pentoses-2-carbon-14; radioactive carbohydrates; Rosenmund reductions; synthesis of radioactive sugars; tetroses-1-carbon-14.

1. Introduction

Prior publications from this laboratory have reported methods for synthesizing pentoses labeled with carbon 14 at C–1 and C–5 [1, 2, 3],[3] and hexoses labeled at C–1, C–2, and C–6 [4, 5, 6, 7], but, heretofore, no methods have been reported for synthesizing tetroses-*1*-^{14}C, pentoses-*2*-^{14}C, and hexoses-*3*-^{14}C. In response to the urgent need for some of these sugars in biological research, the preparation of D-glucose-*3*-^{14}C and certain related compounds was undertaken.

The procedure consisted of a series of three cyanohydrin syntheses, beginning with 2,3-*O*-isopropylidene-D-glycerose and sodium cyanide-^{14}C. In order to avoid the excessive dilution of radioactivity resulting from the addition of carriers in the separation of the epimers in each step, the use of carriers was limited to the separation of the epimeric hexonic acids and the purification of D-glucose-*3*-^{14}C. Separations and purifications at earlier stages were accomplished by means of large-scale paper chromatography.

In the first preparation, the tetronic acids were separated by lactonization and chromatography. D-Erythrose-*1*-^{14}C, prepared from D-erythronic-*1*-^{14}C acid by an improved Rosenmund synthesis, was converted, by a second cyanohydrin reaction, into D-arabinonic-*2*-^{14}C and D-ribonic-*2*-^{14}C acids. These were lactonized, and the lactones were chromatographically separated; the resulting D-arabinono-1,4-lactone-*2*-^{14}C, on reduction with sodium amalgam, yielded D-arabinose-*2*-^{14}C. Starting with this sugar, a third cyanohydrin synthesis yielded D-glucose-*3*-^{14}C and D-mannose-*3*-^{14}C.

In a second, somewhat more efficient, preparation (see fig. 1), it was found convenient to omit separation at the four-carbon level. The tetronic acid mixture was converted into the two D-tetroses-*1*-^{14}C, and thence into a mixture of the four D-pentonic-*2*-^{14}C acids. After lactonization and paper chromatography, this gave, as one fraction, a mixture of *2*-^{14}C-labeled D-arabinonic and D-xylonic lactones. This mixture of lactones was reduced to a mixture of the corresponding sugars, and D-arabinose-*2*-^{14}C was separated chromatographically; this sugar was then used for the third cyanohydrin synthesis.[4]

[1] This work was supported in part by the Psychopharmacology Service Center, National Institute for Mental Health, National Institutes of Health, Public Health Service, Department of Health, Education, and Welfare, Bethesda, Md. 20014.

[2] Preliminary work on this synthesis was reported by one of us (L.T.S.) in a Ph. D. dissertation presented to the University of Maryland (1960).

[3] Figures in brackets indicate the literature references at the end of this paper.

[4] The second prodecure results in the formulation and separation of D-xylose-2-^{14}C and D-lyxono-1,4-lactone-2-^{14}C, in addition to the D-ribono-1,4-lac one-2-^{14}C formed in the first procedure.

FIGURE 1. *Synthesis of* D-*glucose*-3-^{14}C

	Radioactivity (millicuries)
2,3-*O*-Isopropylidene-D-glycerose	
↓ cyanohydrin synthesis ($Na^{14}CN$)	132
Epimeric D-tetronic cyanohydrins	
↓ hydrolysis	
↓ neutralization of acids with $Cd(OH)_2$	
Cadmium D-erythronate-*1*-^{14}*C* and -D-threonate-*1*-^{14}*C*	116
↓	
Tri-*O*-acetyl-D-erythronyl-*1*-^{14}*C* and -D-threonyl-*1*-^{14}*C* chlorides	
↓ Rosenmund reduction	
Tri-*O*-acetyl-*aldehydo*-D-erythrose-*1*-^{14}*C* and D-threose-*1*-^{14}*C*	95
↓ cyanohydrin synthesis (NaCN)	
↓ hydrolysis	
Four D-pentonic acids	
Aliquot Taken for Remaining Steps	68 (71%)
↓ lactonization of acids	
↓ chromatographic separation	
A. D-Lyxono-1,4-lactone-2-^{14}*C* (held on paper)	–
B. D-Ribono-1,4-lactone-2-^{14}*C* (held on paper)	–
C. D-Arabinono-1,4-lactone-2-^{14}*C* / D-Xylono-1,4-lactone-2-^{14}*C*	19.4
↓ reduction of band C ($NaHg_x$)	
chromatographic separation	
D-Xylose-2-^{14}*C* (held on paper)	–
D-Arabinose-2-^{14}*C*	7.0
↓ cyanohydrin synthesis (NaCN)	
Epimeric D-hexonic cyanohydrins	
hydrolysis, and separation of acids by use of carriers	
D-Mannono-1,4-lactone-3-^{14}*C*	3.0
Potassium D-gluconate-3-^{14}*C*	3.6
↓	
D-Glucono-1,5-lactone-3-^{14}*C*	
↓ reduction ($NaHg_x$)	
D-Glucose-3-^{14}*C*	2.8

2. Development of Experimental Methods

2.1. Determination of Completeness of Addition of Cyanide to 2,3-*O*-Isopropylidene-D-glycerose

In order to ascertain the optimal conditions for this reaction, the rate and completeness of addition of cyanide to 2, 3-*O*-isopropylidene-D-glycerose in various buffers were determined. The best results (see table 1) were obtained in a sodium bicarbonate or sodium carbonate buffer; in these, 98 and 94 percent, respectively, of the theoretical uptake of cyanide occurred within ten days. In a sodium acetate–acetic acid buffer, and in a sodium bisulfite buffer, the reaction was less complete.

2.2. Conversion of D-Erythronic-*1*-^{14}*C* Acid Into D-Erythrose-*1*-^{14}*C*

Because of the absence of the stabilizing pyranoid ring in the resulting sugar, tetronic lactones cannot be reduced to tetroses by the methods successfully employed for reducing pentonic and higher lactones. Both sodium amalgam reduction and catalytic hydrogenation of an erythronic lactone lead to the fully reduced product, erythritol [8, 9, 10]. However, a modified Rosenmund reduction [11], as first used by Cook and Major on fully acetylated aldonyl chlorides [12], appeared to provide a possible semimicro method for preparing D-erythrose-*1*-^{14}*C*. The method had already been applied by Glattfeld and Kribben [10] to the macro reduction of DL-erythronic acid to give an overall yield of DL-erythrose of less than 4 percent. Much of the loss occurred during the purification of the *aldehydo* acetate by distillation. Subsequently, Ladenburg et al. [13] improved the yields of acetylated aldonic acids by use of the cadmium salt of the acid in the acetylation. For the semimicro preparation of tri-*O*-acetyl-D-erythronyl chloride, it seemed probable that phosphorus pentachloride, used by Cook and Major, would be more convenient as a reagent than thionyl chloride, employed by Glattfeld and Kribben. In pilot experiments on nonlabeled material, one-millimole quantities of cadmium D-erythronate were freeze-dried, acetylated with a mixture of acetic anhydride and hydrogen chloride, converted into tri-*O*-acetyl-D-erythronyl chloride with phosphorus pentachloride, and reduced by the Rosenmund procedure to tri-*O*-acetyl-*aldehydo*-D-erythrose. The overall yield, as determined by titration, was 90 percent.

2.3. Chromatographic Separations

A variety of chromatographic techniques was developed for separating the isomeric lactones and the sugars obtained in the syntheses. Large-scale separations were carried out on heavy paper [14, 15], and bands of material, located by radioautography, were removed from the paper by elution. Of several solvents evaluated, water-saturated 1-butanol was chosen for separating D-erythronic and D-threonic lactones (R_f 0.34 and 0.52, respectively). The subsequent separation of these lactones was found to be complicated by formation, during attempts to achieve complete lactonization, of a complex mixture containing esterlike compounds. The complication was largely overcome by converting the mixed acids into their butyl esters and then converting these into a mixture of the lactones. However, the separation of the tetronic lactones was further complicated by the forma-

tion of a fairly stable, slow-moving derivative of D-threonic acid,[5] having nearly the same R_f value as that of D-erythronic lactone; consequently, the chromatographic separation of D-erythronic lactone was not sharp.

In a second preparation, the D-tetronic acids, without separation, were carried through the Rosenmund reduction (see secs. 2.2 and 3.4). The resulting mixture of acetylated D-tetroses was converted into a mixture of the four D-pentonic acids. These were lactonized, and the lactones were chromatographically separated into three fractions by use of *tert*-pentyl alcohol, three-quarters saturated with water: A, D-lyxono-1,4-lactone-2-^{14}C; B, D-ribono-1,4-lactone-2-^{14}C; and C, a mixture of D-arabinono-1,4-lactone-2-^{14}C and D-xylono-1,4-lactone-2-^{14}C. Because the lactones in band C are difficult to separate chromatographically, they were reduced, without separation, to a mixture of the corresponding sugars. D-Arabinose and D-xylose, although separable by use of various developing solvents, were found to have widely different mobilities in 9:1:1 2-butanone–acetic acid–saturated aqueous boric acid [16], and so this solvent mixture was used for their separation.

3. Experimental Details

3.1. Materials and General Methods

Sodium cyanide-^{14}C was prepared from barium carbonate-^{14}C, and was analyzed for specific and total radioactivity by methods previously developed [17]. Nonlabeled 1,2:5,6-di-*O*-isopropylidene-D-mannitol was prepared in 82-percent yield by condensing D-mannitol with acetone in the presence of zinc chloride [18].

Most of the radioactivity assays for carbon 14 were made with a liquid scintillation counter by use of a scintillation solution having *p*-dioxane as the solvent [19]. In assaying the salts of aldonic acids (which are relatively insoluble in dioxane), an equal volume of a thixotropic agent[6] was added to the scintillation solution before addition of the radioactive sample [20]. The counting efficiency was determined by means of salts of aldonic acids having known radioactivity. Some of the materials were assayed in formamide solution by means of a 2-π, windowless, gas-flow proportional counter [21].

Reductions of lactones with sodium amalgam (in the form of pellets) [22] were conducted on a semimicro scale, in the presence of sodium hydrogen oxalate as buffer [4, 23].

3.2. Preparation of 2,3-*O*-Isopropylidene-D-glycerose

A solution of 10 mmoles (2.62 g) of 1,2:5,6-di-*O*-isopropylidene-D-mannitol in 40 ml of water was mixed with 11 mmoles (2.35 g) of sodium metaperiodate dissolved in 50 ml of water. The resulting solution was kept in the dark at room temperature for 2 hr, cooled in ice, and passed through a column of ice-cold, mixed, cation- and anion-exchange resins to remove sodium iodate and excess sodium metaperiodate. Measurement of conductivity[8] showed that the effluent was free of ionic materials. The aqueous solution was immediately concentrated under reduced pressure, and the aldehyde content was determined by oxidation of an aliquot with iodine in alkaline solution [24]. The yield of 2,3-*O*-isopropylidene-D-glycerose was, by analysis, 16.4 mmoles (82 percent); the material was used without further purification.

3.3. Reaction of 2,3-*O*-Isopropylidene-D-glycerose With Sodium Cyanide

In order to determine optimal conditions for the cyanohydrin reaction [25], solutions were prepared from equimolar quantities of 2,3-*O*-isopropylidene-D-glycerose, sodium cyanide, and one of the buffers listed in table 1; the concentration of each compound in the solution was 0.09 mmole per ml. The solutions were kept at room temperature, and aliquots were removed periodically for the determination of residual cyanide [26]. The results, expressed as percent of the cyanide that had reacted with the sugar, are given in table 1.

TABLE 1. *Completeness of cyanide addition to 2,3-O-isopropylidene-D-glycerose.*

Buffer	Time (days)				
	3	5	7	10	12
	%	%	%	%	%
$NaHSO_3$	67.3	69.6	70.7	74.1	75.0
$NaHCO_3$	78.6	88.7	94.6	97.7	98.9
Na_2CO_3	72.7	82.7	88.5	93.7	95.6
NaOAc–HOAc	67.3	73.2	75.5	77.9	79.1

For the synthesis outlined in figure 1, the following two solutions were combined:

A. Solution of radioactive sodium cyanide (160 ml) containing:

sodium cyanide	30.4 mmoles
total radioactivity	132.5 millicuries (mCi)
specific radioactivity	4.36 mCi/mmole
sodium hydroxide	21.2 mmoles

B. Solution of 2,3-*O*-isopropylidene-D-glycerose (68 ml) containing:

2,3-*O*-isopropylidene-D-glycerose	33 mmoles
sodium bicarbonate	52 mmoles.[9]

Solution B was added to solution A, previously frozen

[5] On treatment with acid, the compound gave D-threonic acid.

[6] "Cab-O-Sil," Godfrey L. Cabot, Inc., Boston, Mass.

[7] Certain commercial materials and equipment are identified in this paper in order to specify adequately the experimental procedure. In no case does such identification imply recommendation or endorsement by the National Bureau of Standards, nor does it imply that the material or equipment identified is necessarily the best available for the purpose.

[8] All effluents from mixed ion-exchange resins were tested for the presence of ionic impurities by use of a commerical conductivity-meter.

[9] In sodium ion, this amount of sodium bicarbonate is equivalent to the reagents in solution A.

onto the sides of a 750-ml, round-bottomed flask. The flask was allowed to stand at room temperature, and was occasionally shaken until the ice had melted.

After 10 days, a solution of 1 g (25 mmoles) of sodium hydroxide in 20 ml of water was added. The flask, equipped with a gas inlet and a reflux condenser, was heated at 90 °C for 1 hr while a gentle stream of nitrogen was passed through the solution.[10] The solution was then filtered with the aid of 100 mg of a decolorizing carbon; analysis showed 120.4 mCi of radioactivity (90.9 percent). Cations were removed with a cation-exchange resin.[11]

3.4. Conversion of D-Tetronic-*1*-^{14}C Acids Into D-Tetroses-*1*-^{14}C

After concentration under reduced pressure[12] to about 200 ml, the effluent was treated with an excess of cadmium hydroxide, and the suspension was magnetically stirred for two days and filtered. The residue was suspended in water, and the suspension was treated for 15 min with a stream of carbon dioxide gas, heated to boiling, and filtered.[13] The combined filtrates and washings (containing 116.1 mCi) were concentrated under reduced pressure, and the concentrate was divided in two parts; each of these was freeze-dried and separately converted into the mixed D-tetroses-*1*-^{14}C.

To 14.6 millequivalents (meq) of mixed cadmium D-erythronate-*1*-^{14}C and cadmium D-threonate-*1*-^{14}C (containing 63.5 mCi of radioactivity) was added 75 ml of acetic anhydride. The flask was kept in an ice bath for 20 min, while dry hydrogen chloride was bubbled through the suspension. The flask, containing a magnetic stirring bar, was now closed with a drying tube, and the contents were kept at 50 °C for 1 hr, while being stirred. The suspension was immediately filtered on a 15-ml, coarse, glass-fritted funnel, and the residue was thoroughly washed with acetic anhydride.[14] The combined filtrate and washings were concentrated under reduced pressure; traces of acetylating agents were removed by successively adding and evaporating absolute ethanol (twice) and toluene (once). Finally, 50 ml of dry ether, a magnetic stirring bar, and 6.2 g of phosphorus pentachloride were added, the flask was closed with a drying tube, and the contents were stirred overnight at room temperature.

The suspension was filtered through a 15-ml, medium, glass-fritted funnel into a 250-ml, long-necked, round-bottomed flask. Ether and phosphoryl chloride were removed by concentration under reduced pressure. Xylene (50 ml) was twice successively added and distilled.[15]

The acetylated tetronyl chlorides were then catalytically reduced by the Rosenmund procedure [12]. To the sirupy acid chlorides were added 35 ml of dry xylene, a magnetic stirring bar, and 2.75 g of palladium—barium sulfate catalyst [27] (previously heated at 60 °C for 30 min). While the reaction flask was heated under reflux in an oil bath at 130 °C, dry hydrogen was vigorously bubbled through the stirred suspension, and the escaping gases were passed through 15 ml of 0.5-*N* sodium hydroxide. The receiver and contents were replaced every 30 min, and the hydrogen chloride evolved was determined by neutralizing the excess alkali with nitric acid and titrating the chloride ion with silver nitrate (Mohr method). Reduction was rapid during the first 30 min, and slower thereafter; the reaction, which was continued for 4 hr, evolved 13.1 mmoles of hydrogen chloride (90% of the theoretical).

The hot suspension was filtered on a 60-deg funnel bearing a perforated plate (4-cm diam) and filter paper heavily coated with both paper pulp and diatomaceous earth. The residue was well washed with hot xylene, and the filtrate and washings were combined and evaporated under reduced pressure. The residue was dissolved in 50-percent aqueous ethanol, and the solution was passed through a column containing 35 ml of an anion-exchange resin topped by 5 ml of a cation-exchange resin. The neutral effluent contained 54.6 mCi of radioactivity. Elution of the resin with 10-percent aqueous acetic acid yielded 1.45 mCi of radioactivity, largely in the form of unreduced tetronic acids.

A repetition of the acetylation and reduction processes, starting with the second portion of mixed cadmium salts (12.0 meq, 52.5 mCi) yielded neutral products containing 40.2 mCi of radioactivity, and unreduced acids containing 3.6 mCi. The total radiochemical yield of neutral products was 81.7 percent of the tetronic acids.

3.5. Preparation of D-Pentonic-2-^{14}C Acids

The neutral products from the two reductions were combined (21.7 mmoles, 94.8 mCi) and concentrated to about 50 ml under reduced pressure. Sodium bicarbonate (2.18 g, 26 mmoles) was added, and, after the addition of two or three small lumps of solid carbon dioxide, the mixture was frozen onto the sides of the flask. To this solid was added a solution of 1.27 g (26 mmoles) of sodium cyanide in 25 ml of water. The mixture was allowed to thaw in ice water, and was kept at room temperature for one week.

[10] The hydrolysis was conducted in an efficient hood, and no attempt was made to determine the ammonia evolved. Preliminary test-hydrolyses, followed by paper chromatography, had shown that the above conditions are satisfactory.

[11] Because of the evolution of gas in the presence of cation-exchange resin, 50 ml of the resin was first stirred with the solution, which was then passed through a column of the resin (150 ml). The column was back-washed several times during the process, and all of the resin was finally washed until the last portions of the effluent had negligible radioactivity.

[12] With one exception, noted later, if a distillate contained appreciable radioactivity, the distillate was redistilled, and the residue was combined with the main product.

[13] The cadmium carbonate remaining still contained 4.3 mCi of radioactivity. This was not reclaimed.

[14] Cadmium salts were removed at this point, in order to obviate "bumping" during evaporation.

[15] The distillate, containing 250 μCi of radioactivity, was discarded.

Sodium carbonate (2.1 g) was then added, and the solution was heated under reflux (boiling-water bath) for 2 hr, while a gentle stream of nitrogen was bubbled through it. The hydrolyzate was cooled and passed through a column of 125 ml of a cation-exchange resin,[16] which was then thoroughly washed.

3.6. Lactonization and Separation of D-Pentonic-2-^{14}C Acids

A portion of the mixed acids (15.4 mmoles, 67.5 mCi) was lactonized, by way of the butyl esters, by the following rapid method: The solution was concentrated under reduced pressure to a sirup, which was heated at 70 °C for 30 min with a 1-percent solution of hydrochloric acid in 1-butanol. Butanol was removed by two successive additions and evaporations, under reduced pressure (50 °C), of a 1:1 mixture of toluene and acetic acid. The sirup was heated at 80 °C for 1 hr with this mixture, and the solvent was removed by evaporation under reduced pressure. Addition and evaporation of the toluene–acetic acid mixture were repeated twice more. Finally, the sirup was dissolved in acetic acid and freeze-dried.

The residue, dissolved in methanol, was applied at once, as a 0.5-cm band, on four 18 in. × 22 in. sheets of prepared seed-test paper [14, 15]. After being dried for 12 hr in the air, the papers were developed for 94 hr[17] with *tert*-pentyl alcohol, ¾ saturated with water.

Radioautograms of the chromatograms (made with industrial x-ray film by exposure for 15 to 20 min) showed three distinct bands. The fastest band (containing both D-arabinono-1,4-lactone-2-^{14}C and D-xylono-1,4-lactone-2-^{14}C) was located on each sheet of paper, and eluted with 50-percent aqueous methanol until the last of the eluate had negligible radioactivity; the combined eluate from this band of the four chromatograms contained 19.4 mCi of radioactivity.[18]

3.7. Preparation and Separation of D-Arabinose-2-^{14}C and D-Xylose-2-^{14}C

The solution of eluted lactones was treated with a small amount of cation-exchange resin, relactonized, and reduced with sodium amalgam to D-arabinose-2-^{14}C and D-xylose-2-^{14}C by the method previously described [1] for the preparation of D-arabinose-1-^{14}C. The first crop had 13.6 mCi of radioactivity.

Unreduced aldonic acids (containing 5.0 mCi of radioactivity, and contaminated with oxalic acid) were eluted from the ion-exchange resins with 100 ml of 10-percent acetic acid. The acetic acid was evaporated under reduced pressure, an aqueous solution of the residue was treated with excess calcium carbonate, and sufficient solution of calcium hydroxide was added to neutralize it (permanent pink color to phenolphthalein). After filtration of the suspension and passage of the filtrate through a column of a cation-exchange resin, the reclaimed aldonic acids were lactonized by the method described above and reduced with sodium amalgam. The second crop of sugars, containing 2.4 mCi of radioactivity, brought the combined radiochemical yield of D-arabinose-2-^{14}C and D-xylose-2-^{14}C to 16.0 mCi.

The unreduced acids remaining (2.18 mCi) were again removed from the resins, and shown, by a trace analysis with potassium D-arabinonate, to contain 0.7 mCi of radioactivity in the form of D-arabinonic acid.

The mixture of D-arabinose-2-^{14}C and D-xylose-2-^{14}C (3.6 mmoles, 16.0 mCi) was chromatographed on two 18 in. × 22 in. sheets of Whatman paper No. 17, equipped with stirrups and wicks of paper No. 3 [15]. The solvent, 9:1:1 2-butanone–acetic acid–saturated boric acid [16], when used in two developments (17 hr and 12 hr), yielded sharp, well defined bands of D-arabinose-2-^{14}C and D-xylose-2-^{14}C as shown by radioautographs. The D-arabinose-2-^{14}C, eluted with 50-percent methanol, contained 7.0 mCi of radioactivity (1.6 mmoles). Nonlabeled D-arabinose (210 mg) was dissolved in the eluate, and the solution was filtered through a small amount of decolorizing carbon. Boric acid (from the developing solvent) was removed as methyl borate by several successive additions and evaporations of methanol.

3.8. Preparation of D-Glucose-3-^{14}C

The D-arabinose-2-^{14}C was carried through the third cyanohydrin synthesis essentially as described previously for the synthesis of D-glucose-1-^{14}C [4]. However, the D-gluconic acid was separated by means of carrier crops of potassium D-gluconate, instead of barium D-gluconate.[19] Potassium D-gluconate-3-^{14}C, having 3600 μCi of radioactivity, after conversion into D-glucono-1,5-lactone-3-^{14}C and reduction of this, yielded 2380 μCi in the form of chromatographically pure D-glucose-3-^{14}C. Unreduced D-gluconic acid-3-^{14}C was eluted from the ion-exchange resin used in purifying the sugar, and again lactonized and reduced; the total yield of D-glucose-3-^{14}C was 2800 μCi.

Potassium ions were removed from the mother liquor of the potassium D-gluconate-3-^{14}C by a cation-exchange resin, and the D-mannonic-3-^{14}C acid was separated by use of carrier crops of D-mannono-1,4-lactone and held for other work. Part of the lactone was reduced to D-mannose-3-^{14}C by the procedure reported in reference 6.

[16] See footnote 11.

[17] The lactonization of test samples had previously been studied by paper chromatography. The butyl esters, produced by heating with acidified 1-butanol, were almost completely converted into the lactones by the toluene–acetic acid treatment described.

[18] The bands of D-lyxono-1,4-lactone-2-^{14}C and D-ribono-1,4-lactone-2-^{14}C were held on paper and not assayed. The remaining paper, when eluted, yielded 18.1 mCi of radioactivity, of which 2.1 mCi was shown, by an isotope dilution technique, to be in the form of D-arabinonic acid.

[19] The potassium salt crystallizes more freely from impure solutions than the barium salt.

4. References

[1] H. L. Frush and H. S. Isbell, J. Res. NBS **51,** 307 (1953) RP2458.
[2] H. S. Isbell, H. L. Frush, and N. B. Holt, J. Res. NBS **53,** 325 (1954) RP2550.
[3] H. S. Isbell, N. B. Holt, and H. L. Frush, J. Res. NBS **57,** 95 (1956) RP2697.
[4] H. S. Isbell, J. V. Karabinos, H. L. Frush, N. B. Holt, A. Schwebel, and T. T. Galkowski, J. Res. NBS **48,** 163 (1952) RP2301.
[5] H. S. Isbell, H. L. Frush, and N. B. Holt, J. Res. NBS **53,** 217 (1954) RP2536.
[6] H. S. Isbell, H. L. Frush, and R. Schaffer, J. Res. NBS **54,** 201 (1955) RP2581.
[7] R. Schaffer and H. S. Isbell, J. Res. NBS **56,** 191 (1956) RP2667.
[8] D. Hutton, Ph. D. dissertation, Univ. of Chicago. 1930.
[9] J. W. E. Glattfeld and A. M. Stack, J. Am. Chem. Soc. **59,** 753 (1937).
[10] J. W. E. Glattfeld and B. D. Kribben, J. Am. Chem. Soc. **61,** 1720 (1939).
[11] K. W. Rosenmund, Ber. **51,** 585 (1918).
[12] E. W. Cook and R. T. Major, J. Am. Chem. Soc. **58,** 2410 (1936).
[13] K. Ladenburg, M. Tishler, J. W. Wellman, and R. D. Babson, J. Am. Chem. Soc. **66,** 1217 (1944).
[14] H. H. Brownell, J. G. Hamilton, and A. A. Casselman, Anal. Chem. **29,** 550 (1957).
[15] H. L. Frush and L. T. Sniegoski, unpublished work.
[16] W. R. Rees and T. M. Reynolds, Nature **181,** 767 (1958).
[17] J. D. Moyer and H. S. Isbell, Anal. Chem. **29,** 393 (1957).
[18] E. Baer, J. Am. Chem. Soc. **67,** 338 (1945).
[19] W. H. Langham, W. J. Eversole, F. N. Hayes, and T. T. Trujillo, J. Lab. Clin. Med. **47,** 819 (1956); Packard Tech. Bull. No. 1 (Packard Instrument Co., LaGrange, Ill.).
[20] A. Blanchard and I. T. Takahashi, Anal. Chem. **33,** 975 (1961).
[21] A. Schwebel, H. S. Isbell, and J. D. Moyer, J. Res. NBS **53,** 221 (1954) RP2537.
[22] H. S. Isbell, H. L. Frush, and N. B. Holt, J. Res. NBS **64A** (Phys. and Chem.) No. 1, 135–136 (Jan.–Feb. 1960).
[23] H. S. Isbell, U.S. Pat. 2,632,005 (Mar. 17, 1953).
[24] G. M. Kline and S. F. Acree, BS J. Res. **5,** 1063 (1930); Ind. Eng. Chem., Anal. Ed. **2,** 413 (1930).
[25] H. S. Isbell, U.S. Pat. 2,606,918 (Aug. 12, 1952).
[26] I. M. Kolthoff and E. B. Sandell, Textbook of Quantitative Inorganic Analysis, p. 546 (The Macmillan Company, New York, N.Y., 1952).
[27] R. Mozingo, Org. Syntheses, Coll. Vol. **III,** 685 (1955).

(Paper 69A6–376)

JOURNAL OF RESEARCH of the National Bureau of Standards—A. Physics and Chemistry
Vol. 69A, No. 6, November–December 1965

Correlation of Large Longitudinal Deformations With Different Strain Histories

L. J. Zapas and T. Craft

(July 29, 1965)

It is shown that the BKZ incompressible elastic fluid theory is in excellent agreement with experimental results obtained in simple extension. From single step stress-relaxation data, the stress-strain response for a number of other simple extension histories are calculated from the theory and are compared with experiments.

Key Words: BKZ theory, constant rate of strain, creep, elastic fluid, nonlinear behavior, polyisobutylene, polyvinylchloride, recovery, stress relaxation.

1. Introduction

In 1963 Bernstein, Kearsley, and Zapas [1][1] presented a theory of an elastic fluid which gave the correct stress-relaxation response for a large variety of elastomeric materials, including vulcanized rubbers. A principle attractiveness of this theory is its relative simplicity; with a single integral in time, it describes the stress-strain behavior for all types of deformation histories. In the case of simple extension, it predicts the behavior in any uniaxial strain history from the results of single step stress-relaxation experiments which cover the same range of extension and time. We designed a series of experiments to check the validity of this theory and found, as is shown in section 4 of this paper, excellent agreement with experiment in all cases. We are aware that experiments cannot prove a theory. From our results, however, we feel strongly that a single integral expression with a nonlinear integrand such as the BKZ elastic fluid equation is sufficient to describe the stress-strain behavior of elastomeric materials.

2. General Considerations

For an extensive description of the BKZ elastic fluid, we refer the reader to the initial papers [1, 2].

Here we shall use only the definitions and derivations necessary for the description of uniaxial deformations, i.e., simple extension of an incompressible material.

A particular motion of the material may be specified by a relation between the Cartesian components of the position of a particle at time t, $x_i(t)$ and of its position at time τ, $x_i(\tau)$,

$$x_i(t)=x_i(x_k(\tau),\ t,\ \tau) \qquad i,\ k=1,\ 2,\ 3.$$

The relative deformation gradients $x_{ik}(t,\ \tau)$ are defined by

$$x_{ik}(t,\ \tau)=\frac{\partial x_i(t)}{\partial x_k(\tau)}.$$

The left Cauchy-Green tensor $c_{ij}(t,\ \tau)$ is defined by

$$c_{ij}(t,\ \tau)=x_{ik}(t,\ \tau)x_{jk}(t,\ \tau)$$

where, in accordance with Cartesian tensor notation, repeated indices indicate summation over the values 1, 2, 3. The principal invariants of $c_{ij}(t,\ \tau)$ are

$$I_1(t,\ \tau)=\xi_1^2+\xi_2^2+\xi_3^2$$

$$I_2(t,\ \tau)=\xi_1^2\xi_2^2+\xi_2^2\xi_3^2+\xi_3^2\xi_1^2$$

$$I_3(t,\ \tau)=\xi_1^2\xi_2^2\xi_3^2$$

where $\xi_1=\dfrac{\lambda_1(t)}{\lambda_1(\tau)}$, $\xi_2=\dfrac{\lambda_2(t)}{\lambda_2(\tau)}$ and $\xi_3=\dfrac{\lambda_3(t)}{\lambda_3(\tau)}$.

In view of the condition of incompressibility which requires that $I_3(t,\ \tau)=1$, the constitutive equation for the BKZ elastic fluid can be written

$$\sigma_{ij}=-p\delta_{ij}+2\int_{-\infty}^{t}\left[\frac{\partial U}{\partial I_1}c_{ij}(t,\ \tau)-\frac{\partial U}{\partial I_2}c_{ij}^{-1}(t,\ \tau)\right]d\tau \qquad (1)$$

where σ_{ij} are the components of the stress tensor, p is some hydrostatic pressure, U is a function of I_1, I_2, and $t-\tau$,

$$U=U(I_1(t,\ \tau),\ I_2(t,\ \tau),\ t-\tau)$$

and $c_{ij}^{-1}(t,\ \tau)$ are the components of the inverse of $c_{ij}(t,\tau)$.

We may describe isochoric uniaxial strain in a coordinate system in which the x_1 direction corresponds to the direction of strétch. Then the particle which in some reference configuration is located at X_1, X_2, X_3

[1] Figures in brackets indicate the literature references at the end of this paper.

has a position at time t, $x(t)$ given by

$$x_1(t) = \lambda(t) X_1$$

$$x_2(t) = \lambda^{-1/2}(t) X_2$$

$$x_3(t) = \lambda^{-1/2}(t) X_3.$$

The matrix of the left Cauchy-Green tensor $c_{ij}(t, \tau)$ becomes

$$\left\| c_{ij}(t, \tau) \right\| = \begin{Vmatrix} \dfrac{\lambda^2(t)}{\lambda^2(\tau)} & 0 & 0 \\ 0 & \dfrac{\lambda(\tau)}{\lambda(t)} & 0 \\ 0 & 0 & \dfrac{\lambda(\tau)}{\lambda(t)} \end{Vmatrix} \tag{2}$$

and

$$I_1(t, \tau) = \frac{\lambda^2(t)}{\lambda^2(\tau)} + 2\frac{\lambda(\tau)}{\lambda(t)} \tag{3}$$

$$I_2(t, \tau) = 2\frac{\lambda(t)}{\lambda(\tau)} + \frac{\lambda^2(\tau)}{\lambda^2(t)}.$$

From (1), (2), and (3) we get

$$\sigma(t) = \sigma_{11}(t) - \sigma_{22}(t)$$

$$= \int_{-\infty}^{t} \left[\frac{\lambda^2(t)}{\lambda^2(\tau)} - \frac{\lambda(\tau)}{\lambda(t)} \right] h\left(\frac{\lambda(t)}{\lambda(\tau)}, t - \tau \right) d\tau \tag{4}$$

where

$$h\left(\frac{\lambda(t)}{\lambda(\tau)}, t - \tau \right) = 2\left(\frac{\partial U}{\partial I_1} + \frac{\lambda(\tau)}{\lambda(t)} \frac{\partial U}{\partial I_2} \right).$$

Thus, if we know the function h, we can predict the stress response to an uniaxial strain history.[2] For a single step stress relaxation, for which $\lambda(t) = 1$ for $t < 0$ and $\lambda(t) = \lambda$, a constant, for $t \geq 0$, eq (4) becomes

$$\sigma(t) = \left(\lambda^2 - \frac{1}{\lambda} \right) H(\lambda, t) \tag{5}$$

where

$$H(\lambda, t) = \int_t^{\infty} h(\lambda, \zeta) d\zeta \tag{5a}$$

and

$$h(\lambda, t) = -\frac{\partial H(\lambda, t)}{\partial t}. \tag{5b}$$

[2] For discussion of other strain histories we refer the reader to a recent paper by Bernstein [3].

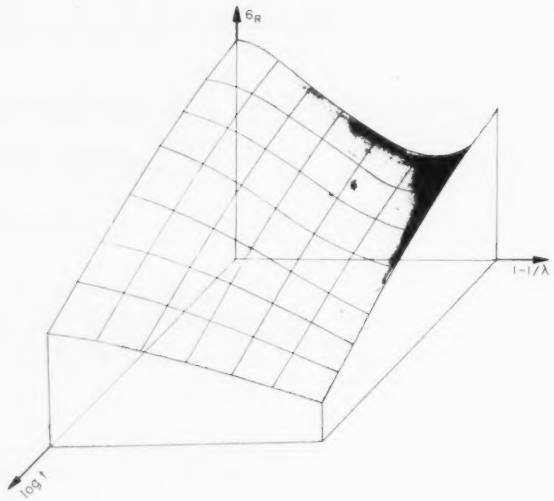

FIGURE 1. *A representative three dimensional plot of* $\sigma_R = H(\lambda, t)$.

In their 1963 article Bernstein, Kearsley, and Zapas [1] plotted isochrones of a reduced stress $\sigma_R(\lambda, t)$ which they defined by

$$\sigma_R(\lambda, t) = \frac{\sigma(t)}{\lambda^2 - \dfrac{1}{\lambda}}.$$

It is evident from (5) that $\sigma_R(\lambda, t)$ is identical with $H(\lambda, t)$. A typical three dimensional plot of H versus log time and $1/\lambda$ is the surface shown in figure 1. We see, then, that with the stress histories of single step uniaxial strains we can measure $H(\lambda, t)$ and predict the stress history of any uniaxial strain history.

3. Experimental Procedure

All our experiments in this work deal with uniaxial deformations on strips with rectangular cross sections. These strips measured about 17 cm long, 0.88 cm wide, and 0.21 cm thick. The data were obtained on polyisobutylene VISTANEX L−100 samples and on polyvinyl chloride samples (plasticized with 50 percent by weight of tricresol phosphate). The stress-relaxation experiments were conducted on a relaxometer whose description has been given in a previous paper [1]. For the creep and recovery experiment we first allowed the sample to creep for a predetermined amount of time by attaching a known weight to the bottom clamp of the sample. We then cut the sample at a place very near the bottom clamp in order to assure an almost instantaneous release of force on the sample and measured the recovery. The constant rate of strain measurements were obtained on an "Instron" machine.

For creep, recovery and constant rate of strain measurements, the motions of two marks on the sample, initially 10 cm apart, were obtained with the aid of two cathetometers. The reference marks were placed far enough away from the clamps to insure that end effects would not disturb the measurements. During the experiments two persons, one at each cathetometer, took readings and a third person recorded the times. Through the use of graphical interpolation, we were able to ascertain accurately the deformation of the sample.

4. Results and Discussion

It has been reported previously by Bernstein, Kearsley, and Zapas [1] that the reduced stress for simple extension measurements can be represented very well by the following equation

$$H(\lambda, t) \equiv \sigma_R(\lambda, t) = \alpha(t)(\lambda^2 - 1) + \frac{1}{\lambda}\beta(t) + \gamma(t). \quad (6)$$

Although we may obtain this equation by assuming a particular form of the potential function U, we shall regard eq (6) as an empirical equation which describes the surface $H(\lambda, t)$. Thus, for the sake of convenience, without committing ourselves to any particular form of U,[3] we shall henceforth present and calculate our data with the three material properties $\alpha(t)$, $\beta(t)$, and $\gamma(t)$ of eq (6). Values of these functions are given in tables 1 and 2. In order to describe the data on plasticized PVC we needed all the three material functions. For the polyisobutylene, however, only two were needed. This is in agreement with previous work [1].

TABLE 1. *Polyisobutylene L-100 at 25 °C*

Time	$\beta(t) \times 10^{-6}$	$\gamma(t) \times 10^{-5}$
min	*Dynes/cm²*	*Dynes/cm²*
2	1.76	6.3
4	1.68	5.1
6	1.63	4.45
10	1.50	3.75
20	1.29	3.00
40	1.064	2.38
60	0.940	2.1
100	.770	1.75
120	.70	1.65

TABLE 2. *Plasticized polyvinylchloride at 27 °C*

Time	$\alpha(t) \times 10^{-7}$	$\beta(t) \times 10^{-7}$	$-\gamma(t) \times 10^{-7}$
min	*Dynes/cm²*	*Dynes/cm²*	*Dynes/cm²*
0.6	2.53	5.28	4.36
1.0	2.38	4.89	4.01
2.0	2.21	4.61	3.64
4.0	2.08	4.39	3.54
6.0	2.02	4.29	3.45
10.0	1.94	4.17	3.34
20.0	1.85	4.04	3.23
40.0	1.78	3.96	3.13
60.0	1.74	3.85	3.07
100.0	1.70	3.77	3.01
120.0	1.68	3.74	2.99

[3] Recently a method of correlating results of experiments in biaxial extension and viscometric flow has been presented which utilizes an empirically determined U with three material properties [4].

4.1. Double Step

Suppose that in a two step stress relaxation we take the first step at time $t = 0$ with extension ratio λ and the second step at $t = t_1$, with extension ratio η, where the extension ratios are taken with respect to the undeformed state. From eqs (4) and (5) we obtain for times greater than t_1,

$$\sigma(t) = \left(\eta^2 - \frac{1}{\eta}\right)\left\{H(\eta, t) + \frac{\eta^3 - \lambda^3}{\lambda^2(\eta^3 - 1)}\left[H\left(\frac{\eta}{\lambda}, t - t_1\right) - H\left(\frac{\eta}{\lambda}, t\right)\right]\right\} \quad (7)$$

In figures 2, 3, and 4 we show the results of two step stress-relaxation experiments for various values of t_1 and the ratio of η/λ. The data are plotted taking as zero time the time of each step. This is done to emphasize the results at early times after the steps which are the more critical data. The black points represent the calculated values as obtained using eqs (7) and (5). The agreement is excellent.

4.2. Triple Step

Consider now a triple step stress relaxation with steps at times 0, t_1, t_2 and extension ratios λ, η, ξ, respectively. For times $t > t_2$ we obtain from eq (4)

$$\sigma(t) = \left(\xi^2 - \frac{1}{\xi}\right)H(\xi, t) + \left(\frac{\xi^2}{\lambda^2} - \frac{\lambda}{\xi}\right)\left\{H\left(\frac{\xi}{\lambda}, t - t_1\right) - H\left(\frac{\xi}{\lambda}, t\right)\right\} + \left(\frac{\xi^2}{\eta^2} - \frac{\eta}{\xi}\right)\left\{H\left(\frac{\xi}{\eta}, t - t_2\right) - H\left(\frac{\xi}{\eta}, t - t_1\right)\right\}. \quad (8)$$

In figure 5, the results of a triple step experiment are shown plotted against the time after each step. The black points represent the calculated values obtained by using eq (5) for the first step, eq (7) for the second step, and eq (8) for the third step. The agreement is very satisfactory. The 3-to 4-percent difference at the early times can be attributed to experimental difficulties. Indeed, because of these difficulties, we know the early time behavior for single step stress relaxation only to within a few percent, and it was these data that were used in calculating our predicted values. The loading time, though small (about 1 sec), may vary by a factor of two, and the manner in which the deformation is applied resembles a very fast ramp function rather than a step function. The temperature change at the early times varies with extension ratio. These effects could contribute significantly at early times after the steps.

787-221 O-65—4

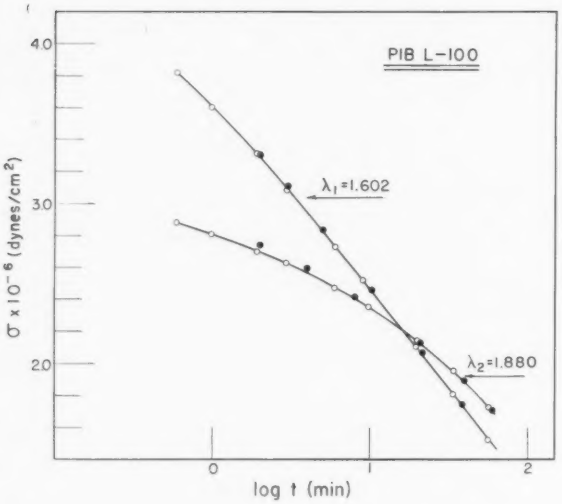

FIGURE 2. *Double step stress relaxation at 25 °C.*
First step with extension ratio $\lambda_1 = 1.602$ from 0 min to 60 min. Second step with extension ratio $\lambda_2 = 1.880$ from 60 min to 130 min.

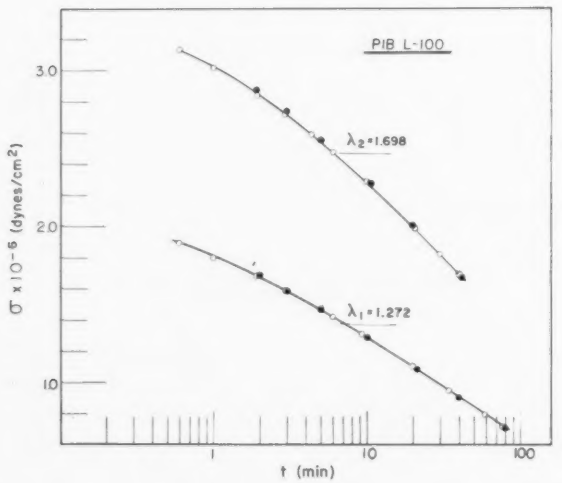

FIGURE 3. *Double step stress relaxation at 25 °C.*
First step with extension ratio $\lambda_1 = 1.272$ from 0 min to 80 min. Second step with extension ratio $\lambda_2 = 1.698$ from 80 min to 125 min.

4.3. Creep and Recovery

In a creep experiment a constant stress or a constant load (as in our experiment) is applied, and the resulting deformation is measured as a function of time. A prediction of the deformation with respect to time requires an inversion of eq (1) or, for the case of simple extension, eq (4). Because this is an arduous task even with the aid of a compr -r, we elected to check our

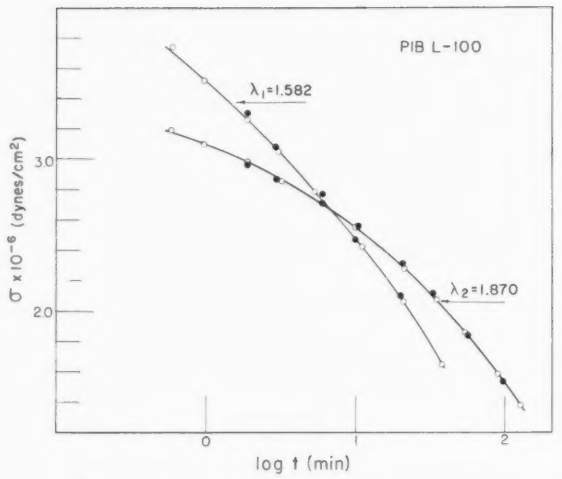

FIGURE 4. *Double step stress relaxation at 25 °C.*
First step with extension ratio $\lambda_1 = 1.582$ from 0 min to 40 min. Second step with extension ratio $\lambda_2 = 1.870$ from 40 min to 165 min.

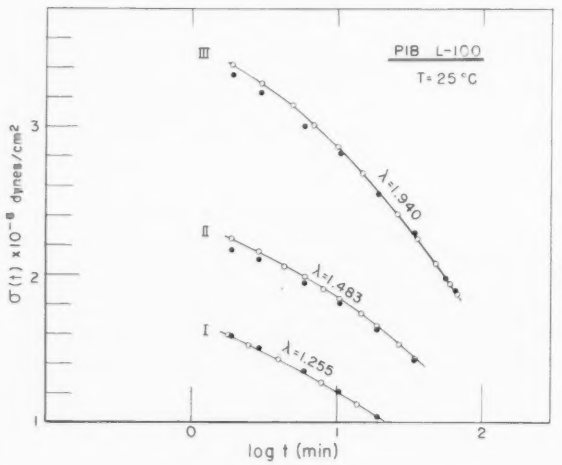

FIGURE 5. *Triple step stress relaxation at 25 °C.*
First step with extension ratio $\lambda = 1.255$ from 0 min to 20 min. Second step with extension ratio $\lambda = 1.483$ from 20 min to 60 min. Third step with extension ratio $\lambda = 1.940$ from 60 min to 125 min.

results by putting into the right-hand side of eq (4) the measured deformation history up to time t and calculating the stress.

Equation (4) can be written as

$$\sigma(t) = \left[\lambda^2(t) - \frac{1}{\lambda(t)}\right] H(\lambda, t) + \int_0^t \left[\frac{\lambda^2(t)}{\lambda^2(\tau)} - \frac{\lambda(\tau)}{\lambda(t)}\right] h\left(\frac{\lambda(t)}{\lambda(\tau)}, t-\tau\right) d\tau. \qquad (9)$$

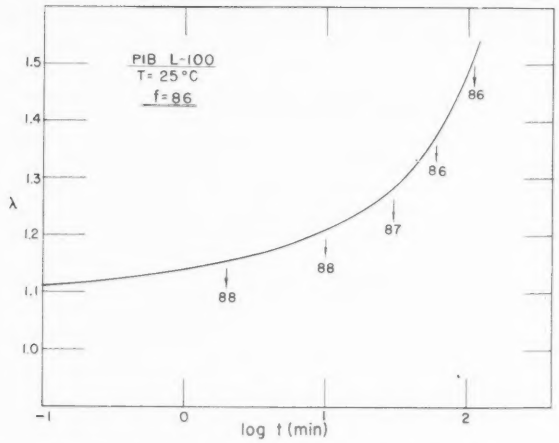

FIGURE 6. *Creep of polyisobutylene L-100 at 25 °C.*
The arrows point to the values of the load calculated using the measured history. The actual load was 86 g.

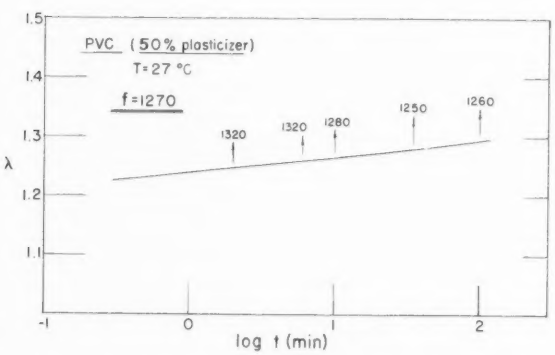

FIGURE 7. *Creep of plasticized polyvinylchloride at 27 °C.*
The arrows are used as in figure 6. The actual load was 1270 g.

The first term of the right-hand side of this equation is the stress necessary to hold a material at an extension ratio λ at time t after a single step deformation (vide eq (5)). The second term may be taken as a correction for deviations of the history of the deformation from that of a single step stress-relaxation experiment.

In figure 6 and figure 7 we exhibit the results of creep experiments on polyisobutylene and plasticized PVC. The line shows the value of λ as a function of time interpolated from direct measurements. The arrows point to values of the load predicted by eq (9) and the measured history of λ up to the indicated times. For PIB L-100 the measured load was 86 g and at the early times we again observe a 2-percent difference from the predicted load, while at the later times the agreement is excellent. The same is observed in figure 7 for plasticized PVC, for which the measured load was 1270 g. Again, this is to be expected, since we do not know $H(\lambda, t)$ accurately at the early times.

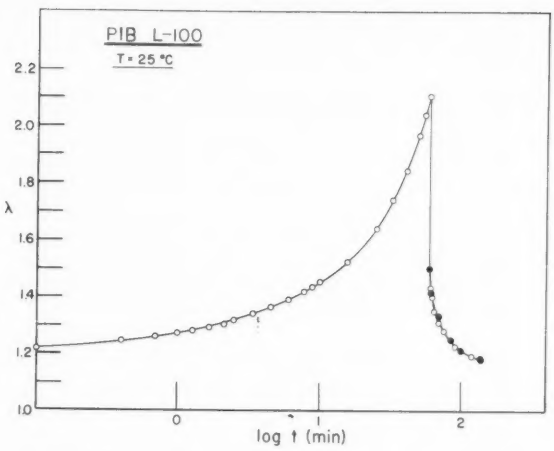

FIGURE 8. *Creep and recovery of polyisobutylene at 25 °C.*
The black circles indicate calculated values. White circles represent measured values.

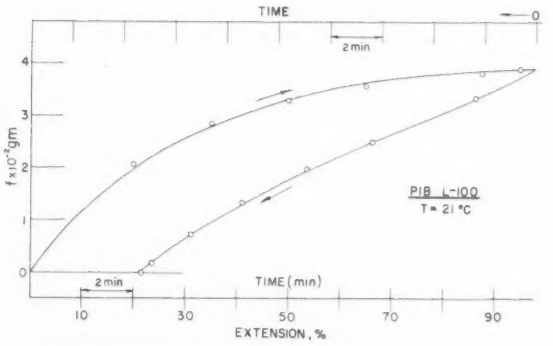

FIGURE 9. *Constant rate of strain of polyisobutylene at 21 °C.*
The circles represent calculated points.

During the recovery after creep, the part of the history for which $\lambda(t) < \lambda(\tau)$ may be considered as a relative compression. Since the part of the surface $H(\lambda, t)$ that we measured from stress relaxation involved only extensions with $\lambda > 1$, we made the assumption in our recovery calculations that eq (6) could be used to describe $H(\lambda, t)$ for values of $\lambda < 1$. In figure 8 we show the data obtained on creep and recovery. The black points are values of λ during recovery, calculated from the measured values of λ prior to recovery using eq (9) with σ set equal to zero.

4.4. Constant Rate of Strain

In experiments of this type, one of the clamps holding the sample is moved at a constant speed, while the other remained stationary. If there were no end effects due to clamping, the sample would be deformed at a rate proportional to the rate of separation of the clamps. In the experiment whose results we show in figure 9, we observed a constant rate of strain different

787-221 O-65—5

from what would be predicted by ignoring end effects. The open circles represent values of the stress calculated from eq (9). Here again, in order to predict the part of the curve where the motion is reversed, we made the same assumptions on extrapolation of $H(\lambda, t)$ to the λ region as we did for the creep recovery. Further, these data were obtained at a lower temperature than the stress-relaxation data. In order to correct for this temperature difference, we adjusted the stress-relaxation data using time-temperature superposition appropriate to the BKZ elastic fluid [2]. The $H(\lambda, t)$ surfaces at absolute temperatures T_0 and T_1 are related as follows [4]

$$T_0^{-1}\rho_0^{-1}H(\lambda, t)_{T_0} = T_1^{-1}\rho_1^{-1}H(\lambda, b_T t)_{T_1}$$

where ρ_0 and ρ_1 are the densities at T_0 and T_1, and b_T is a time shifting factor which can either be obtained experimentally or estimated from semiempirical equations. From previously reported work on polyisobutylene by Leaderman [5] the shifting factor b_T was evaluated to be 1.45 for a shift from 25 °C to 21 °C.

The experimental data and the calculated values shown in figure 9 are in excellent agreement. For creep, recovery, and constant rate of strain the calculation of each point involved graphical integration of the expression

$$\int_0^t \left[\frac{\lambda^2(t)}{\lambda^2(\tau)} - \frac{\lambda(\tau)}{\lambda(t)}\right] h\left(\frac{\lambda(t)}{\lambda(\tau)}, t-\tau\right) d\tau,$$

which is the second term of the right-hand side of eq (9). For values of τ close to t we used values of $h(\lambda, t)$ extrapolated to small values of t. In most of our calculations the first factor in the integrand approached zero as τ approached t, so that we expect the error due to extrapolation to be unimportant.

[4] The validity of this relation for large deformations has been tested and will be presented in a forthcoming publication.

The excellent agreement between the calculated and experimental values for several quite different time histories may be taken as establishing the form of the nonlinear dependence of stress on strain history given by eq (4) for elastomers in the rubbery region. The results reported here, being confined to simple extension, cannot be taken as establishing the potential function, U. They should be considered only as a test of the adequacy of the form in which time effects are brought into the BKZ theory. The development of a potential function, U, adequate for the description of different geometries of deformation will require detailed studies of different types of deformations.

The authors thank B. Bernstein and E. A. Kearsley for their criticism and suggestions on the preparation of this manuscript.

5. References

[1] B. Bernstein, E. A. Kearsley, and L. J. Zapas, A study of stress relaxation with finite strain, Trans. Soc. Rheology **VII**, 391–410 (1963).

[2] B. Bernstein, E. A. Kearsley, and L. J. Zapas, Thermodynamics of perfect elastic fluids, J. Res. NBS **68B**, No. 4, 103–113 (1964).

[3] B. Bernstein, Time-dependent behavior of an incompressible elastic fluid—Some homogeneous deformations, to be published in Acta Mechanica.

[4] L. J. Zapas, Correlations of an elastic fluid with experiments, paper presented at the Society of Rheology meeting, Pittsburgh, October 1964.

[5] H. Leaderman, J. Polymer Sci. **13**, 371 (1954).

(Paper 69A6–377)

JOURNAL OF RESEARCH of the National Bureau of Standards—A. Physics and Chemistry
Vol. 69A, No. 6, November–December 1965

Crystallography of Tetracalcium Phosphate *

Walter E. Brown[1] and Earl F. Epstein[2]

Tetracalcium phosphate, $Ca_4O(PO_4)_2$, has a monoclinic modification with the parameters $a=11.99$, $b=9.48$, and $c=6.97$ A, $\alpha=90.8°$, $z=4$, and space group $P2_1$ or $P2_1/m$. From a comparison with the work of Trömel and Zaminer, it is concluded that this salt has monoclinic and orthorhombic modifications with the most probable space groups being $P2_1$ and $P2_122_1$, respectively.

The results support the view that tetracalcium phosphate has a layer-type structural relationship to hydroxyapatite, $Ca_5(OH)(PO_4)_3$. This would account, in part, for variations in the compositions of apatitic materials in which the ratio Ca/P is greater than 10/6, and it suggests that tetracalcium phosphate may be present in the mineral of tooth and bone.

Key Words: Hilgenstockite, tetracalcium phosphate, hydroxyapatite, bone mineral, tooth mineral, unit cell, symmetry, twinning.

1. Introduction

Tetracalcium phosphate [2] (hilgenstockite), $Ca_4O(PO_4)_2$, the most basic calcium phosphate known, is a constituent of Thomas slag and of other basic calcium phosphate systems at high temperatures. Its major economic importance comes from the fact that it is a product of the reaction between phosphorus, oxygen and lime in the manufacture of iron [2, 22][3] and through this reaction has a significant role in controlling the properties of the metal. Since it has been prepared only at high temperatures and in systems substantially free of water, no biological significance has been attributed to it. The results of a single-crystal x-ray study reported here, however, give evidence that it has a structural relationship to hydroxyapatite, $Ca_5OH(PO_4)_3$, the principal inorganic component of hard tissues, and as a result the possible involvement of tetracalcium phosphate in biological processes cannot be ruled out.

Early optical studies on tetracalcium phosphate have yielded somewhat divergent results. Its symmetry has been described as triclinic [*18*], as monoclinic [*19*], and as orthorhombic [*8, 10, 16*]. Prominent among its crystallographic properties is a pronounced tendency to twin polysynthetically. Its x-ray powder diffraction patterns have similarities to those of hydroxyapatite, and this has been taken to indicate that the two salts are structurally related [*17, 20*]. The two sets of powder patterns are sufficiently different, however, to indicate extensive structural dissimilarities. Trömel and Zaminer [*23*] reported approximate unit-cell constants for tetracalcium phosphate, but made no note of the similarities of the unit-cell dimensions and x-ray intensities of the two salts.

2. Experimental Methods

Equimolar mixtures of $CaHPO_4$ and $CaCO_3$ were heated at 1,500 °C. for 24 hr in a vacuum in platinum foil envelopes. The preparations obtained in this manner were very light green in color. In one instance the central portion of the fused mass was not discolored, indicating that the contamination may have been platinum from the foil. The crystals used in the petrographic and x-ray studies were fragments obtained by lightly crushing the fused product. Examination with the petrographic microscope revealed no significant contaminant phases; the characteristic OH-stretching frequency in the infrared spectrum of hydroxyapatite was completely absent as were peaks attributed to other known calcium phosphates and to carbonate [*26*].

A single setting (a axis) of a small crystal (largest dimension less than 0.1 mm) was used to collect five equi-inclination Weissenberg patterns ($h=0$ through 4) and four precession photographs, $h0l$, $h1l$, $hk0$, and $hk1$, using Cu-Kα radiation ($\lambda=1.542$ A). Several precession photographs were also obtained from a larger crystal with an [021] setting.

3. Results

3.1. Optical Results

The crystalline fragments were birefringent, positive, with indexes of refraction $N_\alpha=1.644$, $N_\beta=1.645$, $N_\gamma=1.648$; wavy extinction was common; many displayed striations due to polysynthetic twinning.

*This investigation was supported in part by research grant DE-00572-02, Crystal Chemistry of Mineralized Tissue, to the American Dental Association from the National Institute of Dental Research.

[1] Research Associate, American Dental Association, National Bureau of Standards, Washington, D.C. 20234.
[2] National Institute of Dental Research, National Institutes of Health, Bethesda, Md. (present address, Department of Chemistry, University of Wisconsin, Madison, Wis.).

[3] Italicized figures in brackets indicate the literature references at the end of this paper.

In some particles the twin domains were wedge shaped; in others the striations were parallel and uniformly spaced. The direction of minimum index in any view of a crystal showing twinning striations was always nearly perpendicular to the striations and closely approximated $N = 1.644$. This shows that the composition plane of the twins studied optically was nearly perpendicular to the N_a direction. Extinction angles relative to the striations were variable and often unsymmetrical. The unsymmetrical extinction is believed to be due to the superpositioning of strain birefringence on the natural (and relatively weak) birefringence of the crystals. Variability in the extinction angle relative to the striations is in accord with the idea that the unique axis of the monoclinic crystal, a, lies in the composition plane. The extinction angles relative to the composition plane appeared to be smaller for the more birefringent views of the crystals.

The crystals for x-ray study were selected because they extinguished sharply and did not display twinning striations. Subsequent examinations showed, however, that most, if not all, of the particles would show twinning striations if rolled into the correct positions. On this basis alone it is probable, therefore, that the crystals used in the x-ray study were polysynthetic twins. As described below, the x-ray effects also revealed twinning.

3.2. X-Ray Results

The x-ray diffraction patterns were indexed on the basis of a monoclinic cell; unit-cell constants are summarized in table 1 along with the results of Trömel and Zaminer [23]. The axial notation was selected to conform with that for hydroxyapatite and the data of Trömel and Zaminer were converted to this notation by an interchange of their a and c axes. The cell dimensions of hydroxyapatite [12] and octacalcium phosphate, $Ca_8H_2(PO_4)_6 \cdot 5H_2O$ [7], are listed in table 1 for comparison.

TABLE 1. *Unit-cell dimensions of tetracalcium phosphate, hydroxyapatite, and octacalcium phosphate*

	Tetracalcium phosphate		Hydroxyapatite [11]	Octacalcium phosphate [7]
	This work	Trömel and Zaminer [21]		
a	11.99 Å	11.9 Å	9.432 Å	19.87 Å
b	9.48	9.4	9.432	9.63
c	6.97	7.0	6.881	6.87
α	90.8°	90°	90°	89.3°
β	90	90	90	92.2
γ	90	90	120	108.9
Cell contents	$Ca_{16}O_4(PO_4)_8$	$Ca_{16}O_4(PO_4)_8$	$Ca_{10}(OH)_2(PO_4)_6$	$Ca_{16}H_4(PO_4)_{12} \cdot 10H_2O$
d_{calc}	3.07	3.10		
d_{obs} [8]	3.06	3.06		
Space group	$P2_1$[a] or $P2_1/m$	$P2_122$	$P6_3/m$	$P\bar{1}$

[a] In this work it is concluded that the most probable space groups are $P2_1$ and $P2_122_1$.

The only systematic absences noted were $h00$ with $h = 2n+1$ and $00l$ with $l = 2n+1$. In this instance, for the monoclinic cell, only the a axis can be a two-fold screw axis, and the indication of a two-fold screw axis paralled to c probably derives from a similarity of the monoclinic structure to one that is orthorhombic. The even orders of $00l$ were intense.

No significant deviation from orthorhombic symmetry was detected in the intensities of the spots; all differences were so slight that they could easily arise from absorption by the crystal or its mount. The 0.8° deviation in α from 90° was clearly visible in both the Weissenberg and the precession photographs; this, along with the optical properties, the inability to detect a deviation from 90° in β and γ in the $h0l$ and $hk0$ precession photographs, and the indication for a 2_1 axis parallel to a led to the conclusion that the symmetry of the crystals studied by us was monoclinic rather than triclinic or orthorhombic. The value of α listed in table 1 was calculated by the method of triangulation [9] using reflections 042 and $0\bar{4}2$ in the zero layer Weissenberg pattern. The values obtained by measuring the separation of the twin spots in the Weissenberg patterns and by direct measurement of the angle in the $0kl$ precession photograph were in agreement with this value for α. It was noted, also, that the 042 and $0\bar{4}2$ reflections appeared in the a-rotation photograph with the expected separation. This is proof that the unit cell of the crystals studied by us was not orthogonal; the separation of spots in the Weissenberg and precession photographs could not have been caused by a multiple crystal with orthorhombic symmetry.

In the Weissenberg patterns for the smaller crystal, the spots could be divided into two groups according to their appearance, and each group could be associated with one member of a twin. The $00l$ spots of the two members were divided by a constant angular separation of 1.6°, but the $0k0$ spots were superimposed. The $0kl$ spots of the two members (e.g., the strong pair 042 and $0\bar{4}2$) differed in both angular and radial position. The relative positions of the two sets of spots, as they appeared in the zero-layer pattern, persisted through the layers, $h = 1$ through 4, indicating that the crystal could be described as a normal twin with b^* the twin axis, and (010) the composition plane, or, alternatively, as a parallel twin with c the twin axis and an $(hk0)$ the composition plane. The four precession photographs of the smaller crystal were fully in accord with these twin relationships; only the $hk1$ photograph showed splitting of the spots. The larger crystal also appeared to be twinned, but in this instance the twinning appeared to be different, corresponding either to a normal twin with c^* the twin axis and (001) the composition plane, or a parallel twin with b the twin axis. Of these four possible types of twins, the normal twins with b^* and/or c^* the twin axes are best supported by the optical study. The other mechanisms could not be eliminated, however, because of difficulties inherent with the petrographic study of anhedral crystals. Usually one should be able to distinguish between normal and parallel twinning of these types in a monoclinic crystal by comparison of spot intensities. In this instance, however, the pseudo-orthorhombic character of tetracalcium phosphate prevented making a distinction.

A precession photograph of a third crystal revealed hexagonal symmetry; the positions and intensities of the spots resembled those of the *hk*0 net of hydroxyapatite. Since no section through the reciprocal lattice of tetracalcium phosphate could yield this net, the third crystal must have been an extraneous phase. Schneiderhöhn, [*18*] has described the occurrence of hydroxyapatite in tetracalcium phosphate. The indexes of refraction of these two salts are so similar that hydroxyapatite would be extremely difficult to detect in tetracalcium phosphate. The absence of an (OH)-stretching band in the infrared spectrum suggests that the phase may have been "oxyapatite", $Ca_{10}O(PO_4)_6$ [*14*].

4. Discussion

4.1. Unit Cell

Our cell dimensions agree with those of Trömel and Zaminer within their indicated accuracy (table 1). Our dimensions yield axial ratios, $c/a = 0.581$ and $a/b = 1.254$. Axial ratios of Termier and Richard quoted by Groth [*11*] and by Winchell and Winchell [25], $A/B = 0.577$ and $C/B = 1.255$ are in good numerical agreement with ours, but they are algebraically inconsistent with ours unless the reciporcal of C/B is used for the ratio 1.255. The inversion of this ratio is confirmed by the average of the interfacial angles quoted by Groth, $(011) \wedge (010) = 51°36'$. This yields $B/C = \tan 51°36' = 1.262$.

The description of tetracalcium phosphate given in Groth and in Winchell and Winchell may be rewritten following the transformation *cab*/*ABC* as, "Monoclinic, $\alpha = 90° \pm$. Crystals (100) tablets with poor (100), (001) and (010) cleavages. Lamellar twinning on (010) and (001). $N_\beta = a$; N_γ near b.

4.2. Crystal Symmetry

The optical and x-ray results clearly show that the crystals studied by us had symmetry lower than orthorhombic. Three explanations would account for the discrepancy between our results and those of Trömel and Zaminer:

(1) Both monoclinic and orthorhombic modifications of tetracalcium phosphate may exist.

(2) Trömel and Zaminer [*23*] may have overlooked or discounted the evidence for monoclinic symmetry in the x-ray patterns.

(3) The crystals we studied may have been distorted because of thermal strain or impurities, or they may have been twinned mechanically when the fused mass was crushed.

The first possibility is strongly indicated by the high degree of pseudosymmetry apparent in our x-ray effects. On the other hand, it is easy to overlook the indications for lower symmetry in the x-ray patterns. The displacements between the twin spots, as seen in the Weissenberg pattern, are so slight that use of too large a crystal, or one that produced diffuse reflections, would make it difficult to detect distortion from orthorhombic symmetry. In this respect, the precession photographs are more revealing than Weissenberg photographs which display a 1.6° angular separation as a constant lateral displacement of only 0.8 mm. Evidence against the view that the lower symmetry is caused by distortion comes from three sources. First, the reflections in the single-crystal x-ray patterns appear too sharp to accord with a simple distortion mechanism. Second, the optical properties show a high degree of uniformity relative to the only morphological feature present (the composition plane) even though there is evidence of strain. Third, the twinning is inconsistent with orthorhombic symmetry; the indicated composition planes are pinacoids and twinning could not be detected optically. The twinning appears to be a persistent feature of tetracalcium phosphate preparations that has been frequently observed by optical methods [18, 19, 20]. Trömel and Zaminer indicate that an attempt to study the crystals with an optical goniometer was unsuccessful because the light reflections were not sharp. They attributed this difficulty to imbedded material. The unevenness in the crystal faces could be caused by polysynthetic twinning.

If, as seems likely, there is a high-temperature orthorhombic modification, and a low-temperature monoclinic modification, the two forms would differ by relatively minor atomic displacements. Of greater importance relative to the symmetry and structure of tetracalcium phosphate is the indication in our x-ray effects that c is a two-fold screw axis rather than a simple diad as reported by Trömel and Zaminer [23]. The presence of this two-fold screw axis would make the most probable orthorhombic space group $P2_12_12_1$ rather than $P2_122$. The absence of glide-plane effects in the diffraction patterns precludes all centrosymmetric orthorhombic space groups. The centrosymmetric monoclinic space group $P2_1/m$ is allowed by the x-ray effects observed by us. If tetracalcium phosphate truly exists in two modifications, it would be highly improbable that a centrosymmetric monoclinic space group is closely related to a noncentrosymmetric orthorhombic space group. It appears, therefore, that the most probable space groups are $P2_1$ and $P2_122_1$ for the monoclinic and orthorhombic situations, respectively.

4.3. Optical Properties

The indexes of refraction for tetracalcium phosphate reported here are in good agreement with the minimum and maximum values given by Schneiderhöhn [*18*] who also studied a synthetic preparation. Trömel and Zaminer [22] reported somewhat higher values ($N_\alpha = 1.649$, $N_\beta = 1.650$ and $N_\gamma = 1.658$) but these were for crystals obtained from a Thomas slag; it appears probable that the higher values were due to the presence of impurities. Trömel and Fix [*21*] reported that the indexes of refraction of a synthetic material were in agreement with those of Schneiderhöhn.

The negative birefringence reported by Schneiderhöhn is in disharmony with the positive birefringence found by Trömel and Zaminer [23] and by us.

There is complete disagreement between the optical directions of Termier and Richard ($N_\alpha \approx c$, $N_\beta = a$, and $N_\gamma \approx b$) [19] and those of Trömel and Zaminer ($N_\alpha = b$, $N_\beta = c$, and $N_\gamma = a$). It was noted above that N_α appeared to be normal to the composition plane. The two sets of indexes are in accord with this observation to the extent that in one N_α appears to be normal to (001) and in the other normal to (010), both of which are composition planes of the possible normal twins.

4.4. Twinning

Trömel and Zaminer state that the tabular plane is (110) although in their drawing it is given as (100) in agreement with Termier and Richard. Tabularity on (100) is consistent with a being the largest unit-cell dimension, since the long dimension of the cell is commonly the short dimension of the crystals.

Trömel and Zaminer give (100) as the plane of the polysynthetic twinning. This contrasts with the findings of Termier and Richard that (010) and (001) are the lamellar twin planes. The x-ray results described above for the two crystals are in accord with the findings of Termier and Richard in that the composition planes for the two normal twins would be (010) and (001). It is not unusual for pseudo-orthorhombic crystals (e.g., some felspars) to have more than one twinning mechanism.

4.5. Structural Relationship to Hydroxyapatite

We attach considerable significance to the apparent structural relationship between hydroxyapatite and tetracalcium phosphate revealed by the comparison of unit-cell dimensions in table 1. The cell constants of octacalcium phosphate, which is known to have a structural relationship to hydroxyapatite [5], are also listed in table 1. It is apparent that the unit-cell lengths, b and c, and the enclosed angle, α, are very nearly the same for all three salts. It was this similarity between the dimensions of octacalcium phosphate and hydroxyapatite, that was initially taken [6] to indicate that the two salts were structurally related. This was later verified by the structure determination of octacalcium phosphate [5]. Analogously it appears that a layer parallel to (100) in tetracalcium phosphate is structurally similar to one parallel to (100) in hydroxyapatite. Differences in the lengths of the a axes and the β and the γ angles relate to the ways in which the layers are stacked. Another indication of similarity between the structures of tetracalcium phosphate and hydroxyapatite was noted in the intensities of the $00l$ reflections. In hydroxyapatite, $00l$ reflections with odd values of l are missing because of two-fold screw axes parallel to c, and the even values of l are strong because all the heavy atoms and 12 of the 26 oxygens have z parameters that are multiples of 1/4. The intensities of the $00l$ reflections of octacalcium phosphate are strikingly similar to those of hydroxyapatite because the heavy atoms and most of the oxygens have z parameters similar to those in hydroxyapatite even though there are no mirror planes restricting them to these positions. The same situation is believed to apply to tetracalcium phosphate, but verification of such a relationship must await determination of the structure.

As noted above, the powder pattern of tetracalcium phosphate, like that of octacalcium phosphate, bears considerable resemblance to that of hydroxyapatite. This makes difficult the detection of tetracalcium phosphate in the presence of hydroxyapatite. This difficulty is compounded by the facts that the indexes of refraction of tetracalcium phosphate are close to those of hydroxyapatite ($n_\epsilon = 1.640$, $n_\omega = 1.646$) [7], and the infrared spectrum of tetracalcium phosphate has no strong peaks that distinguish it in the presence of hydroxyapatite.

Tetracalcium phosphate is the most basic calcium phosphate known, having a Ca/P ratio of 2/1. Hydroxyapatite has a Ca/P ratio of 5/3 and octacalcium phosphate has a ratio of 4/3. It is well known that hydroxyapatite exhibits broad variations in its composition. Most of the materials having low Ca/P ratios, in the range 5/3 to 4/3, are adequately explained on the basis that they are intracrystalline mixtures of octacalcium phosphate with hydroxyapatite [7]. McConnell [15] has emphasized that biological materials tend to have Ca/P ratios higher than 5/3, and he has suggested that such crystals may contain $(OH^-)_4$ and CO_3^{--} groups substituting for PO_4^{---} ions in the hydroxyapatite crystal. In view of the apparent structural relationship between tetracalcium phosphate and hydroxyapatite, it appears that the two salts also may form interlayered mixtures; it would then not be necessary to postulate substitution in the hydroxyapatite lattice to account for high Ca/P ratios. Interlayered crystals of hydroxyapatite and octacalcium phosphate contain the two salts, with their b and c axes collinear. In this connection it is significant that the lamellae of tetracalcium phosphate crystals are reported by Trömel and Zaminer to be parallel to the (100) as they should be if they are caused by interlayering with hydroxyapatite. However, more complex mixtures are possible also. The length of a of tetracalcium phosphate, 11.99 Å., is very nearly 3/2 of $d(100)$ of hydroxyapatite, 8.16 Å. As a result, it may be hypothesized that a block of tetracalcium phosphate two unit cells in thickness could occupy a three unit-cell space in the hydroxyapatite lattice without much distortion. An arrangement of this type, if randomized within the hydroxyapatite, would more nearly fulfill the conditions for a "solid solution" than would an interlayered mixture of the two salts.

A structural similarity between tetracalcium phosphate and hydroxyapatite has bearing on another aspect of considerable importance to the chemistry of apatitic materials. Natural and biological apatites are notorious in their ability to pick up and retain impurities, notably carbonate. There is yet no clear

understanding of the nature of the sites in which the impurities are retained. It is generally accepted that the presence of carbonate influences the chemical properties and the unit-cell dimensions of hydroxyapatite, and is correlated with a decrease in caries resistance. The ease with which tetracalcium phosphate reacts with CO_2 and the suggested structural relationship with hydroxyapatite introduces a new possibility for the understanding of these phenomena.

There is at this time no evidence that tetracalcium phosphate can form from an aqueous system, but this cannot be ruled out. The solubilities of calcium hydroxide and the calcium phosphates in a basic solution are extremely low. The range of compositions where tetracalcium phosphate would be more stable than hydroxyapatite, if one exists, would have to be very basic; the low solubilities would make it difficult to prepare pure tetracalcium phosphate from such systems. The possibility should be kept in mind, however, that under suitable conditions, kinetic factors may facilitate the incorporation of tetracalcium phosphate into the hydroxyapatite crystal.

5. References

[1] Bookey, J. B., J. Iron Steel Inst. **171,** 61 (1952).
[2] Bookey, J. B., Richardson, F. D., and Welch, A. J. E., J. Iron Steel Inst. **171,** 392 (1952).
[3] Bredig, M. A., Franck, H. H., and Füldner, H., Z. Elektrochem. **38,** 158 (1932).
[4] Bredig, M. A., Franck, H. H., and Füldner, H., Z. Elektrochem. **39,** 959 (1933).
[5] Brown, W. E., Nature, **196,** 1048 (1962).
[6] Brown, W. E., Lehr, J. R., Smith, J. P., and Frazier, A. W., J. Amer. Chem. Soc. **79,** 5318 (1957).
[7] Brown, W. E., Smith, J. P., Lehr, J. R., and Frazier, A. W., Nature, **196,** 1050 (1962).
[8] Bücking, H., and Linck, G., Stahl und Eisen, **7,** 245 (1887).
[9] Buerger, M. J., X-ray Crystallography, (John Wiley & Sons, New York, N.Y. 1942).
[10] von Grodbeck, A., and Broockmann, K., Stahl und Eisen, **4,** 141 (1884).
[11] Groth, P., Chemische Krystallographic, vol. 2, Wilhelm Engelmann, Leipzig (1908).
[12] Kay, M. I., Young, R. A., and Posner, A. S., Nature, **204,** 1050 (1964).
[13] Knüppel, H., and Osters, F., Arch. Eisenhüttenw. **32,** 799 (1961).
[14] Körber, F., and Trömel, G., Z. Elektrochem. **38,** 578 (1932).
[15] McConnell, D., Am. Mineral. **45,** 209–16 (1960).
[16] Miers, H. A., J. Chem. Soc. (London), **51,** 608 (1887).
[17] Schleede, A., Schmidt, W., and Kindt, H., Z. Elektronchem. **38,** 633 (1932).
[18] Schneiderhöhn, H., Mitt. Kais.-Wilh.-Inst. Eisenforschg., Düssledorf **14,** 34 (1932).
[19] Termier and Richard, Bull. Soc. franc. Mineral. **18,** 391 (1895), quoted in ref. 11.
[20] Trömel, G., Mitt. Kais.-Wilh.-Inst. Eisenforschg., Düsseldorf **14,** 25 (1932).
[21] Trömel, G., and Fix, W., Arch. Eisenhüttenw. **32,** 209 (1961).
[22] Trömel, G., Fix, W., and Fritze, H. W., Arch. Eisenhüttenw. **32,** 353 (1961).
[23] Trömel, G., and Zaminer, C., Arch. Eisenhüttenw. **30,** 205 (1959).
[24] Welch, J. H., and Gutt, W., J. Chem. Soc. (London), **1961,** 442.
[25] Winchell, A. N., and Winchell, H., The microscopical characters of artificial inorganic solid substances, Academic Press, New York (1964).

[26] We are indebted to Mr. B. O. Fowler, National Institute of Dental Research, for the infrared spectral examination.

(Paper 69A6–378)

JOURNAL OF RESEARCH of the National Bureau of Standards—A. Physics and Chemistry
Vol. 69A, No. 6, November–December 1965

Electrode Potentials in Fused Systems X. Measurement of Cation Concentration in Molten Salts Using Glass Membrane Electrodes

Kurt H. Stern and Susan E. Meador

(June 30, 1965)

A potentiometric method utilizing glass membrane reference electrodes in a concentration cell for the continuous measurement in situ of molten salt composition is presented. Relevant data for the AgCl-NaCl, AgBr-NaBr, and Ag_2SO_4-Na_2SO_4 systems are given. Using cells of the type

$$M_1|M_1A(a_R),\ M_2A(a_R')|\text{glass}|M_1A(a_2),\ M_2A(a_2')|M_1$$

where the a's are activities, the unknown mole fraction X_2 can be calculated from the equation

$$\log\left(\frac{X_2}{1-X_2}\right)=\frac{E}{2.303(RT/F)t'}-\log\left(\frac{1-X_R}{X_R}\right)$$

where t' is a concentration-independent constant of the system and X_R is the concentration of M_1A in the reference electrode. The method is capable of measuring X_2 in molten salt with an accuracy of better than 5 percent over a concentration range of 10^4. Application of the method to cations other than silver is discussed.

Key Words: Analysis, electrodes, glass, membranes, metal ions, molten salts, membrane electrodes.

1. Introduction

Increasing need for reliable reference electrodes in molten salts has led, in recent years, to the development of glass membrane electrodes for use in these media. These electrodes have a number of advantages over electrodes in which a liquid junction is maintained by means of pinholes, asbestos fibers, frits, etc., between the reference and indicator compartments of the cell. They are easily constructed, rugged, and maintain constant potential over relatively long periods of time.

A number of membrane electrode designs, all based on the Ag-Ag^+ equilibrium, have been published [1, 2, 3, 4].[1] In contrast to aqueous systems in which the glass electrode functions as *indicator electrode*, primarily for *p*H measurements, in molten salts it serves as a *reference electrode* with respect to which potential changes at other electrodes can be observed. For this application the primary requirement is stability and reproducibility, i.e., several electrodes of identical design should vary as little as possible in potential behavior. To be useful in this sense it is not necessary that the potential of such an electrode be known on any thermodynamic scale, e.g., with respect to the 1/2 $Cl_2(g)+e=Cl^-$ equilibrium of the chlorine electrode.

It is by now well known that when a glass electrode is combined with another electrode, either in a concentration or in a chemical cell, the measured emf will differ markedly from the Nernst value except in the special case in which the compositions on both sides of the glass are nearly identical [1]. The reason for this deviation lies in the selectivity of every glass for certain ions in the melt. Thus the ionic transport through the glass is relatively independent of melt composition; this leads to a membrane potential which must be taken into account, in addition to the Nernst value.

We have recently studied the behavior of glass in a variety of molten salt media in order to gain more information on ionic transport in glass [5, 6, 7, 8]. One result of this work is that it is now possible to use glass membrane reference electrodes for the determination of melt composition with respect to certain ions. Using these electrodes the melt composition can be measured continuously without disturbing the system by sampling. The purpose of the present paper is to give a more detailed discussion of those aspects of glass electrodes which pertain to the measurement of melt composition, particularly in the dilute range. We have illustrated this by new measurements of the AgCl-NaCl and AgBr-NaBr systems which were previously measured at higher silver concentrations, and of the Ag_2SO_4–Na_2SO_4 system which has not previously been studied.

[1] Figures in brackets indicate the literature references at the end of this paper.

We begin by discussing a simple concentration cell

$$M_1|M_1A(a_1),\ M_2A(a_1')\,|\,\text{glass}\,|\,M_1A(a_2),\ M_2A(a_2')|M_1$$

where the a's represent activities on the mole fraction scale. As shown previously the emf of this cell is

$$E_{\text{cell}}=(RT/F)\left[\ln a_2/a_1-\int_{a_1}^{a_2}\Sigma t_i\, d\ln a_i\right] \qquad (1)$$

which is formally also the potential of the cell with liquid junction. The chief difference between membrane and liquid junction potentials is that in the former case (a) only ions transported across the glass are included in the summation, and (b) if the melt contains more than 2 percent sodium, t_i is a constant in any cell and can be taken outside the integral [5]. For systems containing a single anion only cation terms are included in the summation. Since $\Sigma t_i=1$, eq (1) becomes

$$E_{\text{cell}}=(RT/F)t_{M_2^+}\ln[(a_2/a_1)(a_1'/a_2')]. \qquad (2)$$

Equation (2) is useful for the measurement of an unknown composition only if (a) $t_{M_2^+}$ is really independent of composition over the entire concentration range, (b) no changes occur in the reference electrode, e.g. composition changes by vaporization, and (c) the thermodynamic behavior of the melt, i.e., the activity coefficients of the components, are known. In a study of several silver halide-alkali halide solutions [5] it was found that (a) is satisfied if the melt contains at least 2 percent sodium, but not if it contains only the larger alkali metal cations. Condition (b) can be satisfied fairly well by using small diameter tubing. For the purpose of measuring melt composition condition (c) imposes a great inconvenience. In that case it is probably preferable to write eq (2) in terms of the mole fractions and to let $t_{M_2^+}$ absorb the nonideality of the system. Although this treatment can give misleading results if precise information on ion transport in glass is desired [7], it is justified when the purpose of the measurement is the determination of melt composition. In that case it is more convenient to write eq (2) in terms of the mole fraction, viz

$$E_{\text{cell}}=(RT/F)t'\ln[(X_2/X_1)(X_1'/X_2')] \qquad (3)$$

where

$$t'=t_{M_2^+}\left\{1+\frac{\ln\left[\left(\frac{\gamma_2}{\gamma_1}\right)\left(\frac{\gamma_1'}{\gamma_2'}\right)\right]}{\ln\left[\left(\frac{X_2}{X_1}\right)\left(\frac{X_1'}{X_2'}\right)\right]}\right\} \qquad (4)$$

and the γ's are the Raoult's law activity coefficients of the components. Making use of $X_1+X_1'=X_2+X_2'=1$ gives

$$E_{\text{cell}}=(RT/F)t'\ln[(X_2/X_1)(1-X_1)/(1-X_2)] \qquad (5)$$

t' can then be regarded as the empirical slope obtained in a calibration run when E_{cell} is plotted against $(RT/F)\ln[(X_2/X_1)(1-X_1)/(1-X_2)]$. In practice, it is most convenient to keep one side fixed as a reference and to vary the composition of the other side. Once t' has been determined for a particular melt and glass it can then be used in eq (5) to determine unknown concentrations in this system. For example if $X_1=X_R$, the reference composition, eq (5) can be written

$$\log\left(\frac{X_2}{1-X_2}\right)=\frac{E}{2.303(RT/F)t'}-\log\left(\frac{1-X_R}{X_R}\right). \qquad (6)$$

For dilute melts $1-X_2\simeq 1$.

2. Experimental Part

The general procedure has been outlined previously [4]. Some changes and refinements are discussed below. All experiments were carried out in alumina crucibles open to the atmosphere to duplicate more probable conditions of use.

2.1. Reference Electrodes

Preparation and pretreatment of the glass tubes and silver wire have been described [4]. The reference melt was prepared by melting appropriate quantities of the silver and sodium salts to give ~ 10 mole percent silver. This concentration appears to be suitable for both higher and lower unknown concentrations and minimizes the corrosion of the silver wire [8]. It proved most useful to make up 50 to 100 g of this composition at one time and then use 2 to 3 g of it in each electrode. Since microcrystalline segregation occurs in these melts on cooling (see below) the quenched melt was ground to a fine powder before use. Several representative portions were analyzed by electrodeposition. The precision of the analytical method was better than 1 percent.

2.2. General Procedure

Two identically prepared reference electrodes were placed in an alumina crucible containing ~ 120 g of the sodium salt and heated to the desired temperature. Weighed amounts of the corresponding silver salt were added. Emf's were measured between a 30 mil bare silver wire in the melt and each of the reference electrodes, as well as between the two reference electrodes, using a Leeds and Northrup K–3 potentiometer and electronic galvanometer. The melt, open to the atmosphere, was continually stirred with a stream of dried helium passing through a 4-hole ceramic tube.

In unstirred or insufficiently stirred melts the emf

was always lower, indicating that a layer of higher silver ion concentration surrounds the indicator electrode. The effect is most pronounced in dilute solution and decreases with rising concentration. With increasing stirring rate the emf increases to a limiting value. We assume that this emf then corresponds to that for the bulk melt.

In our initial experiments samples of the melts were taken by dipping a cold ceramic rod and quickly withdrawing it. Analyses of the samples frozen on the rod gave increasingly lower concentrations of silver than the values calculated with a constant transport number as the total silver concentration increased. In other words, if the analytical values are used to calculate transport numbers, these latter decrease markedly as the silver content of the melt rises. These observations are explicable in terms of the phase diagrams of various silver-alkali salts published by Zemczuzny [9]. He showed that in these systems the solid phase is always poorer in silver than the liquid in equilibrium with it. The difference increases with rising silver concentration. Apparently then, the liquid composition cannot be frozen into the solid even by rapid quenching. Consequently, samples for analysis were obtained by dipping a 2 ml platinum bucket attached to a long heavy platinum wire into the melt, equilibrating its temperature with the melt, withdrawing samples and pouring these as rapidly as possible onto a heavy metal tray. This procedure was repeated as many times as necessary to obtain a sufficient sample for analysis. Alternatively, samples were piped into a 9 mm wide fused silica tube equilibrated with the melt and poured into the tray. Samples were taken after the emf had been steady for at least 15 to 20 min. The temperature was measured with a chromel-alumel thermocouple which was placed into a glass tube immersed directly in the melt. Temperatures are estimated to be accurate to within $\pm 1°$.

2.3. Sources of Error

a. Stability and Reproducibility of Reference Electrodes

No extensive stability tests were carried out. However, we found that some electrodes kept in the melts in the 800 to 900 °C range for more than 8 to 10 hr began to deviate increasingly from newly immersed electrodes. This effect appears to be greater in the halides than in the sulfate. Since these electrodes are so easily and cheaply constructed we regard them as the "throw-away" type and suggest replacing them every 8 to 10 hr.

The potential between identically prepared reference electrodes immersed in the same melt varies randomly, but never exceeds 2 mV, this larger difference occurring in the sulfate system. In the halides the difference was usually a few tenths mV. For the determination of actual concentrations the limit of useful measurement is ~ 1 mV; for relative measurements of concentration ratios or rates of change, e.g., in kinetic studies [8], measurements are significant to ~ 0.1 mV.

b. Indicator Electrode Errors

The lower limit of measurable silver ion concentration is imposed by the nearly instantaneous corrosion of the indicator electrode in alkali metal salts. Thus, if an emf is measured between the reference and a bare silver wire in a pure alkali metal salt the calculated silver ion concentration is never lower than 10^{-5} [8]. This is presumably the concentration near the metal surface and not bulk melt composition.

Concentration gradients which build up near the electrode in dilute solution in unstirred melts require good stirring if the bulk composition is to be measured, the difference in emf of stirred and unstirred melts, can easily amount to 20 mV.

As the melt composition approaches that of the reference the emf decreases to zero. It is clear from eq (6) that the accuracy of the measurement must also decrease due to loss of significant figures from E since the uncertainty of the measurement remains fairly constant. It is thus advisable to use a reference composition which differs sufficiently from the melt to be measured to give an emf of ~ 0.1 V.

We illustrate the effect of several errors by calculating the consequence of these on the measured concentration. Since these errors differ somewhat for high and low concentrations, one example of each is given.

Nominal values: $X_R = 0.100$, $t' = 0.95$
$T = 1123$ °K
Case I: $E_{\text{cell}} = 0.300$ V $\quad X_2 = 0.743_7$
Case II: $E_{\text{cell}} = -0.400$ V $\quad X_2 = 1.43_5 \times 10^{-3}$

Error	X(I)	ΔX(I)	X(II) $\times 10^3$	ΔX(II) $\times 10^3$
$\Delta t' = 0.01$	0.739_8	0.004_1	1.47_3	0.03_8
$\Delta X_R = .001$	$.745_7$	$.002_0$	1.45_1	$.01_6$
$\Delta E = .001$	$.745_7$	$.002_0$	1.42_0	$.01_5$
$\Delta T = 2°$	$.742_7$	$.001_0$	1.44_3	.008

On the basis of the above calculation the accuracy of the method is estimated to be approximately 1 percent for fairly concentrated solutions, and 5 percent for dilute ($10^{-4} < X_2 < 10^{-2}$) ones. Since the major source of error results from uncertainties in t' it is important that the calibration run be carried out carefully. In particular, the melt compositions in the calibration must be accurately known. The required accuracy can be obtained by careful weighing of the components for silver-rich melts; for melts dilute in silver it is important that a representative sample of the liquid composition is obtained for analysis (see above).

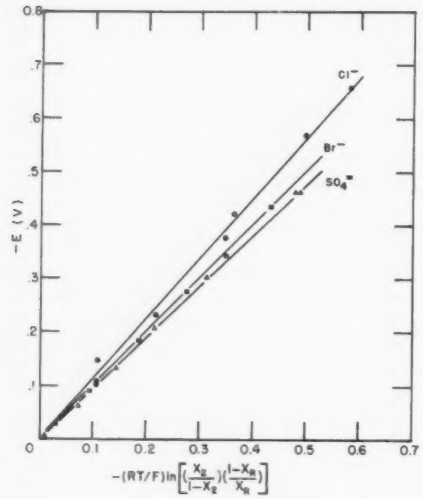

FIGURE 1. *Plot of eq (5).*
$X_1 = X_R$ for three Ag^+-Na^+ systems and Vycor glass membranes. The anions are shown to the right of the respective curves.

3. Results

Plots of eq (5) for the three systems of this study are shown in figure 1. The origin of course represents $X_1 = X_2 \simeq 0.1$. (Slightly different reference compositions were used in the three systems.) The fact that all three plots pass through the origin shows that asymmetry potentials are absent. The range of concentration represented by the plots is $10^{-4} < X_2 < 10^{-1}$. For each of the three systems the plot is linear, i.e., t' is constant over this range. The small differences in the slopes probably arise from differences in the activity coefficient terms. Combined with the data of previous studies [4, 5], these results show that the method presented in this paper is capable of measuring the silver ion concentration in $Ag^+ - Na^+$ melts over a range of 10^4. The values of t' and its standard deviation for the systems studied are

	t'	σ
AgCl − NaCl	1.148	0.0034
AgBr − NaBr	1.009	.008
$Ag_2SO_4 - Na_2SO_4$	0.965	.011

t' is independent of temperature between 800 and 900 °C [4]. A previous comparison between Vycor and Supremax [2, 4], two glasses of quite different composition, indicates that t' is nearly independent of the particular glass used.

4. Conclusions

A potentiometric method has been presented which utilizes glass membrane reference electrodes in a concentration cell arrangement for the continuous measurement of molten salt composition in situ with respect to certain ions.

The method was illustrated by measurements of three melts containing silver and sodium ions. However, the principles which are involved are applicable to other ions as well. For example, data on the CuCl-NaCl system have already been obtained [7]. Thus it should be possible to measure the concentration of any metal ion for which a reversible electrode can be constructed. At present the method appears to be limited to melts containing at least 2 mole percent sodium ion. Another limitation of the method is that the formation of insoluble oxides on and any appreciable corrosion of the metal wires used in the reference and indicator electrodes must be avoided. In some cases this may require an inert atmosphere over the measurement part of the system. In studying any particular system the applicability of the method must be tested and a calibration curve of the type shown in figure 1 constructed.

5. References

[1] J. O'M. Bockris, G. J. Hills, D. Inman, and L. Young, J. Sci. Instr. **33**, 438 (1956).
[2] R. Littlewood, Electrochim. Acta. **3**, 270 (1961).
[3] G. Danner and M. Rey, Electrochim. Acta. **4**, 274 (1961).
[4] K. H. Stern, J. Phys. Chem. **67**, 893 (1963).
[5] K. H. Stern and J. L. Stiff, J. Electrochem. Soc. **111**, 893 (1964).
[6] K. H. Stern, J. Electrochem. Soc. **111**, 208 (1965).
[7] K. H. Stern and S. E. Meador, unpublished results.
[8] K. H. Stern and W. E. Reid, Jr., J. Phys. Chem. **68**, 3757 (1964).
[9] S. F. Zemczuzny, Z. anorg. u. allgem. Chem. **153**, 47 (1926).

(Paper 69A6-379)

JOURNAL OF RESEARCH of the National Bureau of Standards—A. Physics and Chemistry
Vol. 69A, No. 6, November–December 1965

Publications of the National Bureau of Standards*

Selected Abstracts

Determination of the composition of complexes and their instability constant by calorimetry, I. The cuprocyanide complexes, A. Brenner, *J. Electrochem. Soc.* **112,** *No. 6, 611–621 (June 1965).*
The calorimetric method for determining the chemical formula and the instability constant of a complex ion involves the determination of the partial molal heat effects resulting from the separate addition of increments of each of the constituents of the complex to a complete range of mixtures of the constituents. The general mathematical derivations necessary for the utilization of the method have been developed, and the complex copper cyanides have been used as an example. The instability constants for the $Cu(CN)_3^{--}$ and the $Cu(CN)_4^{---}$ ions were found to be 1.0×10^{-5} and 2.3×10^{-3} respectively.

Mass spectrum of yttrium chloride vapor, J. D. McKinley *J. Chem. Phys.* **42,** *No. 6, 2245–2246 (Mar. 15, 1965).*
The mass spectrum of vapor in equilibrium with anhydrous yttrium chloride was examined by a Knudsen effusion technique between 800° and 1000 °K. Ions due to monomeric and dimeric vapor molecules were identified. Heats of evaporation and sublimation for the two species are: dimer $H_e = 86$ kcal/mol, $H = 74$ kcal/mol; monomer $H_e = 57$ kcal/mol, $H = 47$ kcal/mol.

Method of adjusting force constants and its application to H_2O, H_2CO, CH_2Cl and their deuterated molecules. T. Shimanouchi and I. Suzuki, *J. Chem. Phys.* **42,** *No. 1, 296–308 (Jan. 1, 1965).*
A new method for the adjustment of vibrational force constants is presented. It avoids some of the divergence difficulties which may be encountered in perturbation and least-squares procedures. The new method employs an efficient computer program to adjust an initial set of force constants in accordance with the requirement that each successive adjustment leads to a smaller sum of squared deviations between calculated and observed eigenvalues. Several variants of the procedure are given, and their application to a number of actual cases is discussed in detail.

Oxidation of asphalt flux with oxides of nitrogen, P. G. Campbell and J. R. Wright, *Ind. Engr. Chem. Prod. Res. Develop.* **4,** *No. 2, 121–128 (June 1965).*
An asphalt flux of southeastern United States origin was treated with various oxides of nitrogen as the oxidizing gases. Changes in physical and chemical properties were measured by infrared spectroscopy, softening points, and microviscometry. Reaction temperatures did not exceed 166° C. and gas flow rates were well below those used in the commercial air-blowing of asphalts. Nitrous oxide and nitric oxide, alone, gave very little reaction. Nitrogen dioxide, photosensitized nitrogen dioxide, and a nitric oxide-oxygen mixture reacted with the asphalt flux to produce coating-grade asphalts. The reaction time needed to produce a given asphalt softening point with photosensitized nitrogen dioxide, for example, was 1/20 that needed for air alone. Coating-grade asphalts made with oxides of nitrogen were more stable to photooxidation, and to film rupture at any given rate of shear, than was the commercial asphalt from the same flux. A correlation was observed between the extent of photooxidation of exposed asphalts and the changes in viscoelastic properties.

Vacuum-ultraviolet photolysis of ethane in liquid-nitrogen solution, J. A. Pirog and J. R. McNesby, *J. Chem. Phys.* **42,** *No. 7, 2490–2494 (Apr. 1, 1965).*
The photolysis of C_2H_6 in liquid nitrogen was studied at 1470 Å. It was found that the excited ethylene so produced, whose alternative paths are collisional deactivation and decomposition to acetylene plus hydrogen, was entirely deactivated by nitrogen with the acetylene quantum yield falling to zero at very low conversion.

$$C_2H_6^* \rightarrow C_2H_4^\dagger + H_2$$

$$C_2H_4^\dagger + M \rightarrow C_2H_4 + M$$

The excited ethane formed in the primary process is not deactivated by 10^{12} collisions per second with nitrogen. Excited ethylene formed by photolysis of ethylene at 1470 Å is not quenched by the nitrogen but is partially quenched by .001 mole % NO. Thus, electronically excited ethylene is partially deactivated by collisions at a rate of 10^9 sec^{-1}. No positive evidence for reaction of CH_3CH with N_2 was obtained.

Thermodynamic properties of neon from 25 to 300 °K between 0.1 and 200 atmospheres, R. D. McCarty and R. B. Stweart, *Advances in Thermophysical Properties at Extreme Temperatures and Pressures*, p. 84–97 (Am. Soc. Mech. Engr., New York, N.Y., 1965).
Selected P-ρ-T data for liquid and gaseous neon have been fitted to an analytical function. The selected data are the available experimental data, supplemented in regions of pressure and temperature where experimental data are not available by values calculated from the theory of corresponding states and a generalized equation of state. Deviation plots are given which indicate the accuracy with which the analytical function represents the experimental data. The uncertainty of the tabulated properties is also estimated. The equation of state and the zero pressure specific heat were used to calculate tables of density, entropy, and enthalpy for selected temperatures and pressures. These properties are also illustrated in temperature-entropy diagrams.

Work function measurements on field emitters with prescribed orientation, J. W. Little, T. E. Madey, and R. Klein, *J. Appl. Phys.* **36,** *No. 4, 1491–1492 (Apr. 1965).*
Field emitters oriented with a prescribed plane perpendicular to the emitter axis can be prepared simply and economically. This involves the use of the spark erosion technique to machine the emitter blanks from a single crystal rod that may be as small as 1/8" diameter. The method is described in detail, and examples of 100 and 111 oriented tungsten emitters are shown.

Adsorption of polymer molecules at low surface coverage, C. A. J. Hoeve, E. A. DiMarzio, and P. Peyser, *J. Chem. Phys.* **42,** *No. 7, 2558–2563 (Apr. 1, 1965).*
A statistical-mechanical treatment of a polymer molecule adsorbed on a solid surface is given. The surface coverage of adsorbed molecules is assumed to be sufficiently low that the interactions of the adsorbed polymer molecules with each other may be neglected. The partition function is derived for a polymer molecule with sequences of repeating units adsorbed at an interface and with other sequences (loops) held at the surface only at their ends. The assumption of Gaussian statistics for the loops leads to a formulation equivalent to that used for the helix-coil region in DNA molecules. A broad distribution of loop sizes is found, in contrast to Silberberg's theory in which a sharply peaked distribution is assumed. The latter theory predicts also small loops for all values of the adsorption free energy. In contrast, our theory predicts large loops and few units adsorbed for small adsorption free energies and small loops and more units adsorbed for larger adsorption free energies when the chains are sufficiently flexible. This result is also in partial disagreement with earlier theories that predict large loops, even for relatively large adsorption free energies. On the other hand, our theory predicts only a small number of loops and most units at the surface for stiff chains. A relationship between the initial slope of an adsorption isotherm and the molecular weight of the polymer is presented.

Effects of finite heat capacity on spin-lattice relaxation, R. L. Peterson, *Phys. Rev.* **137,** *No. 5A, A1444–A1448 (Mar. 1, 1965).*
The spin-lattice approach to equilibrium is studied for situations in which the "lattice" heat capacity, is not infinite. It is assumed that the spins and the "lattice" each have a well-defined temperature and that the bath either has been removed or is only very weakly coupled to the lattice. It is shown that asymptotically the magnetization relaxes exponentially with a relaxation time which can be very much different from T_1 (the spin-lattice relaxation time for an infinite lattice heat capacity), not only in numerical value but in its functional dependence upon temperature, magnetic field, and spin concentration. Some examples are presented in which the effect of the finite lattice is to "lock" the magnetization in at its initial value for times one to two orders of magnitude longer than the ultimate relaxation time.

Elastic resonances in electron scattering from He, Ne, Ar, Kr, Xe, and Hg, C. E. Kuyatt, J. A. Simpson, and S. R. Mielczarek, *Phys. Rev.* **138,** *No. 2A, A385–A385–A399 (Apr. 19, 1965).*
The transmission of electrons through the rare gases and mercury vapor has been examined as a function of electron energy, with energy resolution of about 0.04 eV. Many anomalies (resonances) localized in energy have been observed, totaling eleven in helium, six in neon, two each in argon and krypton, five in xenon, and thirteen in mercury. The interpretation of these resonances in terms of compound negative ion formation is discussed, and in several cases electron configurations are assigned to the negative ions. In helium, neon, xenon, and mercury, sharp decreases in transmission are observed which are attributed to the onset of inelastic processes. Definite identification of the inelastic processes in the case of helium enables calibration of the absolute electron energy scale to within ± 0.03 eV.

Electronic energy bands in $SrTiO_3$ and related oxide semiconductors, A. H. Kahn and A. J. Leyendecker, *Proc. 1964 Intern. Conf. Phys. of Semiconductors, Paris, pp. 33–39 (Physique des Semiconducteurs, Paris, France, 1964).*
A theoretical examination of the electronic energy bands of cubic strontium titanate has been performed by application of the LCAO (linear combination of atomic orbitals) method. Diagonal energies were determined from ionization potentials and crystalline fields based on a point charge model for the ions. The ionic charges were adjusted to give agreement with the observed energy gap. Overlap integrals were estimated from free ion wave functions. For the crystals studied, the calculations led to filled valence bands derived primarily from oxygen $2p$ orbitals and empty conduction bands derived predominantly from titanium $3d$ orbitals. In cubic strontium and barium titanates, there are six lowest conduction band ellipsoids lying along $<100>$ directions of k-space with minima probably at the edges of the Brillouin zone. The longitudinal mass is about 20–50 m_0 and the transverse mass about 1 m_0. Spin-orbit splitting removes degeneracy at $k=0$ and leads to additional conduction bands several hundredths of an electron volt above the lowest conduction band. Comparison is made with experimental data on conductivity, Hall effect, thermoelectric power, reflectivity, and soft x-ray emission. Results are in substantial agreement with experiment.

Identification of energy levels of negative ions, U. Fano and J. W. Cooper, *Phys. Rev.* **138,** *No. 2A, A400–A402 (Apr. 19, 1965).*
Levels of He^- at 57.1 and 58.2 and of Hg^- at 4.0_7, 4.2_9 and 4.3_7, whose observation is described in an accompanying paper, are identified spectroscopically as $2s^22p\ ^2P$, $2s2p^2\ ^2D$, $6s6p^2\ ^4P_{1/2,3/2,5/2}$, respectively. The identification procedure, which combines elements of spectroscopy and collision theory is described.

Influence of spin paramagnetism on superconductivity, R. A. Kamper, R. S. Collier, and Y. Ohori, *Phys. Rev.* **137,** *1A, A75–A77 (Jan. 4, 1965).*
The Ginsburg-Landau equations are modified to include a magnetic permeability which varies with the order parameter ψ according to the relation: $\mu = \mu_n\psi^2 + \mu_s(1-\psi^2)$. The influence of this on the predicted behavior of a superconducting film in a tangential magnetic field is investigated theoretically. A new value is derived for the upper limit of the critical field for a bulky superconductor and a thin film.

Interpretation of Ar^+-Ar collisions at 50 keV, U. Fano and W. Lichten, *Phys. Rev. Letters* **14,** *No. 16, 627–629 (Apr. 19, 1965).*
An interpretation of the mechanism of ion-atom collisions is presented and discussed.

Mass-spectrometric study of photoionization. II. H_2, HD, and D_2, V. H. Dibeler, R. M. Reese, and M. Krauss, *J. Chem. Phys.* **42,** *No. 6, 2045–2048 (Mar. 15, 1965).*
Mass spectrometric techniques have been used to obtain the photoionization efficiency curves for H_2, HD, and D_2 in the energy range 815 to 700 Å (15.2 to 17.7 eV). A qualitative description of the observed autoionization process, based on a theory proposed by Fano, is applied to an analysis of the results.

Multiple-band conduction in *n*-type rutile (TiO_2), J. H. Becker and W. R. Hosler, *Phys. Rev.* **137,** *No. 6A, A1872–A1877 (Mar. 15, 1965).*
The existence of multiple band conduction in n-type rutile for temperatures above ~ 40 °K is deduced from studies of the Hall coefficients and electrical conductivities from ~ 2 *to* 600 °K. This investigation emphasizes the anisotropy of the Hall coefficients, i.e., the Hall effect measured with magnetic fields along the a- and the c-axis, respectively (R_a and R_c). The pronounced temperature dependence of the ratio of these two coefficients can most easily be interpreted on the basis of two competing conduction processes. Measurements on samples with widely differing charge carrier concentrations prove that the conduction processes involved are due to intrinsic energy states of the crystal. The energy separation between the lowest conduction band and the bottom of the next higher one is calculated to be 0.05 ± 0.01 eV, where the indicated uncertainty denotes estimated limits of error. These concepts are consistent with recent band structure calculations. Impurity and surface conduction are shown to be negligible.

On the behavior of the compressibility along the critical isotherm, S. Y. Larsen and J. M. H. L. Sengers, *Advances in Thermophysical Properties at Extreme Temperatures and Pressures, pp. 74–75 (Am. Soc. Mech. Engr., New York, N.Y., 1965).*
In this note we comment on the use of analytical functions to describe the behavior of a system in the critical region, as proposed by Ulybin and Malyshenko, among others. We also investigate an apparent sharp disagreement noted by these authors between density gradients obtained optically and those derived from P-V-T data, in the critical region. We think that much of the disagreement arises from the way the P-V-T data were analyzed. We conclude that in the critical region the pressure vs. density isotherms are much flatter than has been inferred from P-V-T work. The consequent large gravitational effect together with the difficulty of determining the slope of the isotherm severely limit the use of P-V-T measurement for the investigation of detailed behavior of thermodynamic quantities in the vicinity of the critical point.

On the validity of the Lorentz-Lorenz equation near the critical point, S. Y. Larsen, R. D. Mountain, and R. Zwanzig, *J. Chem. Phys.* **42,** *No. 6, 2187–2190 (Mar. 15, 1965).*
Corrections to the Lorentz-Lorenz equation for the refractive index of a fluid have been evaluated, near the critical point, using Yvon's statistical mechanical theory of the refractive index, together with the Ornstein-Zernike asymptotic form of the two-particle correlation function. For argon, with reasonable values for the numerical parameters, the correction is smaller than one part in 10^4.

Polar modes of lattice vibration and polaron coupling constants in rutile (TiO_2), D. M. Eagles, *J. Phys. Chem. Solids* **25,** *No. 11, 1243–1251 (Nov. 1964).*
Published experimental infrared reflection data are analyzed to obtain information about the long wavelength polar modes of lattice vibration in rutile (TiO_2). Weighted sums of squares of effective charges are found, and are compared with the same quantities calculated on a simple ionic model. The continuum polarization model of electron-phonon interactions is extended to apply to crystals with several types of longitudinal polar phonons, and the results are used to discuss polaron theory in rutile.

Polaron coupling constants in $SrTiO_3$, D. M. Eagles, *J. Phys. Chem. Solids* **26,** *No. 3, 672 (Mar. 1965).*
Using the method described in an article on rutile (D. M. Eagles, to appear), the author has calculated the long wavelength longitudinal polar mode frequencies and coupling constants in $SrTiO_3$.

Pressure dependence of the internal field at the Co^{59} nucleus in a 99.5% Ni–0.5% Co alloy, L. H. Bennett, *J. Appl. Phys.* **36,** *No. 3, Pt. 2, 942–943 (Mar. 1965).*
The room temperature nuclear magnetic resonance absorption of Co^{59} in an alloy of 0.5 percent Co in Ni has been measured under hydrostatic pressures of up to 7 kbars. The change in the resonance frequency with pressure is $\Delta\nu/\rho = 159 \pm 5$ Hz/bar. This is in the same direction (increasing frequency for increasing pressure) as for Ni^{61} in Ni. The ratio of the resonance frequency to the change in frequency with pressure $\nu:\Delta\nu/\rho$ is 700 kbar for Co^{59} and 1100 kbar for Ni^{61} in Ni. The internal field at the Co^{59} nucleus decreases with increasing temperature more slowly than that at the Ni^{61} nucleus in Ni-rich Ni-Co alloys. This discrepancy in the temperature dependences remains as large, when plotted at constant volume, as it was at constant pressure.

Structure of electrodeposited lead dendrites, F. Ogburn, C. Bechtoldt, J. B. Morris, and A. deKoranyi, *J. Electrochem. Soc.* **112,** *No. 6, 574–577 (June 1965).*
Electrodeposited lead dendrites were grown and examined by x-ray diffraction and metallographically. Their structure was essentially that of two crystals having a twist relation about a common [111] pole which was normal to the flat surface of the two dimensional dendrites. Each dendrite contained many small voids or channels. The direction of growth was either about halfway between a $<211>$ direction of one crystal and a neighboring $<211>$ direction of the second crystal or halfway between $<110>$ direction.

SU(6) Clebsch-Gordan coefficients for the product 35×56, J. C. Carter, J. J. Coyne, and S. Meshkov, *Phys. Rev. Letters* **14,** *No. 13, 523–526 (Mar. 29, 1965).*
SU(6) Clebsch-Gordan coefficients for the product 35×56 have been calculated. They have been used to predict a new set of scattering amplitudes which relate widely different final states for reactions in which mesons are incident on proton targets.

The correlation of experimental pressure-density-temperature and specific heat data for parahydrogen, H. M. Roder, L. A. Weber, and R. D. Goodwin (*Proc. XI Intern. Congress Refrigeration, Munich, Germany, Aug. 1963*). *Prog. Refrig. Sci. Technol.* **1,** *187-191 (1963).*
The use of hydrogen in space vehicles and in nuclear devices demands the accurate knowledge of its mechanical and thermal properties.
As mechanical properties of parahydrogen nearly 1200 closely spaced P-ρ-T points have been measured between 14 and 100 °K and between 2 and 350 atm. The P-ρ-T surface was approximated by a large number of polynomials coupled with appropriate interpolation schemes. Use of the virial expansion allows extrapolation to pressures below 2 atm.
Thermal properties may be obtained after relating the experiment above to a second one in which the heat capacity at constant volume was determined for a variety of experimental conditions. At temperatures below critical these heat capacities are used as primary data, while at temperatures above critical they serve as check on the correlation between the statistically calculated specific heats and the P-ρ-T data. Further tests of the correlation arise when calculating thermodynamic functions.
From this correlation it is now possible to compute as function of pressure and temperature such quantities as specific volume, enthalpy, entropy, specific heat at constant volume, specific heat at constant pressure, sonic velocity, the Joule-Thomson coefficient and the heats of vaporization.

Transition from resonant to non-resonant line shape in microwave absorption, A. Ben-Reuven, *Phys. Rev. Letters* **14,** *No. 10, 349-351 (Mar. 8, 1965).*
A new expression is suggested to account for the variation with pressure of the spectral intensity distribution in microwave absorption lines of gases, with specific application to the ammonia inversion spectrum. This expression departs from the conventional Van Vleck Weisskopf expression by adding a new coupling parameter which is proportional to the gas density. The theory is tested by applying it to the observations of Bleaney and Loubser and of Birnbaum and Maryott on ammonia.

Infrared emission spectrum of HBr excited in an electric discharge. Determination of molecular constants, T. C. James and R. J. Thibault, *J. Chem. Phys.* **42,** *No. 4, 1450–1457 (Feb. 1965).*
The infrared emission spectra of HBr^{79} and HBr^{81} have been observed by exciting HBr in an electric discharge. Lines in the 1–0, 2–1, and 3–2 bands have been measured to an accuracy of the order of 0.01 cm^{-1}. Pure rotational transitions of HBr^{79} and HBr^{81} which were not resolved have also been observed and measured with an accuracy of the order of 0.2 cm^{-1}. Values are reported for ω_e, $\omega_e x_e$, $\omega_e y_e$ (only limits for this constant), B_e, D_e, α_e, β_e, γ_e, δ_e, and approximate values of H_0 and H_1 are also obtained. The results are found to be in agreement with Dunham's theory. Values of the potential constants a_1, a_2, and a_3 are calculated. The B_e values for HBr^{79} and HBr^{81} agree with calculations based on microwave measurements of DBr^{79} and DBr^{81}.

Mass spectrometric study of photoionization. III. Methane and methane-d_4, V. H. Dibeler, M. Krauss, R. M. Reese, and F. N. Harllee, *J. Chem. Phys.* **42,** *No. 11, 3791–3796 (June 1965).*
Photoionization efficiency curves for the molecule and fragment ions of CH_4 and CD_4 are obtained in the wavelength region 1000 to 600A. The electronic structure of the molecule ion is related qualitatively to the shape of the parent ionization efficiency curve and the implications of the complicated vibronic behavior of the CH_4^+ ion are discussed. A qualitative explanation is given for the observed isotope effect on the parent ionization efficiency curve and on the fragment ion threshold energies. More nearly correct values of $I(CH_4) = 12.71$ eV and $I(CD_4) = 12.87$ eV are obtained. Other thermochemical values deduced from the study are: $D(CH_3 - H) = 4.41$ eV, $D(CD_3 - D) = 4.55$ eV, $D(CH_2 - H) = 4.87$ eV, and $H_f(CH_2) = 4.07$ eV. Zero-point energy differences for methyl and methylene ions and neutrals are also estimated.

Phase equilibria studies in mixed systems of rare earth and other oxides, R. S. Roth, *Book, Progress in Science and Technology of the Rare Earths, ed. L. Ewring* **1,** *167–202 (Pergamon Press, Inc., New York, N.Y., 1964).*
This paper is a review of the phase equilibra data available on binary systems containing a rare earth oxide, Y_2O_3 or Sc_2O_3 as one component. The review is limited to the oxides of the trivalent rare earth ions only. The phase diagrams are shown when previously published and unit cell dimensions of all compounds are also given where known. From a discussion of the problems involved in the accurate measurement of high temperatures it is concluded that accurate melting point standards are needed for the temperature range 2000–2400 °C in air.

The value of the Faraday, W. J. Hamer and D. N. Craig, *J. Electrochem. Soc.* **111,** *No. 12, 1434 (Dec. 1964).*
This is a brief communication addressed to the Editor of the Journal of the Electrochemical Society briefly discussing the value of the Faraday.

Other NBS Publications

J. Res. NBS 69B (Math. and Math. Phys.), No. 3 (July-Sept. 1965), 75 cents.
A development of the theory of errors with reference to economy of time. M. D. Hersey. Prefatory note by C. Eisenhart.
Transversals and matroid partition. J. Edmonds and D. R. Fulkerson.
Some L_2 Markoff inequalities. L. F. Shampine.
Some theorems on the permanent. R. A. Brualdi and M. Newman.
On Kirchoff's law and its generalized application to absorption and emission by cavities. F. J. Kelly.
On a relation between two-dimensional Fourier integrals and series of Hankel transforms. J. V. Cornacchio and R. P. Soni.

On convex metrics. C. Witzgall.
Some extensions of Banach's contraction theorem. P. R. Meyers.
A variant of the two-dimensional Riemann integral. A. J. Goldman.
The use of finite polynomial rings in the factorization of the general polynomial. D. B. Lloyd.
A primal (all-integer) integer programming algorithm. R. D. Young.

J. Res. NBS 69C (Eng. and Instr.), No. 4 (Oct.-Dec. 1965), 75 cents.

Some applications of the wave front shearing interferometer. J. B. Saunders.
Precision method for evaluating primary aberrations of lenses with a Twyman interferometer. J. B. Saunders.
Comparators for voltage transformer calibrations at NBS. W. C. Sze.
Voltage dependence of precision air capacitors. J. Q. Shields.
Single crystal x-ray diffraction at high pressures. C. Weir, S. Block, and G. Piermarini.
The Sondheimer-Wilson-Kohler formula in platinum resistance thermometry. R. J. Corruccini.
Stress analysis of tape-wound magnet coils. J. Hord.
Centerline correction for precision roughness specimens. J. L. Chamberlin.
Electric currents and potentials resulting from the flow of charged liquid hydrocarbons through short pipes. M. R. Shafer, D. W. Baker, and K. R. Benson.
A transistor screening procedure using leakage current measurements. G. T. Conrad and D. C. Shook.

Radio Sci J. Res. NBS/USNC–URSI, 69D, No. 8, (Aug. 1965), $1.00.

"Ultra Low Frequency Electromagnetic Fields" Papers

Preface to "Ultra Low Frequency Electromagnetic Fields" Papers. W. H. Campbell and S. Matsushita.
Solar wind and its interaction with the magnetosphere. C. P. Sonnett.
Schumann resonances. J. Galejs.
Earth-ionosphere cavity resonances and the propagation of ELF radio waves. J. R. Wait.
Resonances of the earth-ionosphere cavity observed at Cambridge, England. M. J. Rycroft.
Experimental results on the dynamics of the *F* region. W. Becker, R. Rüster, and J. Klostermeyer.
Regular oscillations near 1 c/s observed at middle and low latitudes. L. Tepley.
Preliminary results of a micropulsation experiment at a conjugate points. R. E. Gendrin and V. A. Troitskaya.
Some characteristics of geomagnetic pulsations at frequencies near 1 c/s. W. H. Campbell and E. C. Stiltner.
Propagation of hydromagnetic waves in the magnetosphere. M. Sugiura.
Ionospheric pertubation (the roles played by the ionosphere in geomagnetic pulsations). S. Matsushita.
Effects of induced earth currents on low-frequency electromagnetic oscillations. A. T. Price. Equatorial effects. R. Hutton.
Interpretation of early magnetic transients caused by high-altitude nuclear detonations. S. L. Kahalas and P. Newman.
man.

Regular Contributions

A note on the application of pulse compression techniques to ionospheric sounding. D. C. Coll and J. R. Storey.
Comments on a paper "Measurement of the phase velocity of VLF propagation in the earth ionosphere waveguide" by F. K. Steele and C. J. Chilton. H. F. Bates.
Reply to H. F. Bates' Comments on "Measurement of the phase velocity of VLF propagation in the earth ionosphere waveguide" by F. K. Steele and C. J. Chilton. F. K. Steele and C. J. Chilton.

Radio Sci. NBS/USNC–URSI, 69D, No. 9, (Sept. 1965), $1.00.

Ground-based passive probing using microwave spectrum of oxygen. E. R. Westwater.
Response of NBS microwave refractometer cavities to atmospheric variations. R. O. Gilmer, R. E. McGavin, and B. R. Bean.
Effects of rocket outgassing on rf experiments. W. Pfister and J. C. Ulwick.
Further analysis of propagation of plasma waves in a "spoke-wheel" magnetic field. Richard R. Gold.
Measurement of group velocity of 17.8-kHz VLF radio waves. W. D. Westfall.
On the radio noise level at low and very low frequencies in polar regions. T. Stockflet Jørgensen.
Experimental study on the circular loop antenna immersed shallowly in a conducting medium. Keigo Iizuka.
Directivity of uniformly spaced optimum endfire arrays with equal sidelobes. M. T. Ma.
Extension of Fock theory for currents in the penumbra region. V. H. Weston.
Isometric-circle interpretation of bilinear transformation and its application to VSWR minimization. J. G. Rudolph and D. K. Cheng.
Magneto-ionic propagation in inhomogeneous media. Part I. Transverse propagation. B. K. Banerjea.
Magneto-ionic propagation in inhomogeneous media. Part II. Oblique propagation. B. K. Banerjea.
Editorial comment on the scientific papers of Lord Rayleigh (John William Strutt). J. R. Wait.

Radio Sci. J. Res. NBS/USNC–URSI, 69D, No. 10, (Oct. 1965), $1.00.

Irreversible power and radiation resistance of antennas in anisotropic ionized gases. K. S. H. Lee and C. H. Papas.
Scattering resonances of a cylindrical plasma. W. M. Leavens.
Radiation patterns from plasma enclosed cyclindrical hypersonic vehicles. J. H. Harris, A. T. Villeneuve, and L. A. Broca.
The Schumann resonances. R. K. Cole, Jr.
Atmospheric radio noise bursts in the LF band at Bangalore. S. V. C. Aiya and K. N. Lakshminarayan.
Influence of finite ground conductivity on the propagation of VLF radio waves. J. R. Wait and K. P. Spies.
Model experiments on propagation of groundwaves across an abrupt boundarў at perpendicular incidence. R. J. King and S. W. Maley.

Radio Sci. J. Res. NBS/USNC–URSI, Vol. 69D, No. 11 (Nov. 1965), $1.00.

Propagation of pulses in dispersive media. J. R. Wait.
An anisotropic electron velocity distribution for the cyclotron absorption of whistlers and VLF emissions. H. Guthart.
Nose whistler dispersion as a measure of magnetosphere electron temperature. H. Guthart.
Interference rejection capability of a switched radiometer. R. E. Clapp.
Atmospheric breakdown limitations to optical maser propagation. R. G. Tomlinson.
Phase steps and amplitude fading of VLF signals at dawn and dusk. D. Walker.
Propagation in a model terrestrial waveguide of nonuniform height theory and experiment. E. Bahar and J. R. Wait.
Comments on H. Volland's "Remarks on Austin's Formula." J. R. Wait.
The path integrals of LF/VLF wave hop theory. L. A. Berry and M. E. Chrisman.
Reactive loading of arbitrarily illuminated cylinders to minimize microwave backscatter. Kun-Mu Chen.
On the statistical theory of electromagnetic waves in a fluctuating medium (II) Mathematical basis of the analogies to quantum field theory (a digest). K. Furutsu.

Radio Sci. J. Res. NBS/USNC–URSI, Vol. 69D, No. 12 (Dec. 1965), $1.00.

Symposium on Planetary Atmospheres and Surfaces, May 1965:
I Session: Jupiter, as observed at long radio waves.
II Session: Jupiter, as observed at short radio waves.
III Session: Passive radio observations of Venus, Saturn. Mercury, Mars, and Uranus.
IV Session: Passive radio observations of the Moon.
V Session: Radar observations of the planets.
VI Session: Radar observations of the Moon.

Selected tables of atomic spectra. Atomic energy levels and multiplet tables Si II, Si III, Si IV, C. E. Moore, NSRDS–NBS3, Sec. 1 (June 25, 1965), 35 cents.

Electrical engineering units and constants, NBS Misc. Publ. 268 (June 1965), 10 cents, $6.26 a 100.

Transmission loss predictions for tropospheric communication circuits, P. L. Rice, A. G. Longley, K. A. Norton, and A. P. Barsis, NBS Tech. Note 101, Vol. **I** (May 7, 1965), $1.00.

Transmission loss predictions for tropospheric communication circuits, P. L. Rice, A. G. Longley, K. A. Norton, and A. P. Barsis, NBS Tech. Note 101, Vol. **II** (May 7, 1965), $1.00.

On the effect of heavy ions on I.F propagation, with special reference to a nuclear environment, J. R. Johler and L. A. Berry, NBS Tech. Note 313 (June 7, 1965), 45 cents.

Stability of two-phase annular flow in a vertical pipe, S. Jarvis, Jr., NBS Tech. Note 314 (June 7, 1965), 55 cents.

Grading of abrasive grain for grinding, CS271–65 (April 12, 1965), Supersedes SPR R118–50.

Gas chromotographic determination of the moisture content of grain, E. L. Weise, R. W. Burke, and J. K. Taylor, (Proc. 1963 Intern. Symp. Humidity and Moisture, Wash. D.C.), Book, Humidity and Moisture, ed. A. Wexler, Vol. **IV**, Principles and Methods of Measuring Moisture in Liquids and Solids, ch. 1, pp. 3–6 (Reinhold Publ. Corp., New York, N.Y., 1965).

Isotopic fractionation of uranium in sandstone, Powder River Basin, Wyoming, and Slick Rock District, Colorado, J. N. Rosholt, A. P. Butler, E. L. Garner, and W. R. Shields, Econ. Geol. **60**, No. 2, 199–213 (Mar.-Apr. 1965).

On the twilight sodium emission-2. A theoretical model of sodium abundance, M. Gadsden, Ann. Geophys. **20**, No. 4, 383–396 (Oct.-Dec. 1964).

Strength of fingernails, R. W. Young, S. B. Newman, and R. J. Capott, J. Invest. Dermatol. **44**, No. 5, 358–360 (Dec. 23, 1964).

A miniature helium turbo-expander for cryogenic refrigeration systems, M. T. Norton, (Proc. XI Intern. Congress Refrigeration, Munich, Germany, Aug. 1963), Prog. Refrig. Sci. Technol. **1**, 131–135 (1963).

A simple method for measuring the amount of granular materials in sulfur mortars, C. L. Thompson, Mater. Res. Std. **5**, No. 5, 242–243 (May 1965).

A waveguide noise standard, C. K. S. Miller, W. C. Daywitt, and E. Campbell, (Proc. Intern. Measurements Conf.), Acta IMEKO **3**, 371–382 (1964).

A standard for extremely low values of spectral irradiance, R. Stair, W. B. Fussell, and W. E. Schneider, Appl. Opt. **4**, No. 1, 85–89 (Jan. 1965).

Commercial carbon composition resistors as pressure transducers, C. E. Miller, J. W. Dean, and T. M. Flynn, Rev. Sci. Instr. **36**, 231–232 (Feb. 1965).

Human engineering in the design of a console for the comparison of volt boxes, P. H. Lowrie, Jr., 19th Annual Instr. Soc. Am. Conf. Exhibit, Preprint No. 12.1–3–64, pp. 1–8 (Oct. 12–15, 1964).

Maintenance of maring electronic equipment by personnel not trained in electronic maintenance, G. Shapiro and G. J. Rogers, Proc. Annual Tanker Conf. American Petroleum Institute, pp. A–1–A–18 (June 1965).

Optical instrumentation for the biologist: Microscopy, J. R. Meyer-Arendt, Appl. Opt. **4**, No. 1, 1–9 (Jan. 1965).

Precision detector for complex insertion ratio measuring systems, C. M. Allred and R. A. Lawton, IEEE Trans. Instr. Meas. **IM–13**, No. 2 & 3, 76–81 (June–Sept. 1964).

Stress corrosion cracking of metals, H. L. Logan, Metals Engr. Quart. 5, No. 2, 32–38 (May 1965).

The effect of a fatigue crack on the fatigue strength of an aluminum alloy, J. A. Bennett, Mater. Res. Std. **5**, No. 5, 235–239 (May 1965).

The role of cryogenics in the production of high and ultra-high vacuum, L. O. Mullen and M. J. Hiza, Cryogenics **4**, No. 6, 387–394 (Dec. 1964).

A method for the computation of the error function of a complex variable, O. N. Strand, Math. Comp. **XIX**, No. 89, 127–129 (Jan. 1965).

Bounds for class numbers, M. Newman, Proc. Pure Mathematics, Vol. VIII, Theory of Numbers, p. 70–77 (Am. Math. Soc., 1965).

Comment on "The use of transforms to sum array factors, M. T. Ma, IEEE Trans. Ant. Prop. **AP–13**, No. 1, 174 (Jan. 1965).

Distribution of student's t in samples from a rectangular universe, M. M. Siddiqui, Rev. Intern. Stat. Inst. **32**, No. 3, 242–250 (1964).

Mathematical programming models for selection of diets to minimize weighted radionuclide intake, H. J. Bracken, Environmental Health Series: Radiological Health, Public Health Serv. Publ. 999–R–4 (Dept. Health, Education, and Welfare, Wash. D.C., Aug. 1963).

A comparison between the National Bureau of Standards two-pressure humidity generator and the National Bureau of Standards hygrometer, S. Hasegawa, R. W. Hyland, and S. W. Rhodes, (Proc. 1963 Intern. Symp. Humidity and Moisture, Wash., D.C.), Book, Humidity and Moisture, Measurement and Control in Science and Industry, ed. A. Wexler, Vol. **3**, Fundamentals and Standards, ch. 22, pp. 455–459 (Reinhold Publ. Corp., New York, N.Y., 1965).

A pneumatic bridge hygrometer for use as a working humidity standard, L. Greenspan, (Proc. 1963 Intern. Symp. Humidity and Moisture, Wash., D.C.), Book, Humidity and Moisture, Measurement and Control in Science and Industry, ed. A. Wexler, Vol. **3**, Fundamentals and Standards, ch. 20, pp. 433–443 (Reinhold Publ. Corp. New York, N.Y., 1965).

Letter to the Editor, C. H. Page, Metrologia **1**, No. 2, 73–74 (Apr. 1965).

The evolution of designed experiments, W. J. Youden, Proc. IBM Scientific Computing Symp. Statistics, pp. 59–67 (West Chester County, New York, Sept. 1963).

The NBS standard hygrometer, A. Wexler and R. W. Hyland (Proc. 1963 Intern. Symp. Humidity and Moisture, Wash., D.C.), Book, Humidity and Moisture, Measurement and Control in Science and Industry, ed. A. Wexler, Vol. **3**, Fundamentals and Standards, ch. 19, pp. 389–431 (Reinhold Publ. Corp., New York, N.Y., 1965).

Characteristics of a Raman laser excited by an ordinary ruby laser, H. Takuma and D. A. Jennings, Proc. IEEE **53**, No. 2, 146–149 (Feb. 1965).

Determination of the probability distribution of the number of secondary electrons, Z. Bay and G. Papp, IEEE Trans. Nuclear Sci. **NS–11**, No. 3, 160 (June 1964); Elec. Commun. 40, No. 1, 134 (1965).

Drift-free Mossbauer spectrometer, F. C. Ruegg, J. J. Spijkerman, and J. R. DeVoe, Rev. Sci. Instr. **36**, No. 3, 356–359 (Mar. 1965).

Ice nucleation by photolyzed silver iodide, G. Burley, Phil. Mag. **10**, 527 (Sept. 1964).

Longitude distribution of proton flares, C. S. Warwick, Astrophys. J. **141**, No. 2, 500–504 (Feb. 15, 1965).

Plans for proposed new tables of the thermodynamic properties of moist air, J. C. Davis, T. K. Faison, Jr., and P. R. Achenbach (Proc. 1963 Intern. Symp. Humidity and Moisture, Wash., D.C.), Book, Humidity and Moisture, Measurement and Control in Science and Industry, ed. A. Wexler, Vol. **3**, Fundamentals and Standards, ch. 11, pp. 315–320 (Reinhold Publ. Corp., New York, N.Y., 1965).

Optical quenching of photoconductivity near the band edge in CdS, L. Grabner, Phys. Rev. Letters **14**, No. 14, 551–554 (Apr. 5, 1965).

Stimulated Brillouin scattering in the off-axis resonator, H. Takuma and D. A. Jennings, Appl. Phys. Letters **5**, 239–241 (Dec. 1964).

The absolute photometry of the zodical light, L. L. Smith, F. E. Roach, and R. W. Owen, Planet. Space Sci. **13**, 207–217 (Pergamon Press Ltd., Northern Ireland, 1965).

X-ray spectrochemical analysis of material: cement and dental alloys, B. L. Bean and B. W. Mulligan, Am. Soc. Testing Mater. Spec. Tech. Publ. 373, Application of Advanced and Nuclear Physics to Testing Materials, pp. 25–45 (June 17, 1965).

Measurement and standardization of LF to UHF electrical quantities. Sketch of recent world-wide developments, M. C. Selby, Prog. Radio Sci. 1960–1963, Vol. **I**, Radio Standards and Measurements, pp. 45–55 (Elsevier Publ. Co., Amsterdam, The Netherlands, 1965).

Radio meteorology, J. W. Herbstreit, Science **147**, No. 3653, 76–78 (Jan. 1, 1965).

Stratospheric moisture measurements using infrared spectroscopy, D. M. Gates, (Proc. 1963 Intern. Symp. Humidity and Moisture, Wash., D.C.), Book, Humidity and Moisture Measurement and Control in Science and Industry, Vol. **2**, Applications, Sec. VI, pp. 446–449 (Reinhold Publ., Corp., New York, N.Y., 1965).

The use of electromagnetic signals emitted from nuclear explosions to study long-range VLF propagation, A. G. Jean and J. R. Wait, J. Geophys. Res. **70**, No. 5, 1258–1261 (Mar. 1, 1965).

The uses of oblique ionograms in frequency utilization, K. Davies, ITU Telecommun. J. **31,** No. 10, 1–7 (Oct. 1964).

Tropospheric propagation, P. L. Rice and J. W. Herbstreit, Advan. Electron. Electron Phys. **20,** 199–259 (1964).

Acid bases in analytical chemistry, I. M. Kolthoff, S. Bruckenstein, and R. G. Bates, Interscience Reprint from Kolthoff-Elving "Treatise on Analytical Chemistry", Pt. I, Sec. B, ch. 10, pp. 361–542 (Interscience Publ. Inc., New York, N.Y., 1965).

Acids and bases in alcohol-water solvents, R. G. Bates, Chem. Chem. Ind. (Japan) **18,** 680–685 (May 1965).

Configuration interaction calculation of H_3 and H_2, C. Edmiston and M. Krauss, J. Chem. Phys. **42,** No. 4, 1119 (Feb. 1965).

Constancy of a modified Weston standard cell over long periods, W. C. Bosburgh and R. G. Bates, J. Electrochem. Soc. **III,** No. 8, 997–988 (Aug. 1964).

Crystal structure of gamma-dicalcium silicate, D. K. Smith, A. Majumdar, and F. Ordway, Acta. Cryst. **18,** 787 (Apr. 1965).

Designation of ligand positions in coordination complexes. R. F. Pasternack and P. M. McDonnell, Inorg. Chem. **4,** No. 4, 600–602 (Apr. 1965).

Determination of reducing end-groups by reactions with C^{14}-labeled cyanide, H. S. Isbell, Book, Methods in Carbohydrate Chemistry, ed. R. L. Whistler, **5,** 249–250 (Academic Press Inc., New York, N.Y., 1965).

Direct observation of the decomposition of multiply charged ions into singly charged fragments, K. E. McCulloh, T. E. Sharp, and H. M. Rosenstock, J. Chem. Phys. **42,** No. 10, 3501–3509 (May 1965).

Electron impact studies of aromatic hydrocarbons. III. Anthracene and naphthalene, R. J. Van Brunt and M. E. Wacks, J. Chem. Phys. **41,** No. 10, 3195–3199 (Nov. 15, 1965).

Electron paramagentic resonance and the primarily 3d wavefunctions of the tetrachlorocuprate ion, M. Sharnoff, J. Chem. Phys. **42,** No. 10, 3383–3395 (1965).

Electron paramagnetic resonance spectra of zinc-doped copper acetate monohydrate, G. F. Kokoszka, H. C. Allen, Jr., and G. Gordon, J. Chem. Phys. **42,** No. 10, 3693–3697 (May 15, 1965).

Electron paramagnetic resonance spectrum of bis-8-hydroxyquinolate copper (II) dihydrate, G. F. Kokozska, H. C. Allen, Jr., and G. Gordon, J. Chem. Phys. **42,** No. 10, 3730–3731 (May 15, 1965).

Extinction coefficients of triplet ↔ triplet transitions in aromatic compounds, R. A. Keller and S. G. Hadley, J. Chem. Phys. **42,** No. 7, 2382 (Apr. 1965).

Franck-Condon factors for polyatomic molecules, T. E. Sharp and H. M. Rosenstock, J. Chem. Phys. **41,** No. 11, 3453 (Dec. 1, 1964).

High-precision coulometric titrations with special reference to the determination of uranium, J. K. Taylor and G. Marinenko, Proc. Conf. High-Precision Analysis of Substances of Interest to Nuclear Energy, Jan. 18–22, 1965 pp. 147–161 (Bureau Central des Mesures Nuclaires, Brussels, Belgium, 1965).

High pressure single crystal studies of ice VI, S. Block, C. E. Weir, and G. J. Piermarini, Science **148,** 947 (1965).

High temperature microwave spectroscopy: AlF and AlCl, D. R. Lide, J. Chem. Phys. **42,** No. 3, 1013–1018 (Feb. 1965).

Improved measurement of the electric dipole moment of the hydroxyl radiacal, F. X. Powell and D. R. Lide, J. Chem. Phys. **42,** No. 12, 4201–4202 (June 1965).

Interaction of carbon dioxide with carbon adsorbents below 400 °C., V. R. Deitz, F. G. Carpenter, and R. G. Arnold, Carbon **1,** 245 (1964).

Isotopic fractionation of uranium related to roll features in sandstone, Power River Basin, Wyoming and Colorado Plateau, J. N. Rosholt, A. P. Butler, E. L. Garner, and W. R. Shields, Econ. Geol. **60,** No. 2, 199–213 (Mar.–Apr. 1965).

Method of obtaining a range of current densities with a resistive cathode, M. Brenner and A. Brenner, Plating **56,** No. 6, 527–530 (June 1965).

National Standard Reference Data Program, E. L. Brady and S. A. Rossmassler, D. C. Libraries **35,** No. 4, 57–61 (Oct. 1964).

Negative surface ionization of complex molecules, J. T. Herron, H. M. Rosenstock, and W. R. Shields, Nature **206,** No. 4984, 611 (May 1965).

Nonequilibrium chemical excitation and chemical pumping of lasers, K. E. Shuler, T. Carrington, and J. C. Light, Appl. Opt. Suppl. **2,** pp. 81–104 (1965).

Photolysis of ethane at the argon resonance lines 1067 and 1048 Å, A. H. Laufer and J. R. McNesby, J. Chem. Phys. **42,** No. 9, 3329–3330 (May 1, 1965).

Photooxidation of asphalts in the presence of ozone, J. R. Wright and P. G. Campbell, ACS Div. of Petroleum Chem. Preprints **9,** No. 3, 161 (Aug. 1964).

Precise assay of copper using small samples, T. J. Murphy and J. K. Taylor, Anal. Chem. **37,** No. 7, 929–931 (June 1965).

Pressure-induced trapping phenomenon in silver iodide, H. C. Duecker and E. R. Lippincott, Science **146,** 1295–1297 (1964).

Pyrolytic technique, G. M. Brauer, J. Polymer Sci., Pt. C, No. 8, 3–26 (1965).

Radiochemical methods of analysis (Report on Salzburg Conference), W. W. Meinke, Science **147,** No. 3654, 182–183 (Jan. 1965).

Recommended materials and practices for use with cryogenic propellants, A. F. Schmidt, AIR **839,** 29 pages (SAE Inc., New York, N.Y., Jan. 1965).

Rotational constants of excited vibrational states of $^{14}N_2^{16}O$, W. J. Lafferty and D. R. Lide, J. Mol. Spectry. **14,** No. 4, 407–408 (Dec. 1964).

Second order effects in the phosphorescene of benzophenone crystals at 77 °K, R. A. Keller, J. Chem. Phys. **42,** No. 11, 4050–4051 (June 1965).

Spectrophotometric determination of the rate of dissociation of tetrafluorohydrazine behind a shock wave, L. M. Brown and B. Darwent, J. Chem. Phys. **42,** No. 6, 2158–2165 (Mar. 15, 1965).

Standardization of plastics in the U.S., G. M. Kline, Courrier de la Normalisation No. 182, pp. 280–282 (Mar.–Apr. 1965); Mod. Plastics **42,** No. 9, 176 (May 1965).

Substoichiometric radiometric analysis: Determination of trace amounts of cobalt, A. R. Landgrebe, L. T. McLendon, and J. R. DeVoe, Book, Radiochemical Methods of Analysis, II, 321–333 (Intern. Atomic Energy Agency, Vienna, Austria, 1965).

The constitution of $CuFe_2O_4$, C. F. Jefferson, J. Appl. Phys. **36,** No. 3, 1165–1166 (Mar. 1965).

The gas-phase photolysis of cyclohexane in the far ultra-violet: Modes of decomposition of the neutral excited cyclohexane molecule and reactions of the parent cyclohexane ion, R. D. Doepker and P. Ausloos, J. Chem. Phys. **42,** No. 11, 3746 (June 1, 1965).

The place of radiochemical methods of analysis: Today and tomorrow, W. W. Meinke, (Proc. Intern. Atomic Energy Agency Symp. Radiochemical Methods of Analysis, Salzburg, Austria, Oct. 19–23, 1964), Book, Radiochemical Methods of Analysis I, 13–19 (Intern. Atomic Energy Agency, Vienna, Austria, 1965).

The vibrational assignment of sulfuryl fluoride, D. R. Lide, D. E. Mann, and J. J. Comeford, Spectrochim. Acta. **21,** 497 (1965).

Vacuum-ultraviolet photolysis of ethane at high temperature, R. F. Hampson, Jr., and J. R. McNesby, J. Chem. Phys. **42,** No. 6, 2200–2208 (Mar. 15, 1965).

A comparison of atomic frequency standards, R. E. Beehler and R. C. Mockler, Book, Progress in Radio Science 1960–1963, Vol. **I,** Radio Standards and Measurements, pp. 20–26 (Elsevier Publ. Co., Amsterdam, The Netherlands, 1965).

A DC–RF substitution error in dual element bolometer mounts, G. F. Engen, IEEE Trans. Instr. Meas. IM–13, No. 2 & 3, 58–64 (June–Sept. 1964).

A mechanistic model for the limits of auditory perception, E. L. R. Corliss, Proc. Symp. Models for the Perception of Speech and Visual Form, Boston, Mass., Nov. 11–14, 1964 (Air Force Research Center, Cambridge, Mass., 1964).

A multistub coaxial line tuner, W. E. Little and E. Niesen, IEEE Trans. Microwave Theory Tech. **MTT–12,** No. 5, 570–571 (Sept. 1964).

A survey of research on frozen food transport refrigeration, P. R. Achenbach, ASHRAE J. **6,** No. 11, 29–36 (Nov. 1964).

A two-channel nulling method for measuring attenuation constants of short sections of waveguide and the losses in waveguide joints, R. W. Beatty, Proc. IEEE **53,** No. 6, 642–643 (June 1965).

Advances in electrical instrumentation, F. L. Hermach, Ind. Res. pp. 60–66 (June 1965).

An automatic method for obtaining data in the Weissfloch-Feenberg node-shift technique, R. W. Beatty, Proc. IEEE **53,** No. 1, 79–80 (Jan. 1965).

An unimodulated twin channel microwave attenuation measurement system, D. H. Russell, ISA Trans. **4,** 162–169 (Apr. 1965).

Breakdown characteristics of semi-conductor materials, H. A. Schafft, Electro-Technol. 75, No. 6, 77–82 (June 1965).

Code for electricity metering, revised, F. K. Harris, Mag. Std. 36, No. 5, 143–145 (May 1965).

Color filter nomograph, C. S. McCamy, Am. Cinematographer 46, No. 5, 314–315 (May 1965).

Comments of surface characterization of real metals, D. P. DeWitt, (Symp. Thermal Radiation of Solids, San Francisco, Calif., Mar. 4–5, 1964), NASA **SP–55,** Session II, Paper 12, 141–144 (1965).

Comparison of single-point and two-point loading for determining the strength of flat glass, J. J. Kerper and T. G. Scuderi, Proc. Am. Soc. Testing Materials **64,** 1037–1043 (1964).

Composites in construction, A. A. Bates, Stanton Walker Lecture Series on the Materials Sciences, Nov. 20, 1963, Lecture No. 1, p. 15 (University of Maryland, College Park, Md., 1964).

Computer control of precision instrument inventory, S. N. Alexander and P. E. Doyle, Research/Development pp. 38–43 (May 1965).

Correlation and prediction of thermal conductivity of metals through the application of the principle of corresponding states, A. Cezairliyan and Y. S. Touloukian, Proc. Advances in Thermophysical Properties at Extreme Temperatures and Pressures, Purdue Univ., Lafayette, Ind. Mar. 1965, pp. 301–313 (American Society of Mechanical Engineers, New York, N.Y., 1965).

Current programs in the U.S. Department of Commerce for advancing state science and technology, W. C. Bandy (Proc. 11th Annual Meeting, Denver, Colo., Oct. 19–20, 1964), Mid-Continent Research and Development Council Report, pp. 70–76 (1965).

Design of static elastomeric seals for cryogenic temperatures, D. H. Weitzel, P. R. Ludtke, and R. F. Robbins, Proc. Conf. Design of Leak-tight Separable Fluid Containers 2, 139–165 (NASA, Huntsville, Ala., Mar. 1964).

Effect of surface texture on diffuse spectral reflectance, Part A. Diffuse spectral reflectance of metal surfaces, H. J. Keegan, J. C. Schleter, and V. R. Weidner, (Symp. Measurement of Thermal Radiation of Solids, San Francisco, Calif., Mar. 4–6, 1964). NASA SP–55, Session II, Paper 17, pp. 165–169 (1965).

Effects of connectors and adapters on accurate attenuation measurements at microwave frequencies, R. W. Beatty, IEEE Trans. Instr. Meas. **IM–13,** No. 4, 272–284 (Dec. 1964).

Experimental fires in enclosures, A. F. Robertson, 10th Symp. (Intern.) on Combustion, Cambridge, England, Aug. 1964, pp. 931–942 (1965).

Fire endurance of small gypsum slabs, J. V. Ryan, (Proc. American Society for Testing Materials Annual Meeting on Moisture Influence on Material Behavior During Fire Test, Chicago, Ill., June 1964), Am. Soc. Testing Materials Spec. Tech. Publ. No. 385, pp. 96–111 (May 1965).

Flexural behavior of prestressed split-beam composite concrete sections, J. O. Bryson, L. F. Skoda, and D. Watstein, J. Prestressed Concrete Inst. **10,** No. 3, 77–91 (June 1965).

Flow field in a swirl chamber, D. H. Tsai, AIAA J. Tech. Notes **2,** No. 8, 1504–1505 (Aug. 1964).

Fracture topography, I. Wolock and S. B. Newman, Book, Fracture Processes in Polymer Solids, Phenomena and Theory, ed. B. Rosen, ch. IIC, pp. 235–290 (Interscience Publ. Inc., New York, N.Y., 1964).

Further analysis of the modulated subcarrier technique of attenuation measurement, W. E. Little, IEEE Trans. Instr. Meas. **IM–13,** No. 2 & 3, 71–76 (June-Sept. 1964).

High temperature seal of sapphire windows to ceramics, G. A. Hornbeck, Rev. Sci. Instr. **36,** No. 6, p. 845 (June 1965).

Importance of surface films, J. C. Richmond (Symp. Thermal Radiation of Solids, San Francisco, Calif., Mar. 4–5, 1964), NASA **SP–55,** Session II, Paper 15, pp. 157–158 (1965).

International intercomparison of standards and microwave power measurements, G. F. Engen (Proc. 3d Intern. Measurement Conference, Stockholm, Sweden, 1964), Acta Imeko **1,** 337–346 (1964).

Measuring impedance through an adapter without introducing additional error, R. W. Beatty, Proc. IEEE **53,** No. 6, 656–657 (June 1965).

Method and equipment for measuring thermal emittance of ceramic oxides from 1200° to 1800 °K, H. E. Clark and D. G. Moore (Symp. Thermal Radiation of Solids, San Francisco, Calif., Mar. 4–5, 1964), NASA **SP–55,** Session III, Paper 26, pp. 241–257 (1965).

Microwave and high frequency calibration of the National Bureau of Standards, (Parts I–IV), R. E. Larson, IEEE Trans. Microwave Theory Tech. Part I., **MTT–12,** No. 4, 480–482 (July 1964); Part II, **MTT–12,** No. 5, 572–576 (Sept. 1964); Part III, **MTT–12,** No. 6, 623–624 (Nov. 1964); Part IV, **MTT–13,** No. 1, 138–139 (Jan. 1965).

Microwave discharge cavities operating at 2450 MHz, F. C. Fehsenfeld, K. M. Evenson, and H. P. Broida, Rev. Sci. Instr. **36,** 295–298 (Mar. 1965).

New mode of operation of a phase sensitive detector, Y. Beers, Rev. Sci. Instr. **36,** 696–700 (May 1965).

On the optimum frequency deviation in an FM system over a scatter-propagation path, H. Akima, Proc. IEEE **53,** No. 2, 182–183 (Feb. 1965).

Preliminary studies directed toward determination of spectra absorption coefficients of homogeneous materials in the infrared at elevated temperatures, W. B. Fussell and R. Stair (Symp. Measurement of Thermal Radiation of Solids, San Francisco, Calif., Mar. 4–6, 1964), NASA **SP–55,** Session III, Paper 29, pp. 287–292 (1965).

Progress report on aerosol packaged products, H. F. Wollin and S. Hasko, Aerosol Age Mag. **9,** No. 9, 20 (Sept. 1964).

Project FIST; fault isolation by semi-automatic techniques, G. J. Rogers, Design Disclosure Workbook (Packaging), U.S. Naval Applied Science Laboratory, Brooklyn, N.Y., Draft 5 (June 1965).

Project FIST: fault isolation by semi-automatic techniques, G. Shapiro, G. J. Rogers, O. B. Laug, and P. M. Fulcomer, Jr., IEEE Spectrum, pp. 98–111 (Aug. 1964); p. 130–144 (Sept. 1964).

Radio standards and measurements, microwaves, a progress review from 1960, R. W. Beatty, Book, Progress in Radio Science, 1960–1963, Vol. **I.** Radio Standards and Measurements, pp. 78–81 (Elsevier Publ. Co., Amsterdam, The Netherlands, 1965).

Recent developments in using elastomers for static cryogenic seals, P. R. Ludtke, Proc. Seventh National Society Aerospace Materials Process Engineers Symp., pp. 25–1—25–14 (Western Periodicals, Los Angeles, Calif., 1964).

Sensitivity indices for Hall generators, S. Rubin, Solid State Design Mag. **5,** No. 12, 38–39 (Dec. 1964).

Some factors affecting the sensitivity and spectral response of thermoelectric (radiometric) detectors, R. Stair, W. E. Schneider, W. R. Waters, and J. K. Jackson, Appl. Opt. **4,** No. 6, 703–710 (June 1965).

Standard test for determining alkali resistance of porcelain enamels, M. D. Burdick, Proc. Porcelain Enamel Inst. Forum **26,** 227–236 (Oct. 14–16, 1964).

Standardization of definitions for Hall effect devices, S. Rubin, Proc. Rotating and Stantic Precision Components Symp., Apr. 1964, pp. 344–360 (Bureau Naval Weapons, Washington, D.C., 1964).

Standards-still a continuing project, H. L. Mason, Control Eng. **12,** No. 1, 74 (Jan. 1965).

The evolution of control system standards, H. L. Mason, 1965 Joint Automatic Control Conf., June 22–25, 1965, Session VII, Paper 1, pp. 76–78 (Renssalaer Polytechnic Inst., Troy, N.Y., 1965).

The rapid selector as currently used for information search and replica copy retrieval, T. C. Bagg, (Proc. 26th Annual Meeting of the American Documentation Institute, Chicago, Ill., Oct. 1963) Automation and Scientific Commun. Pt. 2, 227–228 (Oct. 1963).

Waveguide noise-tube mount for use in an interlaboratory noise standard, C. K. S. Miller, W. C. Daywitt, and E. Campbell, Acta Imeko **3,** 371–382 (1964).

Weather resistance of porcelain enamels exposed for seven years at various sites, M. A. Rushmer and M. D. Burdick, Proc. Porcelain Enamel Inst. Forum **26,** 214–226 (Oct. 14–16, 1964).

Weight checking of aerosols, S. Hasko, Mod. Packaging Mag. **38,** No. 11, 141 (July 1965).

A new differential operator of the pure wave type, J. E. Lagnese, J. Different. Eq. **1,** No. 2, 171–187 (Apr. 1965).

Aggregation in matrix models of resource flows, D. Rosenblatt, Am. Stat. 19, No. **3,** 36–39 (June 1965).

An application of the inverse Z-transform theory to the synthesis of linear antenna arrays, M. T. Ma, IEEE Trans. Ant. Prop. **AP–12,** No. 6, 798–799 (Nov. 1964).

Analogies between theories of antenna arrays and passive networks, M. T. Ma., IEEE Intern. Conv. Record **13,** Pt. 5, 150–154 (Mar. 1965).

Application of Bernstein polynomials and interpolation theory to linear array synthesis, M. T. Ma, IEEE Trans. Ant. Prop. **AP–12,** 668–677 (Nov. 1964).

Mechanical translation: U.S.—Japan Joint Conference, F. L. Alt, Science **147,** No. 3665, 1599–1600 (Mar. 1965).

Relation between normal trichromatic vision and dichromatic vision representing a reduced form of normal vision, D. B. Judd, Acta Chromatica **1,** No. 3, 89–92 (Oct. 1964).

Some unorthodox predictions, F. L. Alt, Computers and Automation XIV, No. 1, p. 11 (Jan. 1965).

The standardization of programming languages, Proc. 19th Asso-

ciation for Computing Machinery Conf., Philadelphia, Pa., pp B2-1 (Aug. 1964).

Training a computer to assign descriptors to documents, M. E. Stevens and G. H. Urban, Proc. Spring AFIP Joint Computer Conf., Washington, D.C., April 1964, pp. 563–575 (1964).

Use of general purpose coding systems for statical calculations, J. M. Cameron and J. Hilsenrath, Proc. IBM Scientific Computing Symp. Statistics, Thomas J. Watson Research Center, Yorktown Heights, N.Y., Oct. 21–23, 1963, pp. 281–299 (IBM, White Plains, N.Y., 1965).

You can always tell a computer but you can't tell it much, J. H. Wegstein, Proc. ARO Working Group on Computers, Harry Diamond Laboratories, Washington, D.C., Feb. 4–5, 1964, pp. 129–151 (Feb. 1965).

A system for accurate d-c and a-c voltage measurements, F. L. Hermach, J. E. Griffin, and E. S. Williams, IEEE Intern. Conv. Record **13,** pt. 11, 172–182 (Mar. 1965).

An international comparison of inductive voltage divider calibrations at 400 and 1000 hertz, W. C. Sze, A. F. Dunn, and T. L. Zapf, IEEE Intern. Conv. Record **13,** pt. 11, 126–135 (Mar. 1965).

APPA–TAPPI reference material program. III. A discussion of lambda variance and its application to TAPPI standard T 414 m–49 for internal tearing resistance of paper, T. W. Lashof, Tappi **47,** No. 8, 445 (Aug. 1964).

Comments on Zener diodes as voltage standards, W. G. Eicke, Jr., Comite Consultatif D'Electricite 10e Session, May 2–3, 1963, pp. 27–30 (Gauthier-Villars, Paris, France, 1963).

Construction and behavior of a transportable ten picofarad capacitor, R. D. Cutkosky and L. H. Lee, Comite Consultatif D'Electricite 10e Session, May 2–3, 1963, p. 44–48 (Gauthier-Villars Paris, France, 1963).

Electronic g factor or rubidium, R. L. Driscoll, Phys. Rev. **136,** No. 1A, A54–A57 (Oct. 5, 1964).

Microwave calibration techniques at the National Bureau of Standards, R. E. Larson (Proc. Intern. Measurements Conf.), Acta Imeko **3,** 383–393 (1964).

National Bureau of Standards gas thermometer. III. Constant volume valve, R. L. Anderson and L. A. Guildner, Rev. Sci. Instr. **36,** No. 5, 615–616 (May 1965).

Simultaneous dielectric constant and volume measurements on liquids at high pressures, N. L. Brown, Proc. Electrical Insulation Conf., Cleveland, Ohio, Oct. 1964, Natl. Acad. Sci.-Natl. Res. Council Publ. 1238, pp. 36–40 (1965).

Spacetime coordinate systems, G. E. Hudson, Proc. Intern. Conf. Chronometry, pp. 197–221 (Lausanne, Switzerland, June 1964).

Standards, sources, and detectors in radiation measurements, R. Stair and W. E. Schneider (Symp. Measurement of Thermal Radiation of Solids, San Francisco, Calif., Mar. 4–6, 1964), NASA **SP–55,** Session III, Paper 24, pp. 217–231 (1965).

Planning for better measurement accuracy, R. D. Huntoon and W. A. Wildhack, ISA J. **12,** No. 1, 57–60 (Jan. 1965).

Uncertainties associated with proving ring calibration error, T. E. Hockersmith and H. H. Ku, ISA J. **12,** No. 6, 73–77 (June 1965).

A dumbbell model for dielectric dispersion in paraffin-like solids, M. G. Broadhurst, Proc. Electrical Insulation Conf., Cleveland, Ohio, Oct. 1964, Natl. Acad. Sci.-Natl. Res. Council Publ. 1238, pp. 129–132 (1965).

A method for determination of the tropospheric temperature structure from ground-based measurement of oxygen emission, E. R. Westwater, Proc. 3d Remote Sensing of the Environment, Infrared Phys. Lab., Inst. Sci. Tech., Univ. Michigan, Ann Arbor, Mich., Feb. 1965, pp. 245–256 (Mar. 1965).

A possible mechanism for light absorption by interstellar grains, E. E. Ferguson and H. P. Broida, Astrophys. J. **141,** No. 2, 807–809 (Feb. 15, 1965).

A test of analytical expressions for the thermal emittance of shallow cylindrical cavities, F. J. Kelley and D. G. Moore (Symp. Thermal Radiation of Solids, San Francisco, Calif., Mar. 4–5, 1964), NASA **SP–55,** Session I, Paper 10, pp. 117–121 (1965); Appl. Opt. 4, No. 1, 41–40 (1965).

A theoretical study of the Martian and Cytherian ionospheres, R. B. Norton, Natl. Aeron. Space Admin. NASA Tech. Note D–2333 (July 1964).

Albert Einstein, as I remember him, C. Eisenhart, J. Wash. Acad. Sci. **54,** 325–328 (Nov. 1964).

An experimental study of the backscattering of 5.3 meV alpha particles from platinum and monel metal, D. H. Walker, Intern. J. Appl. Radiation Isotopes **16,** 183–189 (1965).

Annual observatory report from the National Bureau of Standards, C. E. Moore, Astron. J. **69,** No. 9, 696–698 (Nov. 1964).

Beam loading in linear accelerators, J. E. Leiss, IEEE Trans. Nuclear Sci. **NS–12,** No. 3, 566–579 (June 1965).

Calibration of Schlieren systems, J. R. Meyer-Arendt and E. P. Shettle, J. Appl. Opt. Letter **4,** No. 6, 757 (June 1965).

Characteristics of soil and vegetated surfaces to reflected and emitted radiation, D. M. Gates, Proc. 3d Symp. Remote Sensing Environment, Infrared Phys. Lab., Inst. Sci. Tech., Univ. Michigan, Ann Arbor, Mich., Feb. 1965, pp. 573–600 (Mar. 1965).

Chromatography on glass of controlled pore size, W. Haller, Nature **206,** 693–696 (1965).

Compound-atom states for two-electron systems, T. F. O'Malley and S. Geltman, Phys. Rev. **137,** No. 5A, A1344–A1352 (Mar. 1, 1965).

Condensation of tungsten on tungsten in atomic detail: Monte Carlo and statistical calculations vs experiment, R. D. Young and D. C. Schubert, J. Chem. Phys. **42,** No. 11, 3943–3950 (June 1965).

Condensation of tungsten on tungsten in atomic detail: Observation with the field ion microscopy, P. Gurney, Jr., F. Hutchinson, and R. D. Young, J. Chem. Phys. **42,** No. 11, 3939–3943 (June 1965).

Continuum states of H^- and the free-free absorption coefficient, S. Geltman, Astrophys. J. **141,** No. 2, 376–394 (Feb. 12, 1965).

Correction of optical distance measurements for the fluctuating atmospheric index of refraction, P. L. Bender and J. C. Owens, J. Geophys. Res. **70,** No. 10, 2461–2462 (May 15, 1965).

Correlated walk and diffusion equations in a driving force, J. R. Manning, Phys. Rev. **139,** No. 1A, A126–A135 (July 5, 1965).

Coupling of particle-hole states and two particle-two hole states: damping, M. Danos and W. Greiner, Book, Physique Nucleaire, ed. P. Gugenberger, II, 615–616 (Editions due Centre National de la Recherche scientific, Paris, France, 1964).

Critical examination of vibrational energy-transfer theory, F. H. Mies, J. Chem. Phys. **42,** No. 8, 2709–2720 (Apr. 15, 1965).

Crystal growth and thermal etching of argon, G. L. Pollack and E. N. Farabaugh, J. Appl. Phys. **36,** 513 (1965).

Damping of the giant resonance in heavy nuclei, M. Danos and W. Greiner, Phys. Rev. **138,** No. 4B, B876–B891 (May 1965).

Dissociative recombination in helium afterglows, E. E. Ferguson, F. C. Fehsenfeld, and A. L. Schmeltekopf, Phys. Rev. **138A,** A381–A385 (Apr. 1965).

Dynamic collective theory of odd-A nuclei, M. Danos, W. Greiner, and C. B. Kohr, Phys. Rev. **138,** No. 5B, B1055–B1066 (June 1965).

Electron accelerators for food processing, H. W. Koch and E. H. Eisenhower, Proc. Intern. Conf. Radiation Preservation of Foods, Boston, Mass., Sept. 27–30, 1964, Natl. Acad. Sci.-Natl. Res. Council Publ. **1273,** pp. 149–180 (1965).

Electron spin resonance of Mo^{5+} in rutile, T. T. Chang, Phys. Rev. **136,** No. 5A, A1413–A1416 (Nov. 30, 1964).

Empirical relations for energy levels of atoms and ions, A. E. Goertz, J. Opt. Soc. Am. **55,** 742–743 (June 1965).

Energy levels of Pr^{3+} in the vapor state, J. Sugar, Phys. Rev. Letters **14,** No. 18, 731–732 (May 3, 1965).

Energy levels of polarons in a magnetic field, D. M. Larsen, Phys. Rev. **135,** No. 2A, A419–A426 (July 1964).

Energy of the formation of the anion Frenkel pair in calcium fluoride A. D. Franklin, J. Phys. Chem. Solids **26,** 933–934 (1965).

Etch pits in chromic oxide, W. S. Brower, Jr., and E. N. Farabaugh, J. Appl. Phys. **36,** No. 4, 1489–1490 (Apr. 1965).

Excitation of molecular rotation by slow electrons, K. Takayanagi and S. Geltman, Physics Letters **13,** No. 2, 135–137 (Nov. 15, 1964); Phys. Rev. **138,** No. 4A, A1003–A1010 (May 17, 1965).

Expertise or experiments, C. Eisenhart, Science **146,** No. 3647, 997–998 (Nov. 20, 1964).

4fnl configurations of doubly ionized cerium (Ce III), N. Spector, J. Opt. Soc. Am. **55,** No. 5, 492–501 (May 1965).

Γ_6 selection rules in Su(12) $\bar{p}p$ annihilation, H. Harari, H. J. Lipkin, and S. Meshkov, Phys. Rev. Letters **20,** No. 14, 845–847 (May 17, 1965).

Generalized master equation for quantum mechanical systems to all orders in the density, J. Weinstock, Phys. Rev. **136,** 2d series, No. 4A, A879–A888 (Nov. 1964).

High energy x-ray photon albedo, J. S. Pruitt, Nuclear Instr. Methods **27,** 23 (1964).

High voltage Laue x-ray photography of large single crystals, B. Paretzkin and H. S. Peiser, Science **146,** 260 (1964).

Higher-order skewnesses in a turbulent field, F. N. Frenkiel and P. S. Klebanoff, Compt. Rend. **260,** 6026–6029 (1965).

Hyperfine structure of Hg^{193*}, Hg^{195*} by Zeeman level crossings, W. W. Smith, Phys. Rev. **137,** No. 2, 580–591 (Jan. 1965).

Interaction potential between He and H_2, M. Krauss and F. H. Mies, J. Chem. Phys. **42,** No. 8, 2703–2708 (Apr. 15, 1965).

International comparison of atomic frequency standards via VLF radio signals, A. H. Morgan, B. E. Blair, and E. L. Crow, Book, Progress in Radio Science, Vol. **I.** Radio Standards and Measurement, p. 40 (Elsevier Publ. Co., Amsterdam, The Netherlands, 1965).

Isotropic determination of the vibrational numbering for the $B^3\Pi_{0^+_u}$, R. L. Brown and T. C. James, J. Chem. Phys. **42,** No. 1, 33–35 (Jan. 1965).

Laser double-quantum photodetachment of I^-, J. L. Hall, E. J. Robinson, and L. M. Branscomb, Phys. Rev. Letters **14,** No. 25, 1013–1016 (June 21, 1965).

Loop prominences and coronal condensations. I. Non-thermal velocities within loop prominences, J. T. Jefferies and F. Q. Orrall, Astrophys. J. **141,** No. 2, 505–518 (Feb. 15, 1965).

Loop prominences and coronal condensations. II. The sources of mass and energy and a model of the loop prominence mechanism, J. T. Jefferies and F. Q. Orrall, Astrophys. J. **141,** No. 2, 519–525 (Feb. 15, 1965).

Low-Z dye systems for ionizing radiation measurement, W. L. McLaughlin and L. Chalkley, J. Photo. Sci. Engr. **9,** No. 3, 159–166 (May-June 1965).

Master equations and Markov processes, I. Oppenheim and K. E. Shuler, Phys. Rev. **138,** No. 4B, B1007–B1011 (May 24, 1965).

Matrix-isolation study of the reaction of F atoms with CO. Infrared and ultraviolet spectra of the free radical FCO, D. E. Milligan, M. E. Jacox, A. B. Bass, J. J. Comeford, and D. E. Mann, J. Chem. Phys. **42,** No. 9, 3187–3195 (May 1965).

Measurements of the viscosity of parahydrogen, D. E. Diller, J. Chem. Phys. **42,** No. 6, 2089–2100 (Mar. 1965).

Microscopic-astrophysics and the development of astrophysical-laboratories, R. N. Thomas, Bull. Assoc. Devel. Intern. Observatoire de Nice, No. 1, pp. 7–16 (1964).

Microscopic fluctuations and diffusion coefficients of a non-equilibrium plasma in a magnetic field, J. Weinstock, Phys. Fluids **8,** No. 3, 479–481 (Mar. 1965).

Mobilities and reaction rates of ions in helium, E. C. Beaty and P. L. Patterson, Phys. Rev. **137,** No. 2A, A346–A357 (Jan. 1965).

Multipole matrix elements of the translation operator, M. Danos and L. C. Maximon, J. Math. Phys. **6,** 766 (1965).

New odd levels of neutral erbium (Er I), N. Spector, J. Opt. Soc. Am. **55,** No. 5, 576–577 (May 1965).

New Rydberg series in molecular oxygen near 500° A, K. Codling and R. P. Madden, J. Chem. Phys. **42,** No. 11, 3935–3938 (June 1965).

Non-equilibrium thermodynamics of canonically invariant relaxation processes, H. C. Andersen, I. Oppenheim, K. E. Schuler, and G. H. Weiss, J. Chem. Phys. **41,** No. 10, 3012–3019 (Nov. 1964).

Non-equilibrium thermodynamics of creep in polycrystals, R. E. Nettleton, Physica **20,** 1989–2002 (1964).

Note on the theory of cavity ionization chambers, L. V. Spencer, Radiation Res. **25,** No. 2, 352–358 (June 1965).

Nuclear magnetic resonance in $RbMnF_3$, R. E. Payne, R. A. Forman, and A. H. Kahn, J. Chem. Phys. **42,** No. 11, 3806–3808 (June 1965).

Nucleate boiling of hydrogen, D. E. Drayer, Ind. Eng. Chem. Fundamentals **4,** No. 2, 167–171 (May 1965).

Observations of carbon monoxide and oxygen on tantalum with the field emission microscope, R. Klein, J. Chem. Phys. **41,** No. 2, 571 (July 1964).

Observations of dislocation sources in stainless steel, A. W. Ruff, Jr., and H. G. F. Wilsdorf, Acta Met. **13,** No. 6, 694–695 (1965).

On the identification of energy levels of negative ions, U. Fano and J. W. Cooper, Phys. Rev. **138,** No 2A, A400–A402 (Apr. 1965).

On the nature of plasma resonance, W. M. Leavens, Physics Letters **15,** No. 4, 310–311 (Apr. 1965).

Optical constants of iron in the visible region, H. T. Yolken and J. Kruger, J. Opt. Soc. Am. **55,** No. 7, 842–844 (July 1965).

Optical depolarization and scintillation measurements over a terrestrial path, J. R. Meyer-Arendt, Proc. 3d Tropospheric Refraction Effects Meeting **1,** 115–123 (Nov. 1964).

Optical detection of microwave transitions between excited electronic state of CN and the identification of the transitions involved, K. M. Evenson, J. L. Dunn, and H. P. Broida, Phys. Rev. **136,** No. 6A, A1566–A1571 (Dec. 14, 1965).

Optical radar using a corner reflector on the moon, C. O. Alley, P. L. Bender, R. H. Dicke, J. E. Faller, P. Franken, H. H. Plotkin, and D. T. Wilkinson, J. Geophys. Res. **70,** No. 9, 2267–2269 (May 1, 1965).

Optimization of the Czerny-Turner spectrometer, A. B. Shafer, L. R. Megill, and L. A. Droppleman, J. Opt. Soc. Am. **54,** No. 7, 879–887 (July 1964).

Photonuclear reactions, E. Hayward, Book, Nuclear Structure and Electromagnetic Transitions, ed. N. MacDonald, p. 141 (Oliver and Boyd, Edinburgh and London, England, 1965).

Possible implications of the observed profile of (λ 6374) FeX, C. Pecker-Wimel and R. N. Thomas, Astrophys. J. **141,** No. 2, 834–836 (Feb. 15, 1965).

Potential distribution in a rectangular semiconductor bar for use with four-point probe measurements, M. J. Reber, Solid State Electron. **7,** No. 7, 525–529 (July 1964).

Rearrangement kinetics of the liquid-liquid immiscible microphases in alkali borosilicate melts, W. Haller, J. Chem. Phys. **42,** 686–693 (1965).

Report of subcommittee D-atomic spectra, C. E. Moore, J. Opt. Soc. Am. Tech. Notes **55,** No. 6, 745 (1965).

Report of the acoustics research survey committee, R. K. Cook and G. W. Wood, J. Acoust. Soc. Am. **37,** No. 2, 392–395 (Feb. 1965).

Shell model treatment of nuclear reactions, M. Danos and W. Greiner, Phys. Rev. **138,** No. 1B, B93–B103 (Apr. 1965).

Shift of the R(0) and P(1) infrared lines of HCl perturbed by noble gases, A. Ben-Reuven, J. Chem. Phys. **42,** No. 6, 2037–2042 (Mar. 15, 1965).

Some considerations relative to an atomic definition for the unit of time, R. C. Mockler and J. M. Richardson, Proc. Consultative Committee for the Definition of the Second of the International Committee of Weights and Measures, Paris, France, Apr. 1961, pp. 58–65 (Dec. 1964).

Some measured rates for oxygen and nitrogen ion-molecule reactions of atmospheric inportance, including $O^+ + N_2 \rightarrow NO^+ + N$, F. C. Fehsenfeld, A. L. Schmeltekopf, and E. E. Ferguson, Planetary Space Sci. **13,** 219–223 (Mar. 1965).

Spin-orbit coupling constant of nitric oxide. Determination from fundamental satellite band origins, T. C. James and R. J. Thibault, J. Chem. Phys. **41,** No. 9, 2806–2813 (Nov. 1964).

Surface ionization of niobium, M. D. Scheer and J. Fine, J. Chem. Phys. **42,** 3645 (1965).

Tables of dielectric constants, dipole moments and dielectric relaxation times, F. I. Mopsik, 1963 Digest of Literature on Dielectrics Publ. 1230, **27,** 23–55 (1964).

Tables of thermodynamic properties of air in chemical equilibrium including second virial corrections from 1500 °K to 15,000 °K, J. Hilsenrath and M. Klein, Arnold Eng. Develop. Center, Air Force Systems Command, AEDC–TR–65–58 (Arnold Air Force Station, Tenn., Mar. 1965).

The effect of moisture on surface flammability of coated and uncoated cellulosic materials, T. G. Lee, J. L. Loftus, and D. Gross, Am. Soc. Testing Materials Spec. Tech. Publ. **385,** 112–123 (May 1965).

Total photonuclear cross sections for low atomic number elements, J. M. Wyckoff, H. W. Koch, B. Ziegler, and R. Uhlig, Phys. Rev. **137,** No. 3B, B576–B594 (Feb. 1965).

Wave mode modification in liquid helium with clamped normal fluid, G. L. Pollack and J. R. Pellam, Proc. 9th Intern. Conf. Low Temperature Physics, Columbus, Ohio, Sept. 1964, p. 166 (Plenum Press Inc., New York, N.Y., 1965).

Width of the microwave lines of oxygen and their relationship to the thermal noise emission spectrum of the atmosphere, R. L. Abbott, Proc. 3d Symp. Remote Sensing of the Environment, Infrared Phys. Lab., Inst. Sci. Tech. Univ., Michigan, Ann Arbor, Mich., Feb. 1965, pp. 257–269 (Mar. 1965).

Widths of transmission Kikuchi lines in silicon and diamond, H. A. Fowler and L. Marton, J. Appl. Phys. **36,** No. 6, 1986–1995 (June 1965).

W-spin analysis of weak decays in U(12) D. Horn, M. Kugler, H. J. Lipkin, S. Meshkov, J. C. Carter, and J. J. Coyne, Phys. Rev. Letters **14,** No. 17, 717–719 (Apr. 1965).

W-spin and B-spin subgroups of SU(12), H. J. Lipkin and S. Meshkov, Phys. Rev. Letters **16,** No. 14, 670–672 (Apr. 19, 1965).

A comparison of mountain slope and radiosonde observations, C. A. Sampson, Mo. Weather Rev. **93,** No. 5, 327–330 (May 1965).

A study of auroral absorption events at the South Pole: I. Characteristics of the events, J. K. Hargreaves, H. J. A. Chivers, and J. D. Petlock, J. Geophys. Res. **69,** No. 23, 5001–5007 (Dec. 1964).

Attenuation of radio waves in the troposphere, B. R. Bean, Book, Advances in Radio Research **1,** 121–155 (Academic Press Inc., New York, N.Y., 1964).

ESD Maui, Hawaii, measurements, M. C. Thompson, Jr., Proc. 3d Tropospheric Refraction Effects Meeting 1, 89–93 (Nov. 1964).

Fading on microwave line-of-sight paths, H. T. Dougherty, Proc. 3d Tropospheric Refraction effects Meeting 1, 125–135 (Nov. 1964).

Formation of an electron depleted region in the ionosphere by chemical releases, J. W. Wright, D. Golomb, N. W. Rosenberg, and J. A Barnes, (Proc. 4th Intern. Space Science Symp., Warsaw, Poland, June 4–10, 1963), Space Res. **IV,** 389–398 (North-Holland Publ. Co., Amsterdam, The Netherlands, 1964).

Ionosphere explorer I satellite: first ovservations from the fixed-frequency topside sounder, W. Calvert, K. W. Knecht, and T. E. VanZandt, Science **146,** No. 3642, 391–395 (Oct. 16, 1964).

Ionospheric effects observed around the time of the Alaskan earthquake of March 28, 1964, K. Davies and D. M. Baker, J. Geophys. Res. **70,** No. 9, 2251–2253 (May 1, 1965).

Ionospheric propagation on high frequencies, K. Davies, 4U11TU Calling **2,** 112–113 (1965).

Noise tests of an airborne microwave refractometer system, M. C. Thompson, Jr., and W. B. Grant, Rev. Sci. Instr. **36,** No. 6, 758–759 (June 1965).

Prediction of ionospheric characteristics at CRPL for sky-wave radio propagation at high frequencies, K. Davies, Telecommun. J. **31,** No. 12, 339–350 (Dec. 1964).

Radiation efficiencies of half-wave dipole antennas, R. G. Fitz-Gerrell, IEEE Trans. Ant. Prop. **AP–13,** 326–327 (Mar. 1964).

Radio astronomy observations with the $8.4 \times 10^4 m^2$ 50 Mc/s antenna of the Jicamarca radar in Peru, W. K. Klemperer and G. R. Ochs, Astron. J. **70,** No. 1327, 141–142 (Mar. 1964).

Receiver noise factor, E. Hildner, Proc. Intern. Telemetry Conf., Washington, D.C., May 16–20 1964, pp. 326–333 (May 1965).

The contribution of non-thermal electrons to auroral absorption of radio waves, G. C. Reid, J. Geophys. Res. **69,** No. 15, 3296–3298 (Aug. 1964).

The daytime equatorial *F*-layer, R. B. Norton and T. E. VanZandt, J. Atmospheric and Terrest. Phys. **26,** 1047–1054 (1964).

The distribution of electrons in the lower and middle ionosphere, R. W. Knecht, Book, Progress in Radio Science 1960–1963, Vol. III. The Ionosphere, pp. 14–45 (Elsevier Publ. Co., Amsterdam, The Netherlands, 1965).

The light of the night sky: astronomical interplanetary and geophysical, F. E. Roach, Space Sci. Rev. **3,** 512–540 (Nov. 1964).

**Publications for which a price is indicated are available by purchase from the Superintendent of Documents, U.S. Government Printing Office, Washington, D.C., 20402 (foreign postage, one-fourth additional). Reprints from outside journals and the NBS Journal of Research may often be obtained directly from the authors.*

JOURNAL OF RESEARCH of the National Bureau of Standards—A. Physics and Chemistry
Vol. 69A, No. 6, November–December 1965

INDEX TO VOLUME 69A

January to December 1965

A

Page

Absolute temperature scale from 4 °K to 20 °K determined from measurements with and acoustical thermometer 375
Acetamido derivative of sugars 291
Acoustical thermometer, an absolute temperature scale from 4 °K to 20 °K determined from measurements 375
Activity coefficients, tris(hydroxymethyl)aminomethane in 50-percent methanol 263
Additivity rule for the vapor pressure lowering of aqueous solutions 365
Alpha-aluminum oxide crystals, observations 271
Aluminum carbide (Al_4C_3), heat capacity measurements on, from 15 to 1173 °K. Thermodynamic properties from 0 to 2000 °K 423
Aluminum fluoride, heat of formation of, by direct combination of the elements 137
2-Animo-2 (hydroxymethyl)-1, 3-propanediol, dissociation of, in 50-percent methanol 263
Anionic polymerization of isoprene at low concentrations of polyisoprenyllithium 159
Application of precise heat-capacity data to the analysis of the temperature intervals of the NBS–1955 and the International Practical Temperature Scales in the region of 90 °K 5
Aqueous solutions, an additivity rule for the vapor pressure lowering 365
Arc measurement of some argon transition probabilities 495
Archival records current research on preservation of, on silver-gelatin type microfilm in roll form 385
Argon transition probabilities, arc measurement 495
Armstrong, G. T., E. S. Domalski, Heat of formation of aluminum fluoride by direct combination of the elements 137
Atomic absorption spectrum of praseodymium (Pr I) 59
Atomic steps, successive, correlation of, in crystals by relaxation mode analysis 301
Ausloos, P., R. Gordon, Jr., Radiolysis of $N^{15}N^{14}O$ 79

B

Barber, D. J., N. J. Tighe, Observations of dislocations and surface features in corundum crystals by electron transmission microscopy 271
Bates, R. G., M. Woodhead, M. Paabo, R. A. Robinson, Acid-base behavior in 50 percent aqueous methanol: thermodynamics of the dissociation of protonated tris (hydroxymethyl) aminomethane and nature of the solvent effect 263
Berman, H. A., Heat of formation of calcium aluminate tricarbonate at 25 °C 407
—, Preparation of a carbonate-free complex calcium aluminate 45
Beryllium aluminate (chrysoberyl), $BeO \cdot Al_2O_3$, heat capacity and thermodynamic properties of, from 16 to 380 °K 13
Binary mixture: spectral structure of critical opalescence 523
Bis (8-hydroxyquinoline)-Schiff base coordination of polymers, synthesis and thermal stability 53
Bismuth oxide, heats of transformation in, by differential thermal analysis 237
Bolz, L. H., R. K. Eby, Inclusion of perfluoromethyl groups in the lattice of copolymers of tetrafluoroethylene and hexafluoropropylene 481
Boric oxide, liquid, low-frequency dielectric properties 281
Bower, V. E., R. A. Robinson, An additivity rule for the vapor pressure lowering of aqueous solutions 365
—, — Properties of aqueous mixtures of pure salts: thermodynamics of the ternary system water-potassium chloride-barium chloride at 25 °K 439
—, —, Thermodynamics of the ternary system: water-glycine-potassium chloride at 25 °C from vapor pressure measurements 131
—, —, Thermodynamics of the ternary system: water-sodium chloride-barium chloride at 25 °C 19
Brown, W. E., E. F. Epstein, Crystallography of tetracalcium phosphate 547
Bullman, G. W., F. L. Roth, L. A. Wood, Compliance-time temperature relationships form indentation measurements on a pure-gum rubber vulcanizate 347

C

Calcium aluminate, a carbonate-free complex, preparation 45
Calcium aluminate tricarbonate at 25 °C, heat of formation 407
Cataland, G. H., H. Plumb, An absolute temperature scale from 4 °K to 20 °K determined from measurements with an acoustical thermometer 375
—, —, Isotherms determined by the National Bureau of Standards acoustical thermometer in the liquid helium temperature range 531
Compliance-time-temperature relationships from indentation measurements on a pure-gum rubber vulcanizate 347
Compressibility of eleven inorganic materials 29
Corliss, C. H., Oscillator strengths for lines in Ni I 87
Correlation of large longitudinal deformations with different strain histories 541
Correlation of successive atomic steps in crystals by relaxation mode analysis 301
Corundum crystals, observations of dislocations and surface features by electron transmission microscopy 271
Corwin, W. C., J. B. Wachtman, Jr., Internal friction in ZrO_2 containing CaO 457
Craft, T., L. J. Zapas, Correlation of large longitudinal deformations with different strain histories 541
Crystallization kinetics and polymorphic transformation in polybutene-1 335
Crystallography of tetracalcium phosphate 547
Crystals by relaxation mode analysis, correlation of successive atomic steps 301
Current research on preservation of archival records on silver-gelatin type microfilm in roll form 385

D

Page

Deformations, large longitudinal, correlation of, with different strain histories 541
Depolarizers, inorganic, photopolarographic behavior 517
Determination of the intermolecular entanglement coupling spacings in polyisoprene by viscosity measurements 33
D-Glucose-3-^{14}C, synthesis of, and related compounds 535
Diamond, J. J., R. Szwarc, E. R. Plante, Vapor pressure and heat of sublimation of tungsten 417
Dielectric properties of liquid boric oxide 281
Differential thermal analysis, heats of transformations in bismuth oxide 237
Disaccommodation of magnetic spectra of two manganese zinc ferrites 181
Dissociation constant of tris (hydroxymethyl) aminomethane, in 50-percent methanol 263
Dissociation constant of weak bases, in 50-percent methanol 263
Distribution function of the end-to-end distances of linear polymers with excluded volume effects 355
Domalski, E. S., G. T. Armstrong, Heat of formation of aluminum fluoride by direct combination of the elements 137
Douglas, T. B., G. T. Furukawa, W. G. Saba, A. C. Victor, Heat capacity and enthalpy measurements on aluminum carbide (Al_4C_3) from 15 to 1173 °K. Thermodynamic properties from 0 to 2000 °K 423
—, *A. W. Harman*, Relative enthalpy of polytetrafluoroethylene from 0 to 440 °C 149
Durst, R. A., J. K. Taylor, Photopolarographic behavior of inorganic depolarizers 517

E

Eby, R. K., L. H. Bolz, Inclusion of perfluoromethyl groups in the lattice of copolymers of tetrafluoroethylene and hexafluoropropylene 481
Effect of hydrostatic pressure on the refractive indices of some solids 325
Eisenstein, J. C., M. H. L. Pryce, Electronic structure and magnetic of the neptunyl ion 217
Electrical conductivity of dilute solutions of "sea water" from 5 to 120 °C 39
Electrode, potentials in fused systems X. Measurement of cation concentration in molten salts using glass membrane electrodes 553
Electron configurations p^2d and p^3d, matrices of spin-orbit interaction 401
Electron structure and magnetic properties of the neptunyl ion 217
Enthalpy of polytetrafluoroethylene from 0 to 440 °C 149
Epstein, E. F., W. E. Brown, Crystallography of tetracalcium phosphate 547

F

Fetters, L. J., Anionic polymerization of isoprene at low concentrations of polyisoprenyllithium 159
—, Determination of the intermolecular entanglement coupling spacings in polyisoprene by viscosity measurements 33
Franck-Condon factors to high quantum numbers VI: C_2 band systems 397
Franck-Condon factors to high vibrational quantum numbers V: O_2 band systems 369
Franklin, A. D., Correlation of successive atomic steps in crystals by relaxation mode analysis 301
Frush, H. L., L. T. Sniegoski, N. B. Holt, H. S. Isbell, Synthesis of D-glucose-3-^{14}C and related compounds 535
Furukawa, G. T., T. B. Douglas, W. G. Saba, A. C. Victor, Heat capacity and enthalpy measurements on aluminum carbide (Al_4C_3) from 15 to 1173 °K. Thermodynamic properties from 0 to 2000 °K 423
—, *M. L. Reilly*, Application of precise heat-capacity data to the analysis of the temperature intervals of the NBS-1955 and the International Practical Temperature Scales in the region of 90 °K 5
—, *W. G. Saba*, Heat capacity and thermodynamic properties of beryllium aluminate (chrysoberyl) $BeO \cdot Al_2O_3$, from 16 to 380 °K 13

G

Garstang, R. H., J. L. Tech, Matrices of spin-orbit interaction in the electron configurations p^2d and p^3d 401
Gilliland, A. A., D. Wagman, Heat decomposition of sodium and potassium chlorate 1
Glass viscometer 449
Glycine-potassium chloride water at 25 °C from vapor pressure measurements, thermodynamics of the ternary system 131
Gold (Au III), third spectrum, theoretical interpretation 511
Gorden, R., Jr., P. Ausloos, Radiolysis of $N^{15}N^{14}O$ 79

H

Harman, A. W., T. B. Douglas, Relative enthalpy of polytetrafluoroethylene from 0 to 440 °C 149
Hawkins, E. G., A. Napolitano, P. B. Macedo, A wide-range (up to 10^{10}P) rotating cylinder viscometer 449
Heat capacity and enthalpy measurements on aluminum carbide (Al_4C_3) from 15 to 1173 °K. Thermodynamic properties from 0 to 2000 °K 423

Page

Heat capacity and thermodynamic properties of berryllium aluminate (chrysoberyl), $BeO \cdot Al_2O_3$, from 16 to 380 °K 13
Heat of decomposition of sodium and potassium chlorate 1
Heat of formation of aluminum fluoride by direct combination of the elements 137
Heat of formation of calcium aluminate at 25 °C, heat of formation 407
Heats of transformations in bismuth by differential thermal analysis 237
Helium temperature range, liquid, isotherms determined by the National Bureau of Standards acoustical thermometer 531
Herron, J. L., Mass spectrometric study of the effects of nitric oxide 287
Hexafluoropropylene and tetrafluoroethylene, inclusion of perfluoromethyl groups in the lattice of copolymers 481

Hoffman, J. D., J. Powers, J. J. Weeks, F. A. Quinn, Jr., Crystallization kinetics and polymorphic transfogmation in polybutene-1 335
Holt, N. B., H. L. Frush, L. T. Sniegoski, H. S. Isbell, Synthesis of D-glucose-3-^{14}C and relat , compounds 535
Horowitz, E., T. P. Perros, Synthesis and thermal stability of bis (8-hydroxyquinoline)-Schiff base coordination polymers 53

I

Inclusion of perfluoromethyl groups in the lattice of copolymers of tetrafluoroethylene and hexafluoropropylene 481
Indentation measurements on a pure-gum rubber vulcanizate, compliance-time-temperature relationships 347
Inorganic materials, eleven, compressibility 29
Internal friction in ZrO_2 containing CaO 457
International Practical Temperature Scales in the region of 90 °K, application of precise heat-capacity data to the analysis of the temperature intervals of the NBS-1955 temperature scales 5
Iridium and the sesquioxides in air, phase relations between 245
Irregularities in the NBS (1955) provisional temperature scale 527
Isbell, H. S., H. L. Frush, L. T. Sniegoski, N. B. Holt, Synthesis of D-glucose-3-^{14}C and related compounds 535
Isotherms determined by the National Bureau of Standards acoustical thermometer in the liquid helium temperature range 531

L

Levin, E. M., C. L. McDaniel, Heats of transformation in bismuth oxide by differential thermal analysis 237

M

Macedo, P. B., A. Napolitano, E. G. Haukins, A wide-range (up to 10^{16}P) rotating cylinder viscometer 449
Malberg, C. G., Electrical conductivity of dilute solutions of "sea water" from 5 to 120 °C 39
Manganese zinc ferrites, two, disaccommodation of magnetic spectra 181
Mass spectrometric study of the effects of nitric oxide 287
Matrices of spin-orbit interaction in the electron configurations p^5d and p^5d 401
Mazur, J., Distribution function of the end-to-end distances of linear polymers with excluded volume effects 355
McCamy, C. S., C. I. Pope, Current research of preservation of archival records on silver-gelatin type microfilm in roll form 385
McCleary, L. C., H. S. Peiser, J. B. Wachtman, Jr., F. A. Munley, Splitting of equivalent points in noncentrosymmetric space groups into subsets under homogeneous stress 461
McDaniel, C. L., E. M. Levine, Heats of transformations in bismuth oxide by differential thermal analysis 237
McDonald, E. J., Synthesis and ring structure of 7-acetamido-7deoxy-L-*galacto*-heptulose 291
Meador, S. E., K. H. Stern, Electrode potentials in fused systems X. Measurement of cation concentration in molten salts using glass membrane electrodes 553
Meggers, W. F., R. W. Stanley, More wavelengths from thorium lamps 109
Microfilm, silver-gelatin type in roll form, current research on preservation of archival records 385
Molten salts, measurement of cation concentration in, using glass membrane electrodes. Electrode potentials in fused systems X 553
Mountain, R. D., Spectral structure of critical opalescence: binary mixture 523
Munley, F. A., H. S. Peiser, J. B. Wachtman, Jr., L. C. McCleary, Splitting of equivalent points in noncentrosymmetric space groups into subsets under homogeneous stress 461

N

Napolitano, A., P. B. Macedo, E. G. Haukins, A wide-range (up to 10^{16}P) rotating cylinder viscometer 449
NBS-1955 and International Practical Temperature Scales in the region of 90 °K, application of precise heat-capacity data to the analysis of the temperature intervals 5
NBS (1955) provisional temperature scale, irregularities 527
Neptunyl ion, electronic structure and magnetic properties 217
Nicholls, R. W., Franck-Condon factors to high quantum numbers VI: C_2 band systems 397
—, Franck-Condon factors to high vibrational quantum numbers V: O_2 band systems 369
Nitric oxide, mass spectrometric study of the effects 287
Nitrous oxide, radiolysis 79
Noncentrosymmetric space groups, splitting of equivalent points in, into subsets under homogeneous stress 461

O

Observations of dislocations and surface features in corundum crystals by electron transmission microscopy 271
One particle transitions and correlation in quantum mechanics 167
Opalescence, critical, spectral structure of, binary mixture 523
Oscillator strengths for lines of Ni I 87

Page

P

Paabo, M., M. Woodhead, R. A. Robinson, R. G. Bates, Acid-base behavior in 50-percent aqueous methanol: thermodynamics of the dissociation of protonated tris (hydroxymethyl) aminomethane and nature of the solvent effect 263
Peiser, H. S., J. B. Wachtman, Jr., Reduction of crystallographic point groups to subgroups by homogeneous stress 309
—, —, Splitting of a set of equivalent sites in centrosymmetric space groups into subsets under homogeneous stress 193
—, —, *F. A. Munley, L. C. McCleary*, Splitting of equivalent points in noncentrosymmetric space groups into subsets under homogeneous stress 461
Perfluoromethyl groups, inclusion of, in the lattice of copolymers of tetrafluoroethylene and hexafluoropropylene 481
Perros, T. P., E. Horowitz, Synthesis and thermal stability of bis (8-hydroxyquinoline)-Schiff base coordination polymers 53
Perseulose, acetamido derivative 291
Phase equilibria in the system vanadium oxide-niobium oxide 119
Phase equilibrium relationships in the system Gd_2O_3-TiO_2 255
Phase relations between iridium and the sesquioxides in air 245

Photopolarographic behavior of inorganic depolarizers 517
Plante, E. R., R. Szwarc, J. J. Diamond, Vapor pressure and heat of sublimation of tungsten 417
Plumb, H. H., G. Cataland, An absolute temperature scale from 4 °K to 20 °K determined from measurements with an acoustical thermometer 375
—, —, Isotherms determined by the National Bureau of Standards acoustical thermometer in the liquid helium temperature range 531
Polybutene-1, crystallization kinetics and polymorphic transformation 335
Polyisoprene, spacings in, by viscosity measurements, determination of the intermolecular entanglement coupling 33
Polyisoprenyllithium, anionic polymerization of isoprene at low concentrations 159
Polymers, linear, with excluded volume effects distribution function of the end-to-end distances 355
Polytetrafluoroethylene, relative enthalpy of, from 0 to 440 °C 149
Polytetrafluoroethylene, thermodynamic properties 149
Pope, C. I., C. S. McCamy, Current research on preservation of archival records on silver-gelatin type microfilm in roll form 385
Popenoe, C. H., J. B. Shumaker, Jr., Arc measurement of some argon transition probabilities 495
Potassium and sodium chlorate, heat of decomposition 1
Powers, J., J. D. Hoffman, J. J. Weeks, F. A. Quinn, Jr., Crystallization kinetics and polymorphic transformation in polybutene-1 335
Praseodymium (Pr I), atomic absorption spectrum 59
Preparation of a carbonate-free complex calcium aluminate 45
Preservation of archival records on silver-gelatin type microfilm in roll form, current research 385
Properties of aqueous mixtures of pure salts: thermodynamics of the ternary system water-potassium chloride-barium chloride at 25 °K 439
Pryce, M. H. L., J. C. Eisenstein, Electronic structure and magnetic properties of the neptunyl ion 217

Q

Quantum mechanics, one particle transitions and correlation 167
Quinn, F. Q., Jr., J. Powers, J. D. Hoffman, J. J. Weeks, Crystallization kinetics and polymorphic transformation in polybutene-1 335

R

Radiolysis of $N^{15}N^{14}O$ 79
Rasmussen, A. L., Disaccommodation of magnetic spectra of two manganese ferrites 181
Reduction of crystallographic point groups to subgroups by homogeneous stress 309
Refractive indices of some solids, effect of hydrostatic pressure 325
Reilly, M. L., G. T. Furukawa, Application of precise heat-capacity data to the analysis of the temperature intervals of the NBS-1955 and the International Practical Temperature Scales in the region of 90 °K 5
Robinson, R. A., V. E. Bower, An additivity rule for the vapor pressure lowering of aqueous solutions 365
—, —, Properties of aqueous mixtures of pure salts: Thermodynamics of the ternary system water-potassium chloride-barium chloride at 25 °K 439
—, —, Thermodynamics of the ternary system: water-glycine-potassium chloride at 25 °C from vapor pressure measurements 131
—, —, Thermodynamics of the ternary system: water-sodium chloride-barium chloride at 25 °C 19
—, *M. Woodhead, M. Paabo, R. G. Bates*, Acid-base behavior in 50-percent aqueous methanol: thermodynamics of the dissociation of protonated tris (hydroxymethyl) aminomethane and nature of the solvent effect 263
Roder, H. M., Irregularities in the NBS (1955) provisional temperature scale 527
Roth, F. L., G. W. Bullman, L. A. Wood, Compliance-time-temperature relationships from indentation measurements on a pure gum rubber vulcanizate 347
Roth, R. S., J. L. Waring, Phase equilibria in the system vanadium oxide-niobium oxide 119
Rubber vulcanizate, pure-gum, compliance-time-temperature relationships from indentation measurements 347
Ruffa, A. R., One particle transitions and correlation in quantum mechanics 167

S

Saba, W. G., G. T. Furukawa, Heat capacity and thermodynamic properties of beryllium aluminate (chrysoberyl), $BeO \cdot Al_2O_3$, from 16 to 380 °K 13
—, —, *T. B. Douglas, A. C. Victor*, Heat capacity and enthalpy measurements on aluminum carbide (Al_4C_3) from 15 to 1173 °K. Thermodynamic properties from 0 to 2000 °K 423
Schneider, S. J., J. L. Waring, Phase equilibrium relationships in the Gd_2O_3-TiO_2 255
—, —, *R. E. Tressler*, Phase relations between iridium and the sesquioxides in air 245
Sea water from 5 to 120 °C, electrical conductivity of dilute solutions 39
Sesquioxides and iridium in air, phase relations between 245
Shadmi, Y., Theoretical interpretation of the third spectrum of gold (Au III) 511
Shumaker, J. B., Jr., C. H. Popenoe, Arc measurement of some argon transition probabilities 495

Page

Sniegoski, L. T., H. L. Frush, N. B. Holt, H. S. Isbell, Synthesis of D-glucose-3-^{14}C and related compounds 535
Sodium and potassium chlorate, heat of decomposition 1
Solvent effects in 50-percent methanol 263
Spectural structure of critical opalescence: binary mixture 523
Spin-orbit interaction, matrices of, in the electron configurations p^2d and p^4d 401
Splitting of a set of equivalent sites in centrosymmetric space groups into subsets under homogeneous stress 193
Splitting of equivalent points in noncentrosymmetric space groups into subsets under homogeneous stress 461
Stanley, R. W., W. F. Meggers, More wavelengths from thorium lamps 109
Stern, K. H., Low-frequency dielectric properties of liquid boric oxide 281
—, *S. E. Meador*, Electrode potentials in fused systems X. Measurement of cation concentration in molten salts using glass membrane electrodes 553
Synthesis of D-glucose-3-^{14}C and related compounds 535
Synthesis and ring structure of 7-acetamido-deoxy-L-*galacto*-heptulose 291
Szwarc, R., E. R. Plante, J. J. Diamond, Vapor pressure and heat of sublimation of tungsten 417

T

Taylor, J. K., R. A. Durst, Photopolarographic behavior of inorganic depolarizers 517
Tech, J. L., H. H. Garstang, Matrices of spin-orbit interaction in the electron configurations p^2d and p^4d 401
Teflon (see polytetrafluoroethylene) 149
Ternary system, thermodynamics of, water-potassium chloride-barium chloride at 25 °K, properties of aqueous mixtures of pure salts 439
Ternary system: water-sodium chloride-barium chloride at 25 °C, thermodynamics 19
Tetracalcium phosphate 547
Tetrafluoroethylene and hexafluoropropylene, inclusion of perfluoromethyl groups in the lattice of copolymers 481
Theoretical interpretation of the third spectrum of gold (Au III) 511
Thermodynamic properties of polytetrafluoroethylene 149
Thermodynamics of dissociation, tris(hydroxymethyl)aminomethane in 50-percent methanol 263
Thermodynamics of the ternary system water-potassium chloride-barium chloride at 25 °K, properties of aqueous mixtures of pure salts 439
Thermodynamics of the ternary system: water-glycine-potassium chloride at 25 °C from vapor pressure measurements 131
Thermodynamics of the ternary system: water-sodium chloride-barium chloride at 25 °C 19
Thorium lamps, more wavelengths 109
Tighe, N. J., D. J. Barber, Observations of dislocations and surface features in corundum crystals by electron transmission microscopy 271
Tressler, R. E., S. J. Schneider, J. L. Waring, Phase relations between iridium and the sesquioxides in air 245
Tris(hydroxymethyl)aminomethane, in 50-percent methanol 263
Tungsten, vapor pressure and heat of sublimation 417

Page

V

Vanadium oxide-niobium oxide, phase equilibria in the system 119
Vapor pressure and heat of sublimation of tungsten 417
Vapor pressure lowering of aqueous solutions, additivity rule 365
Victor, A. C., G. T. Furukawa, T. B. Douglas, W. G. Saba, Heat capacity and enthalpy measurements on aluminum carbide (Al_4C_3) from 15 to 1173 °K. Thermodynamic properties from 0 to 2000 °K 423
Viscometer, rotating cylinder, wide-range (up to 10^{10}P) 449
Vulcanizate, pure-gum rubber, compliance-time-temperature relationships from indentation measurements 347

W

Wachtman, J. B., Jr., W. C. Corwin, Internal friction in ZrO_2 containing CaO 457
—, *H. S. Peiser*, Reduction of crystallographic point groups to subgroups by homogeneous stress 309
—, —, Splitting of a set of equivalent sites in centrosymmetric space groups into subsets under homogeneous stress 193
—, —, *F. A. Munley, L. C. McCleary*, Splitting of equivalent points in noncentrosymmetric space groups into subsets under homogeneous stress 461
Wagman, D., A. A. Gilliland, Heat of decomposition of sodium and potassium chlorate 1
Waring, J. L., R. S. Roth, Phase equilibria in the system vanadium oxide-niobium oxide 119
—, *S. J. Schneider*, Phase equilibrium relationships in the system Gd_2O_3-TiO_2 255
—, —, *R. E. Tressler*, Phase relations between iridium and the sesquioxides in air 245
Water-potassium chloride-barium chloride at 25 °K, thermodynamics of the ternary system, properties of aqueous mixtures of pure salts 439
Wavelengths from thorium lamps 109
Waxler, R. M., C. E. Weir, Effect of hydrostatic pressure on the refractive indices of some solids 325
Weeks, J. J., J. Powers, J. D. Hoffman, F. A. Quinn, Jr., Crystallization kinetics and polymorphic transformation in polybutene-1 335
Weir, C. E., Compressibility of eleven inorganic materials 29
—, *R. M. Waxler*, Effect of hydrostatic pressure on the refractive indices of some solids 325
Wide-range (up to 10^{10}P) rotating cylinder viscometer 449
Wilson, M., R. Zalubas, Atomic absorption spectrum of praesodymium (Pr II) 59
Wood, L. A., F. L. Roth, G. W. Bullman, Compliance-time-temperature relationships from indentation measurements on a pure-gum rubber vulcanizate 347
Woodhead, M., M. Paabo, R. A. Robinson, R. G. Bates, Acid-base behavior in 50-percent aqueous methanol: thermodynamics of the dissociation of protonated tris(hydroxymethyl)aminomethane and nature of the solvent effect 263

Z

Zalubas, R., M. Wilson, Atomic absorption spectrum of praseodymium (Pr II) 59
Zapas, L. J., T. Craft, Correlation of large longitudinal deformations with different strain histories 541

U.S. GOVERNMENT PRINTING OFFICE 1965 OL—787-221

SJR-A OCT 46129
UNIVERSITY MICROFILMS INC
SERIALS SECTION
313 NORTH FIRST ST
ANN ARBOR MICH

UNITED STATES
GOVERNMENT PRINTING OFFICE
DIVISION OF PUBLIC DOCUMENTS
WASHINGTON, D.C. 20402

OFFICIAL BUSINESS

POSTAGE AND FEES PAID
U.S. GOVERNMENT PRINTING OFFICE

JOURNAL OF RESEARCH of the National Bureau of Standards Vol. 69A, No. 6 November–December 1965
A. Physics and Chemistry

Contents

	Page
Arc measurement of some argon transition probabilities. C. H. Popenoe and J. B. Shumaker, Jr.	495
Theoretical interpretation of the third spectrum of gold (Au III). Y. Shadmi.	511
Photopolarographic behavior of inorganic depolarizers. R. A. Durst and J. K. Taylor.	517
Spectral structure of critical opalescence: binary mixture. Raymond D. Mountain.	523
Irregularities in the NBS (1955) provisional temperature scale. Hans M. Roder.	527
Isotherms determined by the National Bureau of Standards acoustical thermometer in the liquid helium temperature range. G. Cataland and H. Plumb.	531
Synthesis of D-glucose-3-^{14}C and related compounds. Harriet L. Frush, Lorna T. Sniegoski, Nancy B. Holt, and Horace S. Isbell.	535
Correlation of large longitudinal deformations with different strain histories. L. J. Zapas and T. Craft.	541
Crystallography of tetracalcium phosphate. Walter E. Brown and Earl F. Epstein.	547
Electrode potentials in fused systems X. Measurement of cation concentration in molten salts using glass membrane electrodes. Kurt H. Stern and Susan E. Meador.	553
Publications of the National Bureau of Standards.	557
Index to volume 69A, January to December 1965.	567

Library of Congress Catalog Card Number: 62–37059

For sale by the Superintendent of Documents, U.S. Government Printing Office, Washington, D.C., 20402. Price 70 cents (single copy). Subscription price: $4 a year; 75 cents additional for foreign mailing.
UNITED STATES GOVERNMENT PRINTING OFFICE, WASHINGTON : 1965